Combustion of methanol/diesel blends in a compression ignited engine

Research into the effects of methanol/diesel blends on the performance and emissions of a diesel engine based on experiments and simulations

R.S. Tol

P&E report number 3028

TU Delft

Combustion of methanol/diesel blends in a compression ignited engine

Research into the effects of methanol/diesel blends on the performance and emissions of a diesel engine based on experiments and simulations

by

R.S. Tol

to obtain the degree of Master of Science
at the Delft University of Technology,
to be defended publicly on Wednesday August 19, 2020 at 14:00 PM.

Student number:	4974115	
Project duration:	November, 2019 – August, 2020	
Thesis committee:	Prof. Dr. D.J.E.M. Roekaerts,	TU Delft, chairman
	Ir. K. Visser,	TU Delft, supervisor
	Prof. Dr. Ir. R.G. van de Ketterij,	NLDA
	Dr. Ir. L.M.T. Somers,	TU Eindhoven
	Ir. H.D. Sapra,	TU Delft

TU Delft

Preface

Lectori salutem,

This document concerns my master thesis to obtain the degree of Master of Science. I am very grateful to the professors at the Netherlands Defence Academy for getting the opportunity to follow a master track at the Delft University of Technology. My appreciation for these two years is unprecedentedly large.

During my master thesis period an investigation by means of experiments and modelling to the effect of methanol blends in a diesel engine was performed. The COVID-19 period began at a crucial moment for realisation of the experimental setup. Perseverance and hard work made it possible to create a safe and effective experimental setup. Experiments took place in 'Gebouw Medemblik' at the Royal Netherlands Naval College. I would like to express my appreciation to everyone involved in making this project possible. The experiments would especially not have been possible without the help of René d'Hondt, SGT(TD) Jeroen Krieger and Joop van de Laar. We faced ups and downs, but we kept supporting this project. Their hard work and dedication to the realisation of the experiments, even during the period characterized by the 1.5 meter distanced COVID-19 period, made this project a success. Additionally, I would like to thank Ing. Chris Dijkstra and Ing. Marcel Roberscheuten for the time they took to have interesting discussions and for giving me advise during the research period. Again, all of your commitment is greatly appreciated.

Furthermore, I am grateful for the support of my supervisors Prof. dr. D.J.E.M. Roekaerts and Ir. K. Visser. They provided me the opportunity to graduate on this interesting and important topic. Moreover, the daily support and discussions with Prof. dr. ir. R.G. Van de Ketterij and Ir. H. Sapra were very valuable and resulted in interesting discussions and new insights. During these discussions we talked about the problems I faced, which afterwards pushed me mentally back in the right direction.

Last but not least, I would like to say thanks to my family for always supporting me during my thesis period. Even when I converted the living room into an office and while I was facing changing moods, you kept supporting me which provided the opportunity to finish my work.

Thank you all.

R.S. Tol
Delft University of Technology, August 2020

Abstract

In the context of this thesis, the effect of various diesel-methanol blends in a diesel engine compared to conventional marine diesel oil is investigated by experiments and in-cylinder simulations.
The main differences obtained between diesel and methanol are the lower heating value, heat of vaporization and cetane number. During the experiments, the engine was not able to run on M20 at loads lower than 153 [kW]. Pressure signal comparison between the cylinders showed that cylinder one shows better ignition properties for methanol operation compared to cylinder two, three and four. Higher COV's for IMEP and maximum pressure were obtained by methanol blends. Experiments with F76, M10 and M20 fuel have shown that methanol blends increase the specific fuel consumption and slightly decrease the engine efficiency. Specific NO_x emissions decreased with 2.9 up to 14.2 [%] by methanol blends compared to F76. Due to the increased fuel consumption, the CO_2 emissions hardly reduced. Exhaust gas temperatures and CO emissions seems to decrease. The ignition delay of methanol blends increased up to 8°CA for M20 while remaining the brake power constant. Moreover, the combustion duration and air excess ratio decreased by using methanol blends.

A single droplet evaporation model is built to simulate the evaporation heat losses for methanol fuel during the in-cylinder process. Methanol has a longer evaporation time which is a disadvantage for diesel engine applications. By using the single droplet evaporation model combined with an injection model calibrated for dual fuel direct injection, the fuel spray evaporation heat is calculated for implementation in the single zone model. The results are calibrated by using the droplet diameter as a variable. In this way, the evaporation heat required for evaporation of methanol is simulated in the dual fuel single zone model.

Heat release analysis shows that the premixed combustion phase of methanol blends is dominant compared to F76, while the diffusive combustion phase significantly reduces. For methanol blends, the residence time at high temperatures is lower due to the decreased combustion duration and elongated ignition delay. Unfortunately, the results from the dual fuel single zone model are strongly dependent on the position of the pressure signal. Results for the temperature of the mean cylinder two, three and four were not in line with the expectations. Cylinder one showed smoother heat release curves and its temperature result was in line with the expectations based on the exhaust gas temperature. More research to the effects of the fuel injectors on the heat release of methanol/diesel blends is recommended.

Contents

List of Figures

List of Tables

Nomenclature

Abbreviations

AFR	Air to fuel ratio
BSFC	Brake Specific Fuel Consumption
C/H	Carbon-Hydrogen ratio
CI	Compression Ignited
CR	Crank/Rod
D100	$100\%_{energy}$ diesel fuel
ECAs	Emission Control Areas
EO	Exhaust valve open
F76	Conventional marine diesel fuel
GMM	Green Maritime Methanol
HHV	Higher Heating Value
IC	Inlet valve closed
ICE	Internal Combustion Engine
IMO	International Maritime Organisation
LFO	Light fuel oil
LHV	Lower Heating Value
M5	$5\%_{energy}$ - $95\%_{energy}$ diesel fuel
M10	$90\%_{energy}$ diesel fuel, $10\%_{energy}$ methanol
M15	$85\%_{energy}$ diesel fuel, $15\%_{energy}$ methanol
M20	$80\%_{energy}$ diesel fuel, $20\%_{energy}$ methanol
M25	$75\%_{energy}$ diesel fuel, $25\%_{energy}$ methanol
M30	$70\%_{energy}$ diesel fuel, $30\%_{energy}$ methanol
SECA	Sulfur Emission Control Area
SFC	Specific Fuel Consumption
SOC	Start of combustion
SOI	Start of injection
TNO	Netherlands Organisation for applied scientific research

Subscripts

b	Brake
C	Carbon
D	Diesel
d	Droplet
da	Dry air
evap	Evaporation
f	Fuel
gas	Gas, vapor
H	Hydrogen
i	Indicated
j	Exhaust gas component
inj	Liquid
MD	Methanol-Diesel mixture
M	Methanol
m	Mechanical

O	Oxygen
S	Stroke
S	Sulfur
v	Vapor
w	Wall

Greek symbols

α	Crank angle in degrees,	[°]
η	Efficiency	[-]
λ_{CR}	Crank/rod ratio	[-]
ν	Kinematic viscosity	[cSt]
ϕ	Crank angle in radians	[rad]
ρ	Density	[kgm^{-3}]
σ	Stoichiometric air to fuel ratio	[-]
τ	Ignition delay	[° CA]
λ_{tot}	Air excess ratio	[-]
μ	Dynamic viscosity	[m^{2}s^{-1}]
σ	Surface tension	[Nm^{-2}]

Symbols

$\alpha_{\mathrm{g\rightarrow w,i}}$	Heat transfer coefficient	[Wm^{-2}K^{-1}]
A	Fuel dependent constant	[-]
A_0	Area droplet	[m^2]
afr	Air to fuel ratio	[-]
B	Quantity of fuel injected per stroke	[mg/stroke]
Bi	Biot number	[-]
c_{m}	Mean engine speed	[ms^{-1}]
c_{p}	Heat capacity at constant pressure	[kJ(kgK)$^{-1}$]
CN	Cetane number	[-]
$C_{\mathrm{d,cyl}}$	Discharge coefficient	[-]
CRR	Combustion reaction rate	[kgs^{-1}]
d	Diameter droplet	[m]
d_0	Nozzle diameter	[m]
D_{B}	Bore diameter	[m]
D_{AB}	Binary diffusion coefficient	[m^{2}s^{-1}]
E_{A}	Activation energy	[kJ]
E_{f}	Heat of vaporization	[J]
G	Grunnberg-Nissan factor	[-]
$GAHRR$	Gross apparent heat release	[kJs^{-1}]
$\tilde{h}$	Convective heat transfer coefficient	[Wm^{-2}K^{-1}]
$\tilde{h}^*$	Corrected convective heat transfer coefficient	[Wm^{-2}K^{-1}]
h	Enthalpy	[kJkg^{-1}]
h_{fg}	Specific heat of vaporization	[kJkg^{-1}]
$\tilde{h_D}$	Mass transfer film coefficient	[ms^{-1}]
$\tilde{h}^*_{\mathrm{D}}$	Corrected mass transfer coefficient	[ms^{-1}]
i	Number of cylinders	[-]
COV	Coefficient of variance	[-]
$IMEP$	Indicated mean effective pressure	[bar]
K	Evaporation constant	[m^{2}s^{-1}]
K_{f}	Bulk modulus	[Pa]
Pr	Prandtl number	[-]

L_{P}	Length cylinder wall	[m]
M	Molar mass	[kgmol^{-1}]
$\dot{m}$	Massflow	[kgs^{-1}]
m	Mass	[kg]
M_{b}	Brake torque	[Nm]
$\mathrm{mr}_{\mathrm{CO_2}}^{\mathrm{g-out}}$	Emission per kilogram fuel	[gkg^{-1}]
N	Molar fraction	[%]
N	Number of droplets	[-]
n	Fuel dependent constant	[-]
n	Number of carbon molecules	[-]
$NAHRR$	Nett apparent heat release	[kJs^{-1}]
$\dot{P}$	Pressure change	[Pa· s^{-1}]
P	Power	[kW]
p	Pressure	[Pa]
p_0	Pressure in the engine without fuel injection	[bar]
$p_{\mathrm{v,0}}$	Saturated vapor pressure	[Pa]
L_{s}	Stroke length	[m]
P_{b}	Brake power	[kW]
per	Polutant emission ratio	[gkg^{-1}]
P_{n}	Pressure in the injector nozzle	[Pa]
$ppmv$	Parts per million volume	[-]
$\dot{Q}_{\mathrm{loss}}$	Heat loss	[kJs^{-1}]
Q_{evap}	Heat of vaporization	[kJkg^{-1}]
$\dot{Q}_{\mathrm{in}}$	Volume flow pump in	[m^{3}s^{-1}]
$\dot{Q}_{\mathrm{out}}$	Volume flow pump out	[m^{3}s^{-1}]
$\dot{V}$	Volume flow	[m^{3}s^{-1}]
$RACK$	Fuel rack position	[mm]
RCO	Reaction coordinate	[-]
Re	Reynolds number	[-]
SMD	Sauter mean diameter	[m]
Sc	Schmidt number	[-]
sfc	Specific fuel consumption	[g(kWh)$^{-1}$]
Sh	Sherwood number	[-]
spe	Specific emission	[g(kWh)$^{-1}$]
T	Temperature	[K]
t	Time	[s]
t_{c}	Correction factor for time heating period droplet	[-]
t_{h}	Time heating period	[s]
T_{inf}	Temperature in the cylinder	[K]
u	Internal energy	[kJkg^{-1}]
V	Volume	[m^3]
v	Injection speed	[ms^{-1}]
$\dot{W}$	Indicated work,	[kJs^{-1}]
w_{t}	Swirl velocity	[ms^{-1}]
We	Weber number	[-]
x	Mass fraction	[-]
$\mathrm{y}_{\mathrm{O_2}}^{\mathrm{da}}$	Volume fraction of oxygen in air	[%]
$\mathrm{y}_{\mathrm{CO_2}}^{\mathrm{da-out}}$	Volumetric concentration of carbon dioxide in dry exhaust gas	[%$_{\mathrm{v}}$]
$\mathrm{y}_{\mathrm{O_2}}^{\mathrm{da-in}}$	Volumetric concentration of dioxide in dry inlet air	[%$_{\mathrm{v}}$]
$\mathrm{y}_{\mathrm{O_2}}^{\mathrm{da-out}}$	Volumetric concentration of dioxide in dry exhaust gas	[%$_{\mathrm{v}}$]
z	Volume fraction	[%]

1 Introduction

1.1. Motivation

The aim for reducing environmental pollution by harmful emissions from internal combustion engines led to the increase of demand for renewable alternative fuels. The marine industry contributes a significant part in exhaust gas emissions worldwide [27]. One way to reduce harmful emissions is by using bio-fuels produced from renewable sources. Another method is by using electric power from fuel cells in which hydrogen is used as a fuel. Nowadays, alcohols are considered to be an alternative fuel for conventional marine diesel oil.

The governing companies involved in the Green Maritime Methanol project (GMM), in which multiple Dutch maritime companies are involved, started to conduct research to the feasibility of methanol as an alternative marine fuel. Infrastructure, supply chain, several operational profiles, ship configuration, performances and emissions of nine ships are taken into consideration to compare methanol to conventional light fuel oil (LFO).

Nowadays, compression ignited engines are important in power generation for ship propulsion. Therefore, an important part of the GMM is to investigate whether methanol can be used in existing engines. Methanol's ability to replace diesel in existing operational units is investigated by injecting methanol-diesel blends in a diesel engine instead of pure methanol, because methanol normally is non-ignitable in compression ignited engines. The main focus of this research is retaining engine performance and reduction of exhaust gas emissions compared to conventional marine diesel fuel, without adapting the physical properties of the existing diesel engines. In this way, the investigation of the ability of methanol to serve as a renewable fuel source in compression ignited engines contributes to the GMM project.

1.2. Thesis objective

The objective of this thesis is to investigate the effects of methanol as an alternative fuel compared to conventional marine diesel oil by conducting experiments and modelling. Methanol's low cetane number and high heat of vaporization suggests to start the experiments using methanol-diesel fuel blends instead of pure methanol. Measurements on a diesel engine will be performed to investigate the engine performance and combustion parameters for different methanol-diesel mixing ratios. Measurements on varying engine speed and load will be performed. Moreover, exhaust gas measurements are executed including the green house gas emissions.

Combustion parameters are not easy to measure in an engine. Therefore an heat release model will be adapted and applied to study the differences between the fuel blends during the combustion process. One of the objectives regarding the models is to improve the existing in-cylinder models by

implementing the evaporation heat of methanol. The model will be verified based on theoretical experiences and literature expectations.
Results from the measurements and models should provide an indication about the effects of methanol in internal combustion engines.

1.3. Research questions

Before injecting methanol in a diesel engine, the properties of methanol compared to diesel fuel must be known. Based on these properties, an analysis of experimental and simulation results is performed. The research done by experiments and modelling will give answer to the main research question: *What is the effect of blended methanol-diesel fuel on the in-cylinder combustion parameters and exhaust gas emissions of a direct injection compression ignited engine?* The research question is answered by multiple sub questions to give an insight on the effect of methanol in a compression ignited engine. This thesis will answer the following sub questions:

- What are the chemical differences between marine diesel oil and methanol?
- Which in-cylinder combustion parameters are important while studying the effect of methanol/diesel blends?
- Which changes are required to (improve) the dual fuel model C in order to use it for the MAN4L20/27 diesel engine?
- What are the effects on the combustion parameters and emissions of methanol/diesel blends compared to conventional marine diesel oil?
- Can we build a direct injection dual fuel model C such that it can describe in-cylinder engine performance running on methanol/diesel blends?

The results from the research provide information about the use of methanol in compression ignited engines. Differences between methanol and diesel fuel are investigated and will give valuable information about the ability of methanol/diesel blends in existing direct injection compression ignited engines.

1.4. Thesis outline

The research question is answered in this thesis. Chapter 2 provides general information about methanol. Moreover, general applications for the use of methanol in diesel engines and chemical differences between conventional diesel fuel and methanol/diesel blends are discussed. Furthermore, expectations based on literature and theory are proposed. In chapter 3, the dual fuel single zone model and its improvements are discussed. Theoretical background and shortcomings of the existing and new models are treated in detail. Chapter 4 provides information about the experiments performed. Important performance parameters are proposed and supported by theoretical background. Finally, the chapter concludes with a discussion about the experimental results obtained from the measurements. Chapter 5 starts with the modelling verification. Differences observed for fuel performance based on single zone parameters cover the final part of this chapter. Finally, chapter 6 contains the conclusions and recommendations resulting from this research.

2

Methanol as alternative fuel

This chapter describes the motivation and background of methanol as an alternative fuel and discusses different properties, challenges and opportunities by using methanol. Methanol is considered as a reasonable alternative fuel for internal combustion engines based on sustainability, storability and scalability [11]. The topics mainly focus on the use in internal combustion engines (ICE). First, sections 2.1 to 2.3 are giving general information about methanol. After that, in section 2.4 methods to inject methanol in diesel engines are discussed. Important recent developments related to the production of methanol in the Netherlands are discussed. Finally, the chemical properties of methanol and diesel and its blends are evaluated. Expectations based on literature and the chemical properties are described.

2.1. Chemical properties

Methanol has different chemical properties compared to conventional marine diesel oil. To get a first insight in the potential of methanol, this chapter describes the chemical properties of methanol compared to diesel fuel.

2.1.1. Methanol vs. conventional marine diesel oil

Alcohols have deviating properties compared to conventional hydrocarbon fuels such as marine diesel oil. Table 2.1 provides the chemical properties of marine diesel oil (F-76) and methanol.

Heating value

The heating value of a fuel is defined as the amount of energy released during combustion of one kilogram of that specific fuel [51]. There are two defined heating values: higher and lower heating value. The difference between these two is the condensation heat of the water vapour resulting from combustion. If the condensation heat is added, the higher heating value (HHV) is obtained. The lower heat value (LHV) is defined without taking the condensation heat into account.

Comparison between the LHV of methanol and F-76 shows that methanol contains less than 50% energy of the same amount of diesel. This implicates that the specific fuel consumption (SFC) increases by using methanol/diesel blends while maintaining a constant engine load [1, 25].

Hydrogen content

The fuel hydrogen content has a positive impact on the combustion. High hydrogen content contributes to the flammability and ignition characteristics [2].
The difference between both fuels is 0.6 [wt.%], which implicates that methanol has less attractive ignition properties since its hydrogen content is lower.

Table 2.1: Fuel properties: F-76 and Methanol

Parameter	F-76	Methanol [48]	Unit
Lower heating value	42580	20270	[kJkg^{-1}]
Hydrogen content	13.1	12.5	[wt.%]
Carbon content	86.6	37.5	[wt.%]
Sulfur content	0.05	0	[wt.%]
Oxygen content	0	50	[wt.%]
Density	847.4	790	[kgm^{-3}]
Kinematic Viscosity 298.15 [K]	2.5$\cdot$ 10^{-6} [48]	0.75 $\cdot$ 10^{-6}	[cm^{2}s^{-1}]
Kinematic Viscosity 313.15 [K]	3.00 [36]	0.58 [36]	[cSt]
Flash point	342.65	284.15	[K]
Boiling temperature	463.15-553.15 [48]	337.85	[K]
Autoignition temperature	527.15 [48]	737.15	[K]
Cetane number	45.1	4	[-]
Stoichiometric AFR	14.47	6.66	[-]
Heat of Vaporization	0.27 [48]	1.11	[MJkg^{-1}]

Carbon content

Nowadays, one of the main parameters in selecting a fuel is the carbon content. The carbon content is related to the CO_2 and CO emissions. It is therefore advantageous for the reduction of harmful emissions if an alternative fuel contains less carbon.

Comparing both fuels, it shows that the carbon content of methanol is almost 57% lower. Therefore, the expectation is that the CO_2 emissions of methanol automatically are lower. It can be seen that the carbon/hydrogen (C/H) ratio of methanol is over 50% lower.

Sulfur content

Sulfur contributes to the emissions of sulfur oxides (SO_x). However, the amount of sulfur in F-76 is already low due to the strict regulations for ship exhaust gas emissions [51]. A long term disadvantage is that fuel without sulfur has no lubrication effect. On existing engines, the fuel pump is often lubricated by fuel.

Diesel and methanol both have none or very low sulfur content. Lubrication effects already are very low and it is therefore not expected that low sulfur content related problems will suddenly occur by using alcohol diesel blends. Moreover, the exhaust gas emission of sulfur oxides will automatically decrease by adding less sulfur to the engine. This is an advantage to minimize the impact on acid rain [1].

Oxygen content

Oxygen from air mixes with fuel in the cylinder resulting in combustion under the right pressure. Normally all oxygen needed for combustion in a diesel engine comes from the air inlet. Methanol contains an oxygen molecule in its hydroxyl group, which helps in reaching a more complete combustion during the expansion stroke [1].

Density

The fuel density is the mass to volume ratio of a fuel. Fuel density in combination with LHV is important in a practical way. Multiplying these two gives the amount of energy storage in the fuel tanks.

Methanol has a 6.8 [%] lower density compared to diesel. As mentioned before, the LHV is also very low. A higher fuel flow is needed to produce an equal amount of power from an engine. On the long term, this could mean that existing fuel injectors needs to be replaced to inject a sufficient amount of fuel into the cylinders [1]. Assuming an identical engine running on pure methanol or methanol/diesel blends, the range of a vehicle will decrease without adapting the fuel storage capacity. Based on this,

warships have a large operational disadvantage by using methanol as primary fuel. Less energy storage means reduction of fuel supply independency, which results in more frequent visits to harbors or tankers.

Kinematic Viscosity

Viscosity is the internal friction of a fluid in terms of the force per unit area, which is temperature dependent [51]. Viscosity is an important parameter for fuels in a compression ignited (CI) engine since higher viscosity leads to better ignition properties [51]. A low viscosity could cause damage to sub systems of the engine, for instance to fuel pumps and injectors. A decreased fuel temperature in general leads to higher viscosity.

Methanol's viscosity is lower than conventional diesel fuel. A lower viscosity automatically has effect on the combustion in the cylinder for instance due to the methanol spray angle. To prevent disadvantages related to viscosity, fuel additives can be used or methanol must be blended with diesel to maintain the lubricating properties for the existing engines [1].

Heat of vaporization

The heat of vaporization of a fuel indicates how much energy is needed to evaporate a kilogram of that fuel. The required heat comes from the surrounding air in the cylinder of an engine. Therefore, the temperature of the air will decrease while evaporating the fuel. This effect is positive the formation of NO_x, since forming of this is, among other things, dependent on temperature. Moreover, maximum temperatures also decrease which will affect the maximum thermal efficiency of the engine. It is observed that the heat of vaporization of methanol is almost 4 times higher compared to diesel. This causes that the in-cylinder temperature at the start of the in-cylinder process needs to decrease before starting the combustion when liquid methanol is injected. According to literature, it is due to the cooling effect that adding methanol will improve the brake thermal efficiency and power output of the engine [1, 25].

Temperature related parameters

The flash point of a fuel states the temperature at which the fuel vapor above the liquid bulk ignites with a lighter. This is an important parameter for the safety on board of a ship [51]. Methanol has a low flash point which could be a problem on ships. Storage of methanol could force the owner of ships to use additives to increase the flash point. Another point is to take more safety measures for fuel storage rooms. This is however not a discussion point at this phase of the research to methanol.

The boiling point of a fuel is the temperature at which the fuel starts to boil. For methanol, this temperature is low compared to diesel. A low boiling point needs to be considered when a fuel storage room could reach high temperatures. Therefore, is it recommended to have sufficient venting systems to regulate the temperature in this areas and to prevent flammable gases to reach the lower explosive level.

As mentioned before, the auto-ignition temperature is important within a diesel engine. Methanol has a very high auto-ignition temperature which means that using a pilot fuel is necessary in a diesel engine.

Cetane number

The cetane number gives an indication of the fuels flammability. Low cetane number fuels have difficulties with auto-ignition and smooth combustion. In compression ignited engines, fuel is ignited by auto-ignition at a certain pressure. Low cetane fuels have higher auto-ignition pressures, which are difficult to reach with the current compression ignited engines due to limits of the engine's material and cylinder dimensions. Methanol has a low cetane number, indicating that it is not easy to ignite in a CI engine. Therefore, methanol is often ignited by a pilot fuel with a high cetane number. By injecting it as a blend with diesel it is assumed that the diesel fuel will ignite the methanol. Due to the higher heat of vaporization and cetane number, methanol/diesel blends are expected to show a larger ignition delay

compared to diesel fuel.

2.2. Opportunities of methanol as a fuel

2.2.1. Alternative diesel fuel

Since most of the engines are internal combustion engines using diesel fuel, the main focus in the process of finding alternative fuels are the fuel's storability, chemical properties and exhaust gas emissions. Methanol seems to have similar storage properties compared to diesel fuel, except for the LHV and flash point. By using a chemically comparable fuel compared to diesel fuel, research investments and replacing costs of many internal combustion engines on board of ships are reduced. Chemical structure of a fuel helps reducing the harmful exhaust gases by only changing the fuel in an existing engine. The properties affecting storage capability and safety regulations are needed to be evaluated before implementation on operating units. Other parameters influencing the suitability of an alternative fuel are the availability and life cycle emissions.

2.2.2. Emission regulations

The International Maritime Organisation (IMO) regulates the emissions of vessels at sea. Emission control areas (ECAs) are areas were restrictions at sulphur oxides and nitrogen oxides are imposed by MARPOL Annex VI. From January 2020, the sulfur content in fuel is limited to 0.5% by the EU's Sulphur Directive [26]. Methanol as a fuel in vessels helps to decrease the SO_x emissions based on chemical structure. Today, emissions of NO_x for vessels are not yet restricted in the European Union. However, the United States has an ECA where the NO_x emissions are limited. Moreover, researchers from MAN investigated the effect of methanol in diesel engines and concluded that the NO_x emissions reduced by approximately 30% [41]. It seems that by using methanol as a fuel, the tank-to-wheel exhaust gases are reducing. The emissions of CO_2 are not discussed yet, however based on the chemical properties they are expected to be lower compared to diesel fuel. The next section discusses the emissions from the methanol life cycle in more detail.

2.2.3. Methanol production

Emissions related to the production of methanol, or well-to-tank, are not evaluated yet. Although they are not yet evaluated, it is important to be aware of the harmful emissions from the production process because these play a big role in the total emissions of the fuel life cycle [26].

Methanol can be produced by many different processes. It can be produced completely renewable, which is attractive in combination with the low CO_2, NO_x and SO_x emission regulations. Biomass, which often is burned, is more useful to produce methanol from its gasification since its energy is then used in a sustainable way. At the Port of Rotterdam, such a methanol plant is now being built with the aim to make bio-methanol from biomass of over 700,000 house holds and simultaneously reducing the CO_2 emissions with 300,000 tons a year compared to fossil based methanol [16]. Moreover, new techniques show that by extracting CO_2 from the air, methanol can be produced. In Qatar, a new CO_2 recovery plant is built by Mitsubishi to produce renewable methanol [4].

Nowadays, most of the methanol is produced from natural gas. Production based on biomass is less popular, but this method has future opportunities. At this moment, the well-to-tank emissions of natural gas or biomass based methanol production do not differ much according to IMO. However, the tank-to-wheel principle is in favor of biomass, due to the fossil base of natural gas [26]. Those emission numbers are not only shown by the International Maritime Organisation, the European Maritime Safety Agency also affirms the advantages of methanol produced from biomass [15]. Figures 2.1 to 2.3 show the life cycle emissions of conventional fuel and methanol from natural gas and biomass.

In figs. 2.1 to 2.3, tank-to-propeller emissions are shown when burning the fuel in an engine. Well-

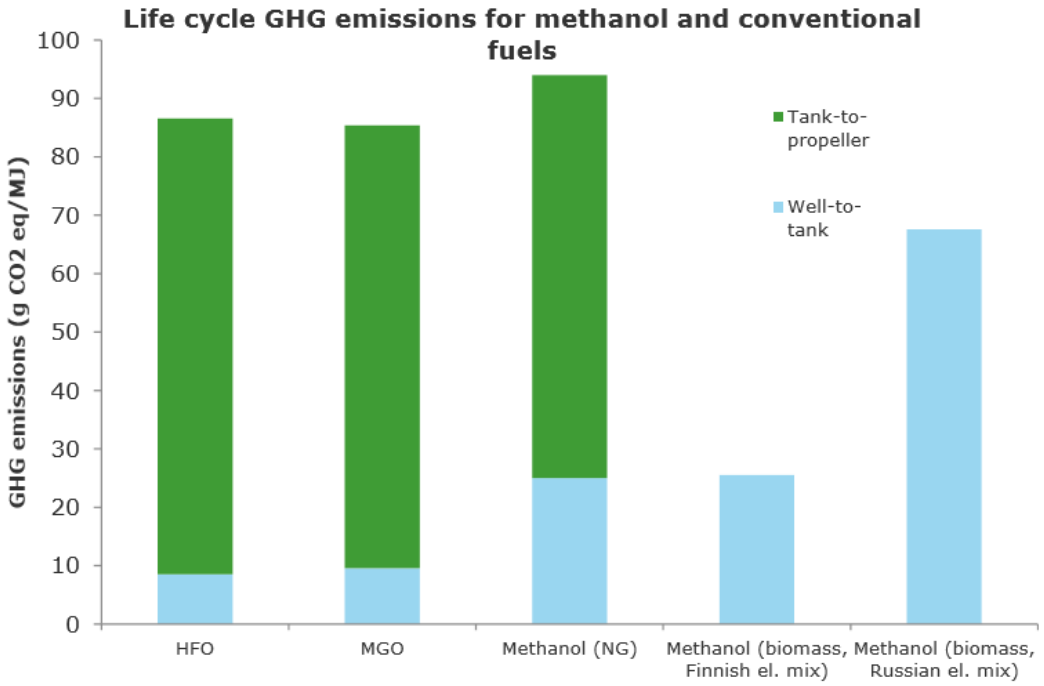

Figure 2.1: Life cycle of CO_2 emissions for conventional fuel compared to methanol produced from natural gas and biomass, taken from IMO [26]

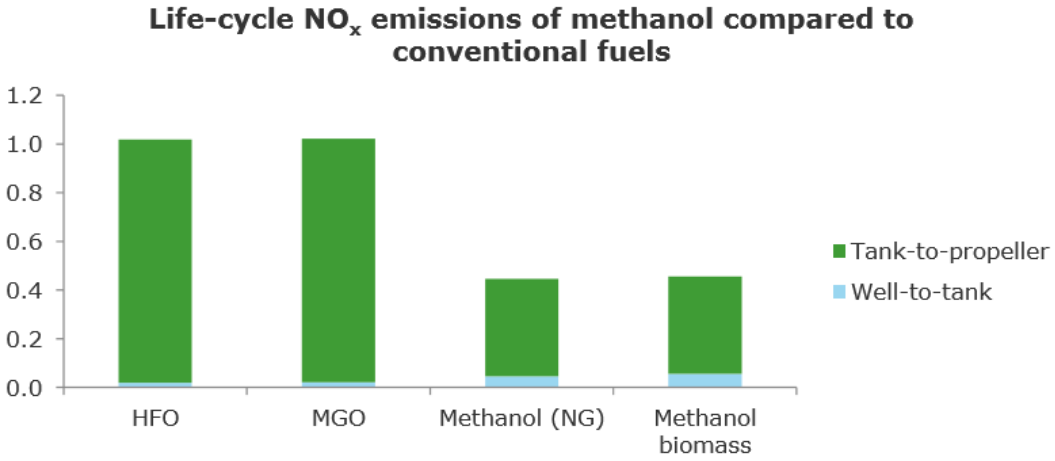

Figure 2.2: Life cycle of NO_x emissions [g/MJ] for conventional fuel compared to methanol produced from natural gas and biomass, taken from IMO [26]

to-tank emissions are related to the production and transport of the fuel until it is in the tank of a ship.

Figure 2.2 shows that the NO_x emissions of methanol combustion are lower compared to conventional diesel oils. Figure 2.3 shows a decrease in SO_x emissions. However, due to the restricted rules on sulfur content in diesel oil the SO_x emissions from conventional diesel are already low. Methanol is sulfur free, which is expected to decrease the sulphur related emissions in the tank-to-propeller phase.

According to the Dutch Organisation for applied scientific research (TNO), the price of production of biomethanol is much higher compared to production from natural gas. It is however expected that companies are willing to pay for biomethanol in order to reach the emission restrictions [21]. The aim of the IMO regulations is to produce 50% less green house gases in 2050 and use 70% less fossil fuel compared to 2008 [21]. Using biomethanol, improving engine efficiency and developments in

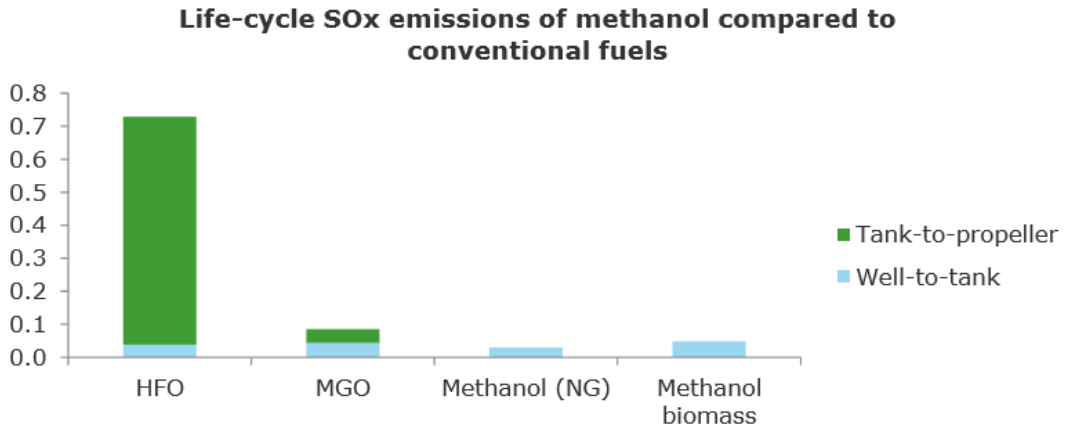

Figure 2.3: Life cycle of SO_x emissions [g/MJ] for conventional fuel compared to methanol produced from natural gas and biomass, taken from IMO [26]

production techniques offer opportunities to reach those targets.

2.3. Challenges of methanol

2.3.1. Technical readiness

Methanol as an alternative fuel for diesel requires technological attention. Methanol is known as a corrosive fluid and is not suitable for much rubbers and plastics. Current combustion systems contain materials which are not methanol proof. Long term effects are still unidentified and it is expected that the life span of existing combustion engines will decrease. MAN suggests that engines already operate in highly corrosive environments. Because of that the impact of methanol is not an issue [40]. Nevertheless, suggested is to re-design engine parts and improve materials of new systems, for instance by the use of stainless steel, to gain a long term sustainability [21]. A direct option is to use corrosion inhibitors as fuel additive. Another challenge is the low energy density compared to diesel oil. Therefore, it is expected that in the long term existing ships needs a re-design of fuel store capacity to maintain the current operation range on methanol.

2.3.2. Availability worldwide

The worldwide production capacity of methanol exceeds 100 million tons a year and is available in all major hubs globally [4]. Nowadays, most of the methanol produced is used by chemical industry. The demand of methanol increased by 2.5 times during the last 10 years whereas the production capacity increased by three times [64]. This implicates that the methanol production is sufficient to meet the demand.

Not every ship is ready to run on methanol due to technical reasons. By only replacing 5% of the total fossil fuel consumption in the Northern European Sulfur Emission Control Area (SECA) by methanol, annually 2 million ton of methanol is required. The main challenge by covering this demand is the transportation by vessel or road transport to the hubs [4].

2.3.3. Human health and environment

Methanol's toxicity is a challenge. Looking at humans health, methanol is toxic by skin exposure, inhalation or eye contact [3, 28, 64]. Exposure to methanol by humans should be avoided at any time, because high concentrations can lead to death according to the methanol safety handling plan of the Methanol Institute. To avoid people from being exposed to methanol, its fuel systems must be designed focused on safety. Moreover, the safety regulations of methanol must be known by the whole crew on

board of vehicles operating with methanol.

2.4. Methanol in internal combustion engines

Several methods exist to inject methanol in an ICE. In this chapter, three methods suitable for diesel engines are discussed. The aim of this research is to test the probabilities of methanol without adapting existing systems. Some methods require more adaptions compared to others, which are for this research less attractive to investigate.

2.4.1. Premixed Direct Injection

Not many researchers have studied premixed direct injection of methanol/diesel blends in a diesel engine. This method is the cheapest to realise for existing engines, because the normal injectors and fuel pipes are used. Before injecting the methanol and diesel blends, it must be made sure that the mixture is homogeneously mixed. Otherwise, problems with the engine could appear if for instance an injection of pure methanol takes place. One of the problems by using this method is that methanol and diesel are immiscible. It is therefore important to monitor the mixtures in the fuel tanks. Methanol/diesel blends can be premixed with an additive to improve the miscibility. Adding an emulsifier helps the mixture to stay homogeneously stable for a certain time varying from hours to days [13].

2.4.2. Port injection

Port injection is attractive in a spark ignited engine, for instance in a gas engine. Port injection means that the fuel is injected in the air inlet of the engine. These engines use a spark plug to ignite the fuel inside the cylinder. Port injection has the advantage that the fuel enters the cylinder already in vapor phase. If the air/fuel ratio is sufficient, the combustion will progresses in an efficient way after the spark. This method seems less attractive for application in a CI engine.

2.4.3. Pilot fuel

Using diesel fuel as a pilot fuel can be combined with injecting methanol into the air inlet. The diesel fuel is injected by direct injection in the engine. Compression of the trapped air in the cylinder will ignite the small amount of pilot fuel. This reaction ignites the methanol vapor and air mixture. However, it is necessary to built a new injection system in the air inlet which could be difficult in some existing applications. Furthermore, the high heat of vaporization of methanol requires an evaluation of the air inlet temperature. Moreover, a fuel control system is needed to regulate the methanol injection. Another disadvantage is that safety measures has to been taken. For instance, flame arresters has to be installed in the air inlet and a new fuel injection control system is needed. This method seems to require high investment costs for new parts and research into engine capabilities for normally direct injection CI engines.

2.5. Methanol-diesel blend properties

Because methanol has poor auto-ignition properties, which can be seen in table 2.1, CI engines can not run on pure methanol. However, diesel fuel can act as a pilot fuel as described in section 2.4.1 to ignite methanol. In this chapter, properties of methanol-diesel blends are described based on theoretical fuel properties. Engine properties are based on the MAN4L20/27 diesel engine located at the Royal Netherlands Naval College. Moreover, a theoretical study on the combustion characteristics of methanol-diesel blends is discussed.

2.5.1. Energy based blends

The search for an alternative fuel in a diesel engine can be carried out in various ways. This research will focus on methanol-diesel blends based on energy replacement. Replacing an amount of energy from diesel fuel by methanol has effect on the liquid properties. This section discusses the change of

fuel properties for methanol-diesel blends compared to diesel fuel. For the property calculations, it is assumed that methanol and diesel are miscible. However, referred to section 2.5.2 this is not realistic.

The effect of methanol added to diesel fuel is investigated by adapting the methanol-diesel ratio of the fuel. Due to the bad ignition properties and the unknown engine behaviour of methanol, the blends will start at a low methanol-diesel ratio. After the first measurements, the amount of methanol is increased until engine knocking appears. Engine knocking is when the engine starts to show heavy fluctuations in the pressure signal. Eventually, it will damage the engine. Chapter 4 contains more information about the measurements with methanol/diesel blends. For the fuel blends, different abbreviations are used in this report. For clarity, these are explained here: D100 is 100% diesel fuel (F76) and M5 means that 5% from the total energy of diesel in the mixture is replaced by methanol.

As mentioned earlier, different mixture ratios will be injected to investigate the effect of adding an alcohol fuel. Replacing diesel fuel for methanol while the total amount of energy injected must be constant, results in an increased fuel flow into the cylinder. If the fuel flow can not be adapted sufficiently, the engine will not reach its nominal power.

Fuel parameters change when blending diesel fuel with methanol. Most significant changes appear in the density, heat of evaporation, viscosity, oxygen content and stoichiometric air to fuel ratio (AFR). Blend properties for different ratios are shown in table 2.2. The mass fraction of methanol is calculated based on the LHV of a kilogram diesel fuel. A percentage of the total energy is replaced by methanol, which is calculated by eq. (2.1).

$$\mathrm{LHV_{MD}} = x_\mathrm{D} \cdot \mathrm{LHV_D} + x_\mathrm{M} \cdot \mathrm{LHV_M} \tag{2.1}$$

In eq. (2.1), $\mathrm{LHV_D}$ and $\mathrm{LHV_M}$ are lower heating values of diesel and methanol respectively, x_D and x_M are mass fractions of diesel and methanol based on the total energy of one kilogram diesel. When replacing 5% energy of diesel by methanol, x_D is equal to the mass fraction of methanol per kilogram fuel. The mass fraction methanol is higher than 0.05 due to the decreased $\mathrm{LHV_M}$. Assuming a mixture with equal energy compared to diesel, the total mass of the mixture will be higher. The lower heating value is given per kilogram and will decrease with more methanol blended.

Density is one of the parameters in which both fuels differ. According to literature, density properties are changing linear with the blending ratio [36]. By replacing the LHV values in eq. (2.1) by the densities, the mixtures density is obtained in eq. (2.2).

$$\rho_\mathrm{MD} = \frac{x_\mathrm{D} \cdot \rho_\mathrm{D} + x_\mathrm{M} \cdot \rho_\mathrm{M}}{x_\mathrm{D} + x_\mathrm{M}} \tag{2.2}$$

The heat of vaporization of methanol increases the total heat to vaporize methanol-diesel mixtures compared to pure diesel. From the total heat available in methanol, in perspective almost 5.5% of total added energy will be lost due to evaporation losses. The evaporation heat losses of diesel fuel are relatively low. Evaporation heat thus is an important parameter to take into account while simulating combustion in a cylinder.
It is assumed that the heat of vaporization of the fuel mixture increases as a function of the methanol-diesel ratio as shown in eq. (2.3).

$$Q_\mathrm{evap,MD} = \frac{x_\mathrm{D} \cdot Q_\mathrm{evap,D} + x_\mathrm{M} \cdot Q_\mathrm{evap,M}}{x_\mathrm{D} + x_\mathrm{M}} \tag{2.3}$$

where Q_evap is the heat of vaporization given in table 2.1.

Viscosity in a diesel engine has an effect on lubrication, spray development, injection timing and pressure [34]. Methanol has bad lubrication properties and it is therefore important to see which effect it has on the viscosity of a mixture. The viscosity is however not linear related to the blending ratio. Grunnberg and Nissan developed a non-linear relation for the viscosity of alcohol-diesel blends given

in eq. (2.4) [18, 36].

$$\nu_{MD} = \frac{\exp(N_D \cdot \ln(\rho_D \nu_D) + N_M \cdot \ln(\rho_M \nu_M) + N_D \cdot N_M \cdot G_{MD})}{z_D \cdot \rho_D + z_M \cdot \rho_M} \tag{2.4}$$

$$G_{MD} = 0.11 \cdot n_M^2 - 1.242 \cdot n_M + 2.897 \tag{2.5}$$

In eq. (2.4), the mole fraction of a component is given by N, the density ρ, kinematic viscosity ν (in [cSt]), volume fraction z and G the Grunnberg-Nissan parameter which is defined in eq. (2.5). In eq. (2.5), n is the number of carbon in a molecule of the alcohol. The reliability of the Grunnberg-Nissan equation is experimental verified by Lapuerta et al. [34]. However, the viscosity of methanol-diesel blends is in practice difficult to calculate due to the immiscibility. More information about miscibility of both componenents is given in section 2.5.2.

Diesel fuel hardly contains oxygen. Adding methanol, according to its molecular structure and equation CH_3OH, automatically includes oxygen in the fuel. The oxygen content in the mixtures linearly increases with the amount of added methanol and is calculated by eq. (2.6).

$$x^f_{O,MD} = \frac{x^f_{O,M} \cdot x_M}{x_D + x_M} \tag{2.6}$$

where x^f_O is the oxygen mass fraction, x_D and x_M are the mass fractions of both fuels in a blend. Related to the oxygen content in fuel is the stoichiometric AFR (σ). Methanol already contains oxygen and therefore σ of methanol is much lower compared to diesel. In eq. (2.7), the stoichiometric AFR of diesel is given based on dry air [51].

$$\sigma_{da} = \frac{M_{da}}{y^{da}_{O_2}} \cdot \left(\frac{x^f_C}{M_C} + \frac{1}{4} \cdot \frac{x^f_H}{M_H} + \frac{x^f_S}{M_S}\right) \tag{2.7}$$

where M_{da} is the molar mass of each component. $y^{da}_{O_2}$ is the volume fraction oxygen in dry air. x^f_C, x^f_H and x^f_S representing the mass fractions of carbon, hydrogen and sulfur in the fuel.

Complete combustion of methanol requires less air due to the oxygen in its molecular structure. The chemical reaction of complete methanol combustion is shown in eq. (2.8).

$$CH_3OH + \frac{3}{2}O_2 \rightarrow CO_2 + 2H_2O \tag{2.8}$$

Nitrogen in air is in this case considered to be an inert gas and not noted in the equation. In reality, if high temperatures in the cylinder appear nitrogen oxides form which will be discussed in detail section 2.6.1. From eq. (2.8), the stoichiometric AFR of methanol is obtained by rearranging the chemical reaction to eq. (2.9).

$$\sigma_{da} = \frac{M_{da}}{y^{da}_{O_2}} \cdot \left(\frac{x^f_C}{M_C} + \frac{1}{4} \cdot \frac{x^f_H}{M_H}\right) \cdot \frac{3}{4} \tag{2.9}$$

According to table 2.1, for diesel and methanol the stoichiometric AFR is 14.47 [-] and 6.67 [-] respectively. Mixing both fuels decreases the total required air for stoichiometric combustion.

$$\sigma_{da,MD} = \frac{x_D \cdot \sigma_{da,D} + x_M \cdot \sigma_{da,M}}{x_D + x_M} \tag{2.10}$$

In eq. (2.10) is assumed that the relation of the fuel to fuel ratio is linear to the stoichiometric AFR to give an indication of the air requirement for complete combustion. Table 2.2 provides the blend properties of diesel and methanol at various ratios. An important assumption related to this values is that the fuel is completely miscible. Unfortunately, this assumption is not based on reality, see section 2.5.2 for more information.

Table 2.2: Methanol-diesel energy based blend properties

Parameter	**Unit**	D100	M5	M10	M15	M20	M25	M30
Diesel	[$\%_{energy}$]	100	95	90	85	80	75	70
Methanol	[$\%_{energy}$]	0	5	10	15	20	25	30
Density	[kgm^{-3}]	847.4	841.7	836.5	831.9	827.6	823.8	820.2
Lower heating value	[$kJkg^{-1}$]	42580	40359	38358	36546	34898	33392	32010
Heat of vaporization	[$kJkg^{-1}$]	270	354	429	497	559	616	668
Viscosity	[cSt]	3.00	2.03	1.60	1.35	1.19	1.08	1.00
Oxygen Content	[$\%_{mass}$]	0	4.98	9.46	13.52	17.22	20.59	23.69
Stoichiometric AFR	[-]	14.47	14.19	13.42	12.72	12.09	11.50	10.97

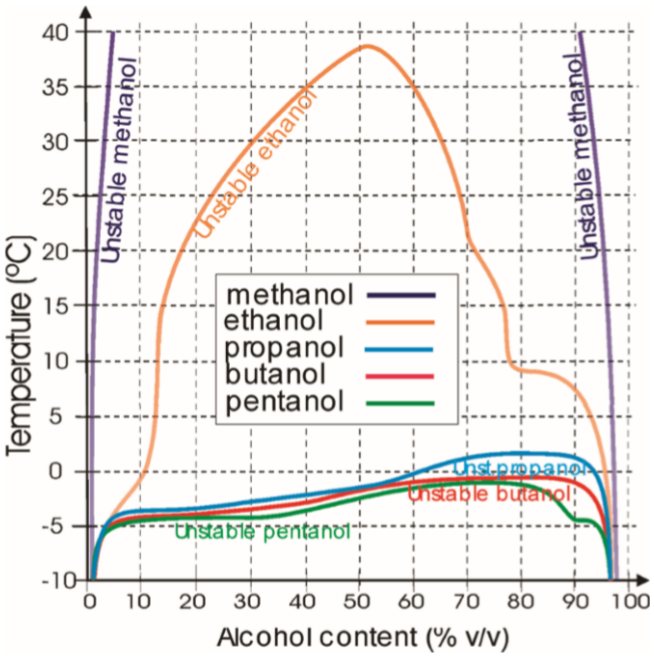

Figure 2.4: Miscibility alcohol in diesel fuel, taken from Lapuerta et al. [34]

2.5.2. Miscibility

Methanol is immiscible with diesel fuel in a wide operating range. Lapuerta et al. did experimental research to the properties of alcohol-diesel blends [34]. Figure 2.4 shows the miscibility of different alcohols from this research. Figure 2.4 shows that there is only a small range at which methanol is miscible with diesel oil at low temperature. During this research, the temperature is expected to be between 15 and 20 [°C]. The miscibility problem could be solved by using additives such as dodecanol or SPAN mixtures [1, 13].

Propanol, butanol and pentanol have only a small range of instability with diesel fuel. Diesel blends with these alcohols will require less adjustments to current diesel engine systems since fuel separation is of less importance.

2.5.3. Brake specific fuel consumption

The brake specific fuel consumption (BSFC) is defined as the burned fuel mass related to the brake power or the effective power delivered by the engine in [$g(kWh)^{-1}$] [53]. Equation (2.11) shows the equation to calculate the BSFC for an engine.

$$\text{BSFC} = \frac{\dot{m}_f}{P_b} \tag{2.11}$$

Table 2.1 describes the chemical properties of methanol and diesel fuel. When using an existing diesel engine, based on the lower heating value, it is expected that the BSFC of the engine increases as function of the methanol-diesel ratio of the fuel injected [10, 19, 49]. It is difficult to predict the fuel consumption in advance. Nevertheless, based on existing measurements with D100, an indication of fuel consumption of methanol-diesel blends can be made based on its lower heating value.

2.5.4. Air consumption

Section 2.5.1 discussed the variation of stoichiometric AFR when using fuel blends. An higher methanol volume decreases the amount of air required for stoichiometric combustion as shown in table 2.2. It is therefore expected that by using fuel mixtures, the fuel air mixture will be more lean which automatically results in a lower in cylinder temperature and a larger air excess ratio if the engine setup is unchanged.

2.5.5. Heat of vaporization

The heat vaporization of methanol is almost four times higher than that of fossil fuel oil. In a diesel engine, injected fuel is vaporized by heat transfer from the trapped air in the cylinder to the fuel droplets. Adding methanol to diesel fuel leads to an increase in heat of vaporization. For a constant pressure flow, the temperature decrease due to heat of vaporization is for methanol five times higher compared to diesel [22]. In the cylinder, the pressure is not a constant. However, the exchanged heat is not only supplied by trapped air, but also by heat transfer from the wall and pressure fluctuation. The effect of heat of vaporization is shown in the heat release analysis from Heywood in fig. 2.5 [22]. Larger

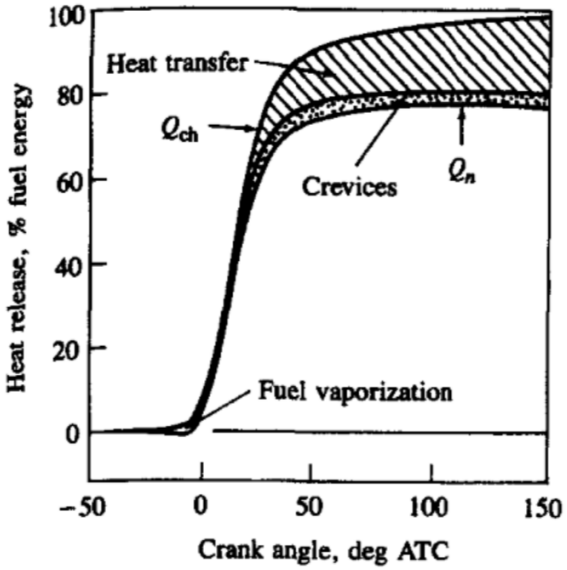

Figure 2.5: Heat release analysis, taken from Heywood [22]

heat of vaporization increases the negative part of the heat release in the engine. Therefore, injected fuel needs more time to evaporate and therefore causing a fluctuation in the peak pressure and heat release. Wei shows this phenomena in his pressure signal [61].

2.5.6. Ignition delay

Fuel does not ignite directly after injection. The time between start of injection (SOI) and the start of combustion (SOC) is defined as the ignition delay. Ignition delay of a fuel is strongly dependent on the

cetane number which is described in eqs. (2.12) and (2.13) by Semenov [22, 51].

$$\tau_{\text{id}} = A \cdot p^{-n} \cdot \exp\left(\frac{E_{\text{A}}}{R \cdot T}\right) \tag{2.12}$$

$$E_{\text{A}} = \frac{618,840}{\text{CN} + 25} \tag{2.13}$$

where τ_{id} is the ignition delay in crank angle, E_{A} the activation energy for the fuel auto-ignition, R is the universal gas constant and T the temperature. A and n are described as fuel dependent constants [22]. For diesel fuel according to Wolfer, n is considered to be 1.19 and A is equal to 0.44 [51].

The ignition delay is dependent on the activation energy of a fuel, which is described in eq. (2.13). CN is the cetane number of the fuel. From heat release analysis, the ignition delay can be obtained by studying the difference between the injection point and the crank angle where the heat release rate crosses the zero line from the negative side.

2.5.7. Combustion duration

Combustion duration is the time that fuel inside a cylinder actually burns. The combustion time is influenced by different parameters and is fuel dependent. For instance, Merker described the laminar and turbulent flame speed of methanol and diesel fuel with a mathematical description: the height of turbulence level in a cylinder influences the flame speed. More details about these parameters can be found in the work of Merker [42]. According to Verhelst, methanol has a high flame speed compared to gasoline [58]. Wei investigated the effect of methanol by port injection and published a report showing that the combustion duration in the cylinder decreased with a larger amount of methanol added [61].

2.5.8. Heat release rate

The heat release rate gives the rate of heat released by fuel due to combustion. Methanol-diesel blends will show different heat release rates at equal engine operation levels. Due to the longer evaporation time of methanol, as described in section 2.5.5, diesel fuel is expected to ignite first. As a result of diesel combustion, methanol will continue to vaporize before it finally starts to burn. This phenomena is expected to be visible in the heat release rate.

Heat release can be divided in multiple combustion phases. First, the premixed combustion is typical the largest peak in the heat release rate for diesel fuel. Second, the diffusive heat release follows in which the resulting fuel burns while the piston is moving away from TDC. During diffusive combustion, late combustion is defined. For diesel fuel, the heat release rate and its different combustion phases are shown in fig. 2.6 [51].

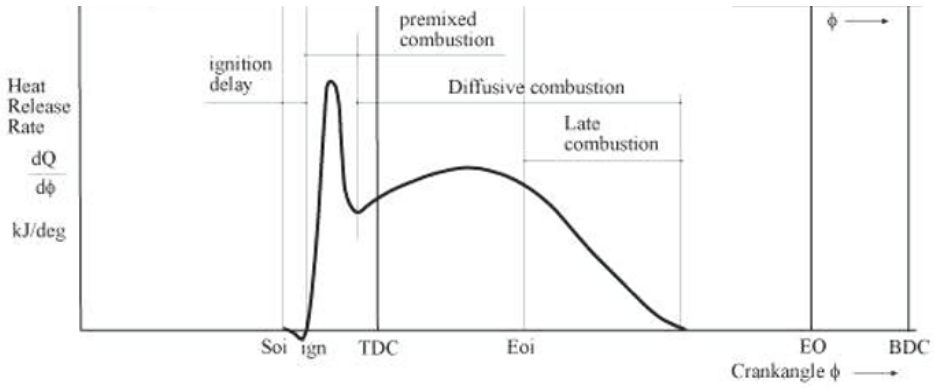

Figure 2.6: Heat release rate for diesel fuel and its combustion phases, taken from Stapersma [51]

Premixed combustion during diesel fuel operation is dominant. While running on methanol-diesel blends, this peak is expected to be lower. Less diesel is injected and methanol has to evaporate first

before it is able to ignite. By adding more methanol, the effect of methanol has to be more visible in the heat release. Wei has shown that by adding more methanol to the cylinder, the larger the dip in the heat release of premixed combustion appears [61]. However, he used premixed port injected methanol diesel operation which is different from direct injection. According to literature, Jamrozik et al. showed that the premixed combustion increased and the diffusive combustion decreased by increased methanol ratio [29]. The effect by direct injected blends has not widely been investigated yet.

2.5.9. Spray angle

The spray angle is dependent on the injector geometry, injection and cylinder pressure and fuel viscosity. Methanol differs from diesel and therefore the spray angle of these blends will be different compared to D100 operation. Yanfeng et al. investigated the spray angle of methanol and diesel and showed that the spray angle of methanol is larger compared to diesel [17]. The consequence of a larger spray angle is that there exists a higher risk of wall and piston head impingement of the fuel causing a reduction in combustion efficiency and a possible increase of the formation of toxic aldehydes, which is not desirable.

2.6. Emissions

This section discusses the effect of methanol-diesel blends on exhaust gas emissions based on previous research results and chemical structure.

2.6.1. NO_x and SO_x emissions

NO_x emissions are very important in today's discussions regarding harmful exhaust gas emissions for ships. Reducing these harmful emissions is one of the biggest challenges for the development diesel engines. The main important parameters for NO_x formation are the high temperatures combined with a long residence time in the cylinder. Moreover, oxygen content and pressure in the cylinder contribute to NO_x formation. Figure 2.7 shows the different parameters which are important to the formation of the main important particle in NO_x emissions.

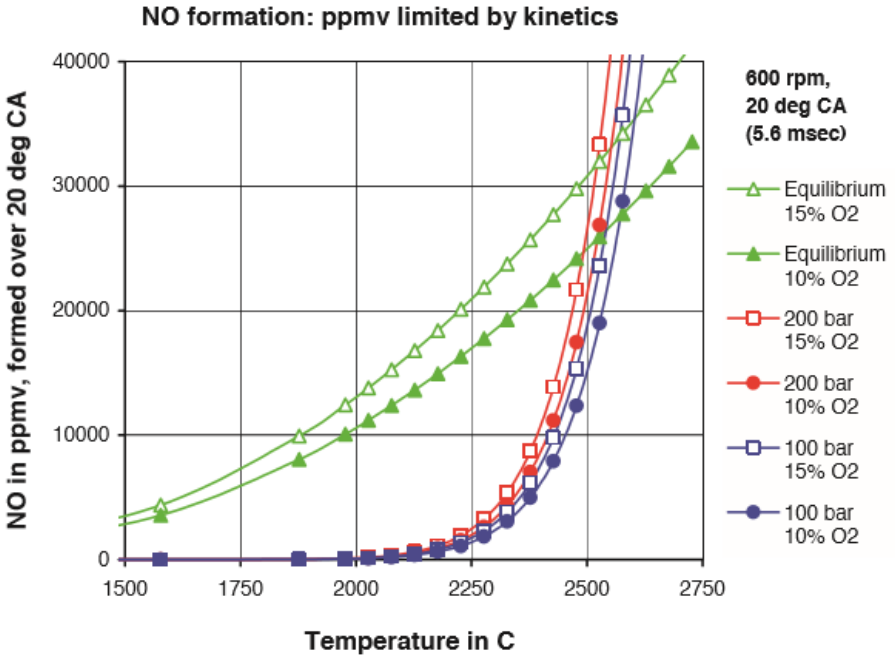

Figure 2.7: NO formation in a diesel engine based on different parameters, taken from Stapersma [52]

NO_x is a group of different nitrogen-oxide groups which are formed during different combustion equilibrium reactions. The main important particles are NO, NO_2 and N_2O. Zeldovich described the formation of NO with three equilibrium reactions described as the Zeldovich mechanism, shown in eqs. (2.14) to (2.16).

$$O + N_2 \Leftrightarrow NO + N \tag{2.14}$$
$$N + O_2 \Leftrightarrow NO + O \tag{2.15}$$
$$N + OH \Leftrightarrow NO + H \tag{2.16}$$

NO is the most significant part of the total NO_x emissions, followed by 5-10% NO_2. N_2O is only 1% of the NO_x formed in the diesel engine [52]. NO_2 formation is described by eqs. (2.17) and (2.18).

$$NO + HO_2 \rightarrow NO_2 + OH \tag{2.17}$$
$$NO_2 + O \rightarrow NO + O_2 \tag{2.18}$$

Under normal in-cylinder conditions, NO_2 is converted to NO. According to Heywood, low-temperature fluid mixtures could stop eq. (2.18) which could increase the concentration of NO_2 in the exhaust gases [22].

Previous research of Song et al. looked into the effect of oxygenated fuel blended with diesel. He observed that the NO_x emissions increased despite the higher heat of vaporization and low cetane number. He argued that the oxygen in the fuel increased the maximum in-cylinder temperature and therefore the NO_x emissions [50]. Moreover, Sayin et al. investigated the effect of various methanol-diesel blends. Their conclusion regarding the effect on NOx emissons was in line with Song et al.: a larger amount of methanol leads to higher temperatures in the cylinder and thus contributes to NO_x formation. The oxygen content thus has a larger impact on the combustion compared to the cooling effect of the heat of vaporization and cetane number [49]. Blending methanol with diesel fuel is also done by Berber [7]. The result here was that the NO_x formation again increased up to 17% running on M15 (volume based) due to higher in-cylinder temperatures.

SO_x is a fuel dependent emission and contains two species: sulphur tri-oxide and sulphur di-oxide. Although in diesel fuel the amount of sulphur is already very low as can be seen in table 2.1, the emissions are mentioned. Methanol does not contain any sulphur, which automatically means that it is expected that these emissions will reduce by replacing diesel for methanol.

2.6.2. CO and CO_2 emissions

Formation of carbon monoxide (CO) and carbon di-oxide (CO_2) is dependent on the carbon molecules in fuel and on the combustion process. If CO is measured in the exhaust gas, incomplete combustion took place [52]. In the chemical process, this means that the equilibrium reaction stops forming CO_2 due to an insufficient amount of hydroxyl (OH) particles as shown in eq. (2.19).

$$CO + OH \Leftrightarrow CO_2 + H \tag{2.19}$$

The amount of C injected in an engine can be measured by fuel consumption measurements combined with the chemical composition of a fuel. If the combustion efficiency of an engine is 100%, all C molecules will be deformed to CO_2 and no CO will appear in the exhaust gases because both of the components are balanced [52]. Sayin et al. observed a decrease in CO emissions with an increasing amount of methanol. Reduction of CO is related to the oxygen content in methanol which causes more complete combustion [49].

As already expected, Berber measured a reduction in CO_2 and CO emissions due to the lower C content in methanol. CO reduction is related to the extra O_2 from methanol used in the combustion process leading to higher exhaust gas temperatures and more complete combustion [7].

2.6.3. O_2 emissions

Diesel does not contain oxygen in its molecular structure and uses oxygen from air for combustion. The stoichiometric air/fuel ratio, as explained in eq. (2.7) gives the amount of air needed for complete combustion. In practise, the diesel engine has an air excess ratio of around 2.5 [-]. This indicates that more 2.5 times more air is injected then necessary for stoichiometric combustion. This gives a cooling effect and results in a lower in-cylinder temperature and less formation of harmful emissions such as NO_x. Since methanol already contains oxygen, this will compete in the combustion process. Therefore, the required stoichiometric air/fuel ratio of methanol and its blends in eq. (2.9) is much lower compared to diesel.

Methanol-diesel mixtures are expected to use less air due to methanol's oxygen content as shown in table 2.2. The O_2 emissions are an important indication to evaluate the relationship between the combustion process and the theoretical required air for complete combustion.

2.6.4. Unburned hydrocarbons

Hydrocarbons in the exhaust gases are the result of incomplete combustion. After fuel injection, fuel mixes with air due to air entrainment and spray penetration. If the air/fuel mixture in the cylinder is not ideally, rich and lean zones appear. Lean zones contain more air than the stoichiometric ratio and too much air could result in non-ignitable overlean air/fuel mixtures. In the fuel spray centre, the mixture can appear to be overrich which means there is too much fuel to form an stoichiometric fuel air mixture. In this way, the combustion appears to be inefficient in particular zones in the cylinder resulting in unburned hydrocarbons.

Unburned hydrocarbons concentration depends on the fuel used. At high temperatures, methanol forms aldehydes, which are toxic for human beings. If methanol is not burned in the cylinder, aldehydes appear in the exhaust gases. However, the unburned hydrocarbon concentration in the exhaust gas flow should be low, because the combustion efficiency of diesel engines usually is 99% [22, 52]. Expected is that the effect of methanol addition must be measurable in the exhaust gases.

2.7. Discussion and expectation

Previous chapter provided information about diesel engine operation with methanol/diesel blends. Based on the chemical properties of methanol it is expected that fuel consumption increases when more methanol is mixed with diesel. Moreover, for long term methanol operation, low viscosity appears to be a problem for oil lubricated high pressure fuel pumps. From the heat of vaporization, which increases significantly with the rate of methanol, the expectation is that this will lead to an increased ignition delay and a period of lower temperatures in the cylinder. Moreover, less air is required for stoichiometric combustion of methanol. Lean combustion is a risk without adapting the turbine to the fuel's air consumption.

Emissions are expected to change. On beforehand, literature concluded an increase in NO_x emissions while other show a significant reduction. It is mentioned that the amount of carbon dioxide is strongly dependent on the fuel's carbon content. Fuel consumption is expected to increase significantly which makes it questionable whether the CO_2 emissions will decrease. Methanol contains oxygen and has a low stoichiometric air to fuel ratio. Expected is that the blends will use less air compared to diesel fuel. Finally, sulphur dioxide and unburned hydrocarbons are considered. Methanol does not contain sulphur dioxide implicating a decrease of the already low sulphur dioxide emissions from F76. Incomplete combustion results among other things in unburned hydrocarbons. The cooling effect of methanol gives the expectation that combustion will be less complete compared to diesel fuel operation and also an increase in unburned hydrocarbons is expected.

3

Modelling of combustion in a dual fuel engine

3.1. Overview

Several models are available to simulate combustion in compression ignited engine cylinders. When modelling combustion, it is important to know how the model calculates its properties and how accurate these calculations are. A model's complexity increases depending on the requirements of the accuracy and points of interest. A more detailed model predicts a more accurate envelope of combustion on different locations in the cylinder.

Insight in various variants of heat release and in cylinder models is important when working with one of them. Therefore, there is an overview of different in-cylinder models discussed in this chapter. After that, the model used in this thesis is broadly explained by its thermodynamics and sub models. Furthermore, some alternative sub models are mentioned to get an insight in the different possibilities with combustion simulations.

A diesel cycle contains a compression, expansion, outlet and inlet stroke for a four-stroke engine. While studying heat release measurements, the in- and outlet stroke are of less interest thermodynamic wise. Optimizing the thermodynamic process during compression and expansion is the aim of such a model. Therefore, the models discussed in this chapter only calculate the process from inlet valve closes (IC) until exhaust valve opens (EO).

3.1.1. Single zone model

According to Stapersma [51], heat release analysis can be done using a single zone model which uses a correlated crank angle and pressure signal as input parameters. The combustion inside the cylinder is considered to take place in a single volume with no distinct difference between the unburned fuel and air zone [12, 37]. In reality, the cylinder usually contains many different zones during combustion. Therefore, the output of a single zone approach is evaluated as a mean value of the complete cylinder volume. Moreover, any detailed information of the combustion is generated using this model. However, the single zone approach gives a decent estimate of what happens in the cylinder and gives an implication of the thermodynamic process during combustion.

An important assumption when using this model is that the fuel injected directly evaporates. The evaporated fuel is immediately assumed to be burned and is therefore automatically equal to the combustion rate. This implicates that all fuel injected is burned. Another assumption is that the mass inside the cylinder is constant except for the fuel injection rate. However, in reality fuel leakage may occur which causes a decrease of the total in-cylinder mass. This is however often neglected [51].

3.1.2. Dual fuel single zone model

As mentioned in chapter 3.1.1, previous research into the combustion of dual fuel in internal combustion engines has been done by Lee using a single-zone model [37]. He improved the diesel model by adding chemical properties of methanol for dual fuel operation. One assumption he made was that methanol enters the cylinder in vapor phase using premixed port injection. Diesel fuel was used as a pilot fuel to ignite the premixed methanol-air mixture.

3.1.3. Double zone model

A more complicated approach of heat release modeling is by using a double zone model. The main assumption is that the cylinder consists of two different zones and an undefined flame front. A double zone model is more realistic regarding the real combustion process compared to the single zone model and gives the possibility to predict exhaust gas composition in more detail. Linden used a two-zone in cylinder simulation model to predict NO emissions in a diesel engine. He made use of the Hohlbaum approach and included gas properties by means of equations of state to the model [38]. However, is was proven that it is difficult to get reliable results using such a complex model and more investigation to in cylinder flow profiles was recommended by the author.

In order to reach higher accuracy of two zone models combined with a suitable calculation speed, a quasi-dimensional model is introduced [58]. Multi-dimensional models have a multiple number of zones in the cylinder and solve the mass- and energy balances for each zone. The cylinder is considered to be infinitesimal among the z-axis, while one layer of the cylinder represents the whole volume. Sub-models are needed to get a detailed description of different phenomenon regarding combustion in a cylinder. These phenomena are for instance turbulence kinetic, internal droplet mixing, wall impingement or break up models, to increase accuracy of the calculations.

3.1.4. Package models

When in-dept information of in-cylinder combustion is desired, package models are available to increase model accuracy. In this section, some information about available package models is described.

After the single zone approach described in chapter 3.1.1, higher level models can be reached by extending the cylinder into multiple zones: the unburned and burned zones. Each zone is an open thermodynamic system in which the heat and mass can exchange. Important assumptions in this approach are the homogeneity of temperature and gas composition in each zone. Moreover, the pressure is assumed to be equal in every zone [56].

Multi-zone modelling in principle is described with any number of zones preferred. The method however does not take geometry effects of the cylinder into account. Fuel spray by direct injection is affected by cylinder geometry and injector design. Taritas and Rakopoulos designed extended multi-zone quasi-dimensional models in which the fuel spray is modelled in detail [47, 56]. Taritas included combustion chamber geometries, injector data, deflection of the chamber walls, spray zone position, flame propagation and interaction between flame and cylinder walls. The quasi-dimensional approach is combined with in-cylinder turbulence kinetics, modelling of spray processes and exhaust gas emission calculations. A widely applied combustion spray model is developed by Hiroyasu, from which also NO emissions predictions can be derived from [23]. Depending on the number of zones defined, the time consumption of quasi-dimensional models increases significantly [46].

The multi-zone model makes it possible to take temperature and chemical component fluctuations in the cylinder into account. To improve combustion rate analysis accuracy, turbulence and spray models could be used.

3.2. Simulation model by Lee

A single zone model is able to predict the overall combustion process based on average properties. Details during combustion, for instance flame fronts, emission formation or hot spots can not be simulated

by using single zone models. However, this project marks the start in a broader research spectrum regarding methanol-diesel combustion. The research target is to find out whether the engine is able to run on methanol-diesel blends and which overall differences can be observed compared to D100. For reaching this targets, measurements have to be done. The single zone model approach is able to give the in-cylinder information. Combined with real engine performance and emission measurements a general indication of methanol-diesel combustion can be provided. When the general working principles of the model are tested and verified, model improvements to go in to further detail are to be covered in future research. Furthermore, when modelling the combustion process in a diesel engine there is always a trade off between calculation speed and accuracy. Single zone modeling offers a compromise between both of them. Due to general thermodynamic assumptions the accuracy of the single zone approach decreases. However, the calculation speed makes it more attractive compared to time consuming multi zone models.

3.2.1. Model features

This section describes the fundamentals of the single zone model of Ding Yu including the adaptation of Buyongjoo Lee [12, 37].

The single zone model consists of two sub-models presented in figs. 3.1 and 3.2. Heat release

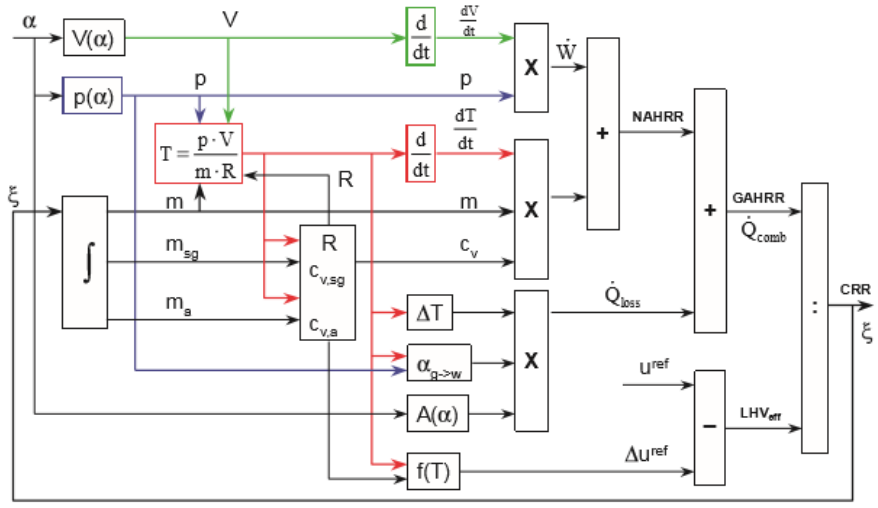

Figure 3.1: Heat release model based on pressure and crank angle input from measurements, taken from Stapersma [51]

calculations based on the model shown in fig. 3.1 are based on a correlated pressure and crank angle. By implementing the engines geometry, ideal gas law and the first law of thermodynamics, the combustion reaction rate (CRR) is calculated. The CRR is used as the input for the in-cylinder model in fig. 3.2. The integrated CRR, which is the reaction coordinate (RCO), is fitted by multiple Vibe functions to reproduce the temperature and pressure signal. The output from the in-cylinder model can for instance be deployed to determine seiliger parameters of a diesel cycle [12]. In-dept details of the heat release model in fig. 3.1 are described later in this chapter. The in-cylinder part of the model is not implemented during this research.

3.2.2. Assumptions

Several assumptions were made about the single zone model. The assumptions are simplifications of reality to make the calculation process faster while maintaining an appropriate accuracy. First the assumptions regarding losses during combustion are mentioned followed by general assumptions of

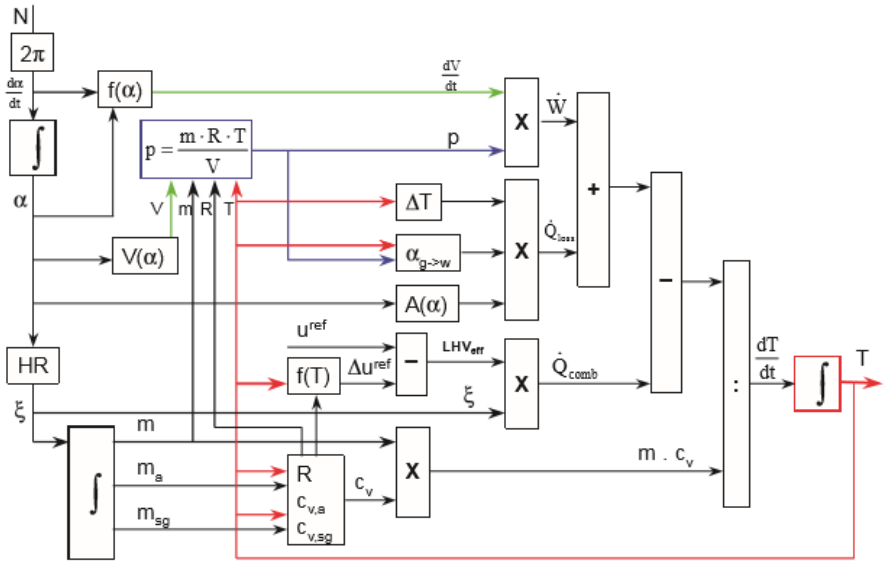

Figure 3.2: In-cylinder model based on combustion ratio from the heat release model, taken from Stapersma [51]

the model. Finally, constant inputs are mentioned.

- Losses
  - Fuel leakages between piston rings and the cylinder wall is neglected
  - Combustion efficiency is 100%
  - Heat losses only transferred to cylinder wall, cover and piston head
- Model calculations
  - Gas properties are a function of temperature (ideal gas law)
- Inputs
  - Atmospheric conditions are equal at any time
  - Inlet receiver temperature is constant
  - Fuel injection temperature is constant
  - Cylinder wall, cover and piston head temperatures are constant

The main assumption for the combustion process is noted in eq. (3.1).

$$\dot{m}_{\text{inj}} = \dot{m}_{\text{evap}} = \dot{m}_{\text{comb}} \tag{3.1}$$

For methanol/diesel blends, eq. (3.1) is expected to be invalid since the plausible ignition delay caused by methanol makes the assumption of equal injected, evaporated and burned mass rates in time questionable. Section 3.5 explains more about the validity of this assumption.

3.2.3. Engine geometry

Combustion in a CI engine is related to the geometry of the engine. Heat release parameters can be calculated based on pressure and crank angle measurements. The position of the crank is directly related to the in-cylinder volume. Important parameters of the engine geometry are shown in table 4.1. Based on the crank angle, the cylinder's change in volume is calculated at any position as shown in eq. (3.2) [51].

$$\frac{dV}{d\phi} = \frac{\pi}{360} \cdot V_S \cdot \left(\sin(\alpha) + \lambda_{CR} \cdot \left(\frac{\sin(\alpha) \cdot \cos(\alpha)}{\sqrt{1 - \lambda_{CR}^2 \cdot \sin^2(\alpha)}} \right) \right) \tag{3.2}$$

where V_S is the cylinder stroke volume, ϕ the crank angle and λ_{CR} the crank/rod ratio. During simulations the volume changes constantly dependent on the crank position.
With the help of the bore (D_B) and stroke length (L_S) the cylinder volume is determined. These parameters are fixed and are obtained from the engine manufacturer data sheets.

3.2.4. Ideal gas law

To calculate the state parameters in the model, the ideal gas law is applied. The ideal gas law implies that the state parameters of air and stoichiometric gases in the cylinder satisfy the equations of state of eq. (3.3) [24].

$$p(\alpha) \cdot V(\alpha) = m \cdot R \cdot T(\alpha) \tag{3.3}$$

where p is the pressure, V cylinder volume, m the mass of the gases, R the universal gas constant and T the temperature. The gases are considered to be semi-perfect implicating that the heat capacity is a function of the temperature.

3.2.5. Mass balance

Single zone in-cylinder models describe the combustion between IC and EO. Theoretically, this means that the trapped mass is constant during this process. However, fuel injection is the parameter which changes the mass during the closed cylinder process. Fuel leakage over the piston rings and incomplete evaporation is not taken into account. The total change of mass inside the cylinder can be obtained by integrating the mass balance given in eq. (3.4) [12, 37, 51].

$$\frac{\mathrm{d}m_{cyl}}{\mathrm{dt}} = \frac{\mathrm{d}m_f}{\mathrm{dt}} \tag{3.4}$$

where m_{cyl} is the total mass in the cylinder and m_f the mass of fuel injected. Current single zone models assume that the injected fuel is evaporated immediately followed by combustion. Therefore, the combustion, evaporation and injection rate are equal resulting in eq. (3.5).

$$\frac{\mathrm{d}m_{cyl}}{\mathrm{dt}} = \xi \tag{3.5}$$

where ξ is the fuel combustion rate. The total mass in the cylinder finally contains air, stoichiometric gas and fuel. During simulation, no air or gas leaves the cylinder. The only reason why heat release in the cylinder takes place is due to the injected fuel under influence of increasing pressure in the cylinder. Heat release calculations are derived from the energy balance as discussed in section 3.2.6.

The total mass balance in the dual fuel single zone model is described in two different parts. One side describes the combustion reaction of methanol, the other the reaction of diesel fuel. In the end, both fuels are added to the mass balance, which is equal to the total mass in the cylinder in time. The total mass in the cylinder is given in eq. (3.6).

$$m = m_f + m_a + m_{sg} \tag{3.6}$$

The total burned mass of each fuel is calculated separately. Each fuel has its own stoichiometric air to fuel ratio and own air consumption. From the engines parameters and known temperature and pressures at IC, the trapped mass in the cylinder is calculated. Therefore, the model is able to calculate the air excess ratio. The air excess ratio is usually known by the results of measurements. This parameter combined with the fuel consumption of the engine could be used for verification of the calculations.

The total mass in the cylinder does not change except for fuel injection as discussed earlier. Equation (3.6) contains the total mass in the cylinder including air, stoichiometric gas and resulting fuel. During combustion, the mass of each component changes. Those functions are described in eqs. (3.7) to (3.9). The amount of fuel changes with the combustion ratio in eq. (3.5).

$$m = m_1 + \int_{t_1}^{t} \xi \cdot \mathrm{dt} \tag{3.7}$$

$$\frac{\mathrm{d}m_a}{\mathrm{dt}} = -\sigma \cdot \xi \tag{3.8}$$

$$\frac{\mathrm{d}m_{sg}}{\mathrm{dt}} = (1+\sigma) \cdot \xi \tag{3.9}$$

where m_1 is the trapped mass at IC calculated by the ideal gas law. Equations (3.7) to (3.9) are calculated separately for methanol and diesel. The total mass in the cylinder is therefore the sum of the mass equation of both fuels. It is assumed that combustion and air consumption are reacting according to the stoichiometric air to fuel ratio (σ). Air and fuel used for combustion is transformed to stoichiometric gas. In the end, both fuel and required air is transformed to stoichiometric gas. It is assumed that only excess air and stoichiometric gas are in the cylinder at the end of the closed cylinder process. Moreover, the cylinder contains 0.1% of stoichiometric gas which was left behind from the previous cycle. All equations used in the mass balance are described in [12, 51].

3.2.6. Energy balance

Single zone in-cylinder modelling is based on energy conservation by the first law of thermodynamics. All energy in the system is constant and can not be produced or get lost. The total energy in the cylinder is divided in three components: indicated work, combustion heat and heat losses The sum of those three components is described as the total energy change of the system as described by Stapersma and Ding [12, 51]. Indicated work is described in eq. (3.10).

$$\dot{W} = p \cdot \frac{\mathrm{d}V}{\mathrm{d}t} \tag{3.10}$$

where p is pressure and $\frac{\mathrm{d}V}{\mathrm{d}t}$ the change of volume in time. Furthermore, the combustion heat is described as the temperature and time dependent heat input by fuel in eq. (3.11).

$$\dot{Q}_{\mathrm{comb}} = \left(u^{\mathrm{ref}}_{\mathrm{comb}} - \Delta u^{\mathrm{ref}}_{\mathrm{comb}}\right) \cdot \xi \tag{3.11}$$

where $u^{\mathrm{ref}}_{\mathrm{comb}}$ is the internal energy reference value. The combustion heat is dependent on temperature and since temperature is not a constant, the reference value is corrected by the temperature dependent correction factor $\Delta u^{\mathrm{ref}}_{\mathrm{comb}}$ [51]. ξ is the combustion rate as described in eq. (3.5).

The third term associated in the first law of thermodynamics, $\dot{Q}_{\mathrm{loss}}$, are the heat losses to cylinder wall, cylinder head and piston crown. Moreover, evaporation losses after injection are considered as a heat loss too. The heat losses to the cylinder parts are described using Woschni's heat transfer theory dependent on crank angle, temperature, pressure and among others engine speed [62]. Section 3.2.7 gives an in dept analysis of Woschni's heat transfer coefficient. The total change of internal energy is the sum of the indicated work, heat of combustion and the heat losses in eq. (3.12) [12, 51].

$$m \cdot c_v \cdot \frac{\mathrm{d}T}{\mathrm{d}t} = \dot{Q}_{\mathrm{comb}} - \dot{Q}_{\mathrm{loss}} - p \cdot \frac{\mathrm{d}V}{\mathrm{d}t} \tag{3.12}$$

where the left hand side of eq. (3.12) is the total change of internal energy. Equation (3.12) is written as one equation which consists of multiple definitions. First the nett apparent heat release rate ($NAHRR$) is defined in eq. (3.13), the net heat released by temperature and volume changes in the cylinder [51].

$$NAHRR = \dot{Q}_{\mathrm{comb}} - \dot{Q}_{\mathrm{loss}} = m \cdot c_v \cdot \frac{\mathrm{d}T}{\mathrm{d}t} + p \cdot \frac{\mathrm{d}V}{\mathrm{d}t} \tag{3.13}$$

Equation (3.13) ignores the heat losses in the cylinder and therefore a second definition is defined by the gross apparent heat release rate ($GAHRR$). This term, given in eq. (3.14), includes heat losses

to the walls. Heat losses are difficult to measure and often for diesel engine measurements, these losses are calculated using Woschni.

$$GAHRR = \dot{Q}_{\text{comb}} = m \cdot c_{\text{v}} \cdot \frac{\mathrm{d}T}{\mathrm{d}t} + p \cdot \frac{\mathrm{d}V}{\mathrm{d}t} + \dot{Q}_{\text{loss}} \tag{3.14}$$

Now the gross apparent heat release rate is obtained, the combustion reaction rate (CRR) is defined combined with eq. (3.11).

$$CRR = \frac{m \cdot c_{\text{v}} \cdot \frac{\mathrm{d}T}{\mathrm{d}t} + p \cdot \frac{\mathrm{d}V}{\mathrm{d}t} + \dot{Q}_{\text{loss}}}{u^{\text{ref}}_{\text{comb}} - \Delta u^{\text{ref}}_{\text{comb}}} = \xi \tag{3.15}$$

The CRR is important while modelling the in cylinder process, based on this parameter the fuel injection rate is calculated. Integration of eq. (3.15) results in the reaction coordinate (RCO), the end value of the RCO should be unity implying complete combustion of the fuel injected.

Lee added methanol properties to the single zone model from Ding [37]. Methanol's heat of vaporization is not taken into account in this model. Based on data from the paper of Wei et al., several methanol/diesel ratios are investigated [61]. The gross apparent heat release of both fuels is calculated using eq. (3.16), where he divided the total energy injected by the methanol/diesel ratio to obtain the heat release per fuel component.

$$GAHRR_{\text{MD}} = (1 - X_{\text{g}}) \cdot GAHRR_{\text{diesel}} + X_{\text{g}} \cdot GAHRR_{\text{methanol}} \tag{3.16}$$

where X_{g} refers to the amount of energy stored in methanol in the gas phase. The variable is copied from Lee where methanol was assumed to enter the cylinder in the gas phase. The part of total energy injected per fuel defines the height of X_{g} varying between zero and one.

During simulations, the heat release benchmark from D100 is used to represent the diesel combustion. Based on this value, the percentages of energies are used to obtain the heat releases for the methanol and diesel dual fuel operation. Unfortunately, the method described above implies that the start of combustion of methanol and diesel is at the same point. Apart from the fact that separate heat release is not easy to measure, it is not expected that this is what actually happens in the cylinder. Diesel acts as pilot fuel and ignites first resulting in the combustion of methanol. Moreover, heat of vaporization is not taken into account which could be considered as an important parameter causing ignition delay and cylinder cooling. However, it is difficult to model fuels with different combustion duration since it is not measurable. Diesel fuel is expected to ignite first, while the resulting liquid particles of methanol finish evaporation before participation in the combustion.

Each heat release analysis is based on a pressure signal obtained by experiments. The method to split the heat release rate based on energy fractions per fuel is necessary to work with this model. Lee used the D100 signal for each simulation with methanol as his reference heat release. Each methanol/diesel blend was based on the diesel fuel heat release rate. By multiplying the heat release from diesel fuel by the methanol energy rate, he obtained the simulations of methanol operation.

The simulations obtained by the new experiments are based on the experimental pressure data on a dual fuel diesel engine. Using the D100 benchmark is not a requirement and each simulation has its own pressure signal. The heat release is still divided in diesel and methanol fuel. The difference is that it is now based on the heat release calculated from a real methanol dual fuel pressure signal. In this way, the model's performance is improved.

3.2.7. Heat losses

Heat losses to cylinder head, walls and piston crown are modelled using Woschni's heat transfer coefficient. Heat transfer depends on temperature differences, variable cylinder wall area due to reciprocating piston movement and heat transfer coefficients of gas and engines material. Woschni described the heat transfer from the in-cylinder gases to cylinder walls by convective heat transfer for the different cylinder components. Equation (3.17) describes the heat losses to several cylinder parts.

$$\dot{Q}_{\mathrm{loss}} = \sum_{\mathrm{i}=1}^{3} \left\{ \alpha_{\mathrm{g\to w,i}} \cdot \left(T - T_{\mathrm{wall,i}} \right) \cdot A_{\mathrm{wall,i}} \right\} \tag{3.17}$$

with:
$\mathrm{i} = 1$ cylinder wall
$\mathrm{i} = 2$ cylinder cover
$\mathrm{i} = 3$ piston crown

where $\alpha_{\mathrm{g\to w,i}}$ is the heat transfer coefficient from gas to wall, T the temperature and A the area of each cylinder part. During engine operation, the area of the cylinder wall and the gas temperature constantly change. According to Woschni, the wall temperature is assumed to be constant and must be an approximation between the highest and lowest temperature of the cylinder wall. Furthermore, heat transfer can be calculated at any point during a cycle.

Cylinder wall area is dependent on the position of the piston and can be calculated as a function of the crank angle using eq. (3.18). The area of the piston head and cylinder cover does not change during the cycle.

$$A_{\mathrm{wall,1}} = \pi \cdot D_{\mathrm{B}} \cdot L_{\mathrm{P}}(\phi) \tag{3.18}$$

where D_{B} is the bore diameter and $L_{\mathrm{P}}(\phi)$ the length of the cylinder wall above the piston. The equation for convective heat transfer is now defined. Woschni's definition for the heat transfer coefficient is defined in eq. (3.19). Woschni describes the heat transfer coefficient including radiation since this is assumed to be only a small part of the total heat transfer [62].

$$\alpha_{\mathrm{g\to w}} = C_1 \cdot \frac{1}{D_{\mathrm{B}}^{0.214}} \cdot \frac{p^{0.786}}{T^{0.525}} \cdot \left(C_3 \cdot c_{\mathrm{m}} + C_4 \cdot \frac{p - p_0}{p_1} \cdot \frac{V_{\mathrm{S}}}{V_1} \cdot T_1 \right)^{0.786} \tag{3.19}$$

where C_1, C_3 and C_4 are parameters described in detail in the work of Ding and Woschni [12, 62]. c_{m} is the mean piston speed and p_0 is the gas pressure in the engine without fuel injection.
Parameter C_3 depends on the swirl velocity (w_{t}) inside the cylinder, which is the phenomena that the air is moving in a spiral form inside the cylinder. Since this is difficult to measure, the ratio between swirl and mean piston speed is set as a constant between 5 and 50 dependent on the engines specifications [12].

Ding used this heat loss calculation model while simulating diesel engines running on D100. It is not proven that Woschni's equation is accurate for using other fuels such as methanol. Results for alternative fuel can be adversely affected by misplaced heat loss calculations. For methanol and diesel, Woschni parameters from literature are used and shown in table 3.1[12, 42]. These values are identical for each fuel. Since knowledge about the heat losses is limited for this engine, future research to the effect of alternative fuels on heat losses is necessary to simulate the heat losses more accurate.

Table 3.1: Woschni parameters for diesel and methanol

Parameter	Diesel	Methanol	Units
C_3	2.28+0.308 $\frac{c_c}{c_m}$	2.28+0.308 $\frac{c_c}{c_m}$	[-]
C_4	$3.24 \cdot 10^{-3}$	$3.24 \cdot 10^{-3}$	$\left[\frac{\mathrm{m}}{\mathrm{s \cdot K}}\right]$
C_1	127.93	127.93	[-]
T_{piston}	600	600	[K]
T_{wall}	400	400	[K]
$T_{\mathrm{cyl.head}}$	580	580	[K]

3.3. Uncertainties

3.3.1. Pressure signal

The pressure signal used for implementation in the model is based on a mean signal. Cycle to cycle variations are not considered in the heat release analysis, even though in reality they do exist. The mean pressure signal has lower peak pressures, because the noise is removed. Furthermore, the Kibox has its own measurement accuracy and a time delay between data capturing and the real process. These errors are structural for each measurement and are considered to be small.

3.3.2. Woschni

Woschni describes the heat losses to the piston, cylinder wall and head. Woschni's formula is used widely in many models to describe heat losses by engines running on diesel fuel with its standard parameters [12]. The effect of heat losses by using methanol in a diesel engine is not investigated and an uncertainty in the dual fuel model. Heat losses have an impact on the GAHRR and influence the reaction coordinate of the model.

3.3.3. Temperature

The temperature is strongly dependent on the cylinder volume and thus the position of the crank angle related to the pressure signal. Moreover, the temperature determines the fuel's specific energies and thus the model's results.

Based on the mean temperature provided by this model, only general indications of the temperature in the cylinder can be observed. Locally, hot spots and cool regions exist in the engine and are not taken into account. These local temperature fluctuations have impact on the formation of harmful emissions.

3.3.4. Combustion

The combustion process is difficult to measure. For methanol and diesel fuel, the combustion process is assumed to occur simultaneously. In the cylinder, there could be a difference between the real combustion process and the assumption of equal combustion times.

The residual gas which is left in the cylinder during the exhaust stroke is taken as 5 [%], which was found in literature [51]. Assumed is that the exhaust stroke almost removes all the combustion gases from the previous cycle. In reality, this number is different and not easy to measure.

3.4. Discussion on the existing model

The dual fuel single zone model from Lee will give insight in the heat release rate of dual fuel operation. The method used to simulate the dual fuel combustion is simplistic and is not verified by engine measurements and literature. To do this, complete pressure signals for dual fuel combustion are required to study the in-cylinder process in the model. Pressure signals from the measurements include the complete four stroke combustion cycle. Adding the heat of vaporization for methanol is required to simulate the combustion process for dual fuel direct injection operation compared to port injection. Experiments will give the opportunity the check whether the model calculates the thermodynamic process sufficiently.

3.5. Model improvements

The in-cylinder dual fuel model described in chapter 3 does not take evaporation heat into account and is based on port injection. Later in this report, experiments are described in which premixed fuel blends are injected by a direct injection nozzle. In order to model use the current dual fuel model for direct injection engines, the heat of vaporization of methanol must be added to the current dual fuel single zone model. By direct injection, the methanol is injected in liquid form, which was for port injection assumed to be vapor.

The heat of vaporization for methanol is calculated by different models. First of all, an injection model

built by Zeng is used to simulate the fuel injection rate into the cylinder [63]. After fuel injection, the fuel starts to evaporate which is described by a single droplet evaporation model. From the results of both described models, the heat of vaporization for the injected fuel can be calculated. Finally, this result is used to simulate the heat of vaporization of methanol in the single zone model. A detailed description of the way that the models are connected is given in section 3.5.1.

3.5.1. Model connections

The injection and evaporation model can be combined to calculate the evaporation heat of the injected fuel. The calculated heat of vaporization is used to implement the vaporization of methanol in the single zone model.

The first step in this process concerns the fuel injection. Using the injection model, the fuel injection rate is calculated. By assuming a SMD for the injected fuel droplets, the number of droplets injected per time step is known. The total heat subtracted from the cylinder to evaporate the droplet is calculated per droplet by the evaporation model. Multiplying the heat of vaporization by the number of droplet gives the total heat of vaporization per time step. The injection happens during multiple time steps, which means that the fuel spray is determined by the sum of the heat of vaporization of each time step during injection. Each time step then follows its own vaporization process based on single droplet evaporation. A first indication of the evaporation effect of methanol in the single zone model is obtained by using this method. The general process is shown schematically in fig. 3.3.

Figure 3.3 shows an additional step before implementing the evaporation heat into the single

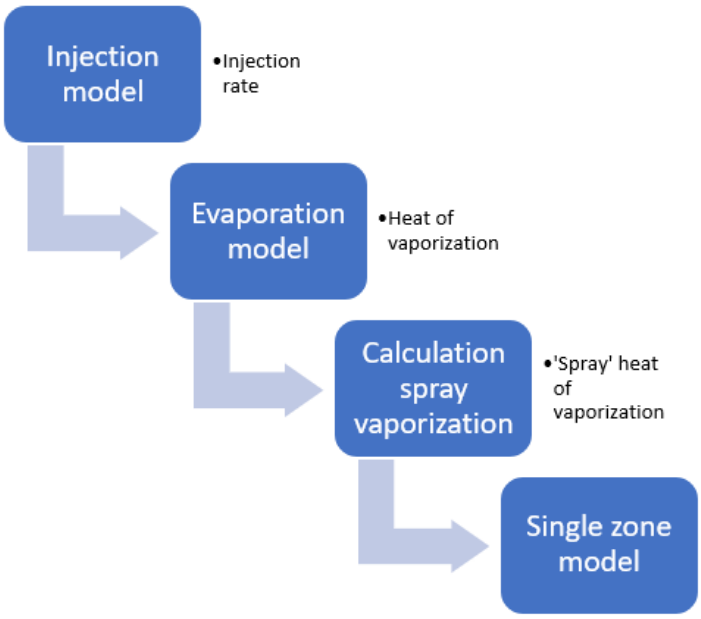

Figure 3.3: Scheme of important model connections

zone model. The main reason for this is that the time steps of the models are not identical. The evaporation process of a single droplet takes less time compared to the in cylinder process of the single zone model. Therefore, the evaporation model has a smaller time step, which must be converted to the larger time step without losing important data. Therefore, the time step is adapted after the spray signal is calculated. In that case, the signal can be represented without losing the trend of the original signal.

3.6. Injection model

The original dual fuel single zone model used in this thesis is based on port injection of methanol. It is assumed that all methanol is evaporated at IC. Port injected fuel subtracts heat from the air inlet before entering the cylinder, resulting in a lower in-cylinder temperature. Direct injection engines inject fuel in liquid phase, which needs to evaporate in the cylinder. In this project, a direct injection engine is used. More details of the engine specifications can be found in chapter 4.

Galindo mentioned that the diesel evaporation and combustion kinetics are almost reacting simultaneously [39]. The assumption that the injection, evaporation and combustion rates are equal is therefore plausible for pure diesel simulations. However, methanol's heat of vaporization contains a much larger percentage of its total combustion heat. Evaporation heat must be supplied by heat from in-cylinder air and walls. Since this is more energy, it is expected that the methanol evaporation process needs reaction time. Subsequently, increased methanol/diesel ratios leads to slower evaporation and an elongated ignition delay.

To determine the evaporation heat of methanol/diesel blends, the injected fuel rate is calculated by using the plunger injection model of Zeng [63]. The mechanical injection model is connected with the single zone model in MATLAB/Simulink. After post processing and solving minor mathematical and programming errors, the model is able to simulate the right amount of fuel injected into the cylinder. Section 3.6.1 gives general information regarding the working principles of the injection model. More in-dept details can be found in the work of Zeng [63].

3.6.1. General configuration

The plunger injection model is constructed by combining three separate models. In specific, a cam, plunger pump and injector model are combined to simulate a complete mechanical injection system. All three components are connected in order to simulate the fuel injection into a cylinder. The main purpose of this model is to connect the output to the in-cylinder model to simulate the fuel injection.

The model is designed based on the cam movement in the engine. Related to the cam movement, the plunger pump reacts by moving up and down. The position of the plunger and the velocity of the cam determines the amount of fuel injected to the injector. The pressure in the plunger increases until the spring force from the pump to the injector lifts the ball valve. From there on, the fuel causes an increase of the pressure in the injector. When the injector's spring force resistance is reached, the needle lifts and injection starts. At a certain point in the cycle the nozzle starts to move down, which is caused by a pressure decrease in the injector. This is the moment that the pressure inside the injector compared to the in-cylinder pressure is lower, which is at the end of injection. The model is built in the MATLAB/SIMULINK environment.

3.6.2. General working principle of the injection model

In this section, the general working principles of the injection model are discussed. The aims of this section are to discuss the general methods regarding the model and to explain the improvements for the simulation of methanol/diesel blends.

The cam model is related to the engine's speed, which is an input and drives the model. The camshaft of fuel injectors have a special designed shape to move the plunger up and down during each cycle at the right moment. The shape of the cam is modelled by using a polynomial function found in literature [20, 63].

The cam movement determines the plunger lift and controls the fuel supply flow into the fuel pump. This process is modelled in four parts: supply from the tank, flow to the injector, leakage flow and a spill flow. In the plunger pump model, the flow to the injector is important. A typical plunger system is shown in fig. 3.4.

Figure 3.4 shows the working principle of the plunger in the pump chamber. A fuel rack is connected to the plunger, which controls the position of the helical design of the plunger. Depending on the engine

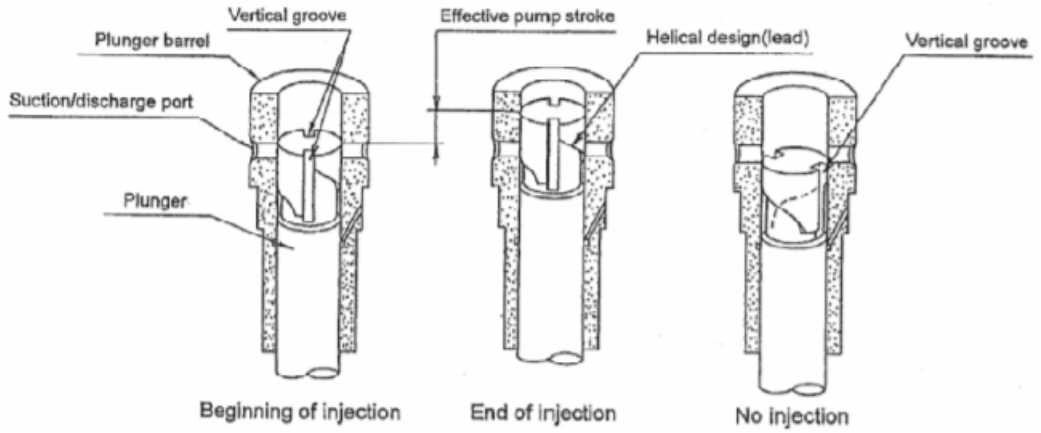

Figure 3.4: Plunger pump system, taken from Bejger [6]

load, the fuel rack turns to a specific position. At high loads, the vertical distance of the helix on the plunger will be extended, which means that the inlet and outlet ports of the pump chamber are blocked for a longer time. The effective plunger stroke is in that case larger and a larger amount of fuel is delivered to the injector. When the helix reaches the suction and discharge ports, the remaining fuel leaves the system through the vertical grooves and flows through the helix back into the fuel pipes.

The pressure in the pump chamber is important for delivering a sufficient amount of fuel. This process is modelled using the diesel bulk modulus and the mentioned volume flows in and out the pump chamber. Equation (3.20) shows the equation calculating the pump pressure.

$$\dot{P} = \frac{K_\mathrm{f}}{V_\mathrm{P}} \left(\dot{Q}_\mathrm{in} - \dot{Q}_\mathrm{out} + \dot{V} \right) \tag{3.20}$$

where $\dot{Q}_\mathrm{in}$ is the volume flow into the pump chamber, $\dot{Q}_\mathrm{out}$ is the volume flow leaving the pump chamber which contains leakage, to injector and spill flow. The volume flow $\dot{V}$ is dictated by the movement of the cam and assumes the fuel volume in the pump chamber is equal to the plunger movement. K_f is the diesel bulk modulus in [Pa] and V_P is the volume of the pump chamber. From this point, the flow to the injector and the pump pressure are used for the injector model.

The injector receives the volume flow from the pump. To calculate the volume flow that goes from the injector into the cylinder, the cylinder pressure must be known. The in-cylinder pressure signal from the experiments is used to simulate the cylinder pressure. Using the pressure difference between the cylinder and the nozzle, the nozzle effective area, fuel density and a discharge coefficient, the volume flow to the cylinder is calculated in eq. (3.21).

$$\dot{Q}_\mathrm{out} = C_\mathrm{d,cyl} \cdot A_\mathrm{cyl} \sqrt{\frac{2}{\rho} \left| P_\mathrm{n} - P_\mathrm{cyl} \right|} \tag{3.21}$$

The pressure in the nozzle is calculated in a similar way as shown in eq. (3.20). Moreover, the spring, damping and hydraulic forces and opening of the nozzle are modelled using a second order differential equation. Details of these modelling parts can be found in the work of Zeng [63].

3.6.3. Model improvements and tuning

This section discusses the improvements made to the injection model of Zeng and the tuning of the model. During the study of the model, it became clear that parts of the model needed improvement. Therefore, the model needed to be calibrated again to the operating profile of the engine. One of the main improvements of the model is the calculation of pressure and volume flows. An internal error was found: the units of the pressure were in [bar] instead of [Pa], therefore the pressure and volume

flows were incorrect. Moreover, the calculation of the leakage flow was found to be mistaken by a factor of 10, due to a conversion error from [bar] to [mH_2O]. The improvements did not result in a large difference between the model results.

At this point, these bugs are fixed and the model can be calibrated to use it for methanol/diesel blends. To implement methanol properties, the density and the viscosity in the model needs to be changed. The bulk modulus was not found for methanol/diesel blends and has remained equal. By changing these parameters, the fuel flow changes. Moreover, the position of the fuel rack has to be adapted. The fuel consumption and power relation of the engine changes by injecting lower energy dense fuel mixtures and thus the position of the fuel rack for a certain engine power needs to be adapted.

Some parameters can be used in the model to tune the results to experimental values. The parameter available to tune the model is the discharge coefficient of the injector. According to literature, the discharge coefficient depends on the needle lift in the injector. The needle lift is dependent on the pressure in the cylinder and thus on the engine load. Therefore, the discharge coefficient of the accumulation chamber is used to calibrate the injection flow of the model at several engine loads and speeds. The relation between the needle lift and discharge coefficient is shown in fig. 3.5 [45].

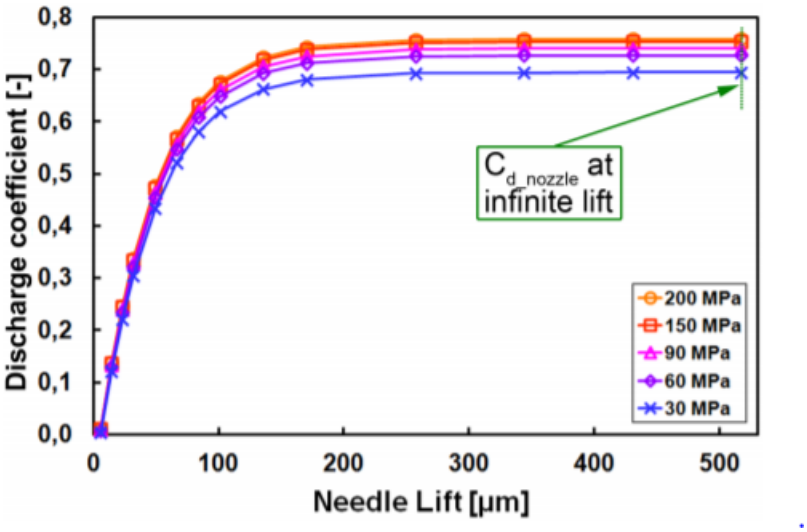

Figure 3.5: Relation between needle lift and discharge coefficient [45]

Figure 3.5 shows that the discharge coefficient of the nozzle should not exceed 0.75 at 200 [MPa]. The discharge coefficient includes velocity and effective area losses of the flow in the equations. The pressure in the cylinder is measured by experiments and is used in this model.

3.7. Single droplet evaporation model

Galindo developed a liquid zone model for diesel injection in a diesel engine [39]. In Galindo's model, he described the liquid phase and the evaporation process after injection. The most complex phenomena that occur during spray development are not implemented in the model and are replaced by assumptions to keep calculation times short. However, the model is able to describe the heat and mass transfer processes in detail. The development of the current model starts by building an unsteady single droplet evaporation model for methanol and diesel droplets comparable to the diesel evaporation model of Galindo [39]. The aim for this part of this thesis is to describe the evaporation process of fuel droplets and to capture the heat of vaporization of methanol in the dual fuel single zone model.

Dual fuel experiments will be executed to verify the dual fuel single zone model of Lee [37]. In the original model of Lee, evaporation losses for methanol fuel were not included. By building a single droplet evaporation model for methanol and diesel, the difference between the evaporation process of both fuels is investigated. After verifying the evaporation models, the heat of vaporization for a com-

plete fuel spray is calculated. Since the evaporation heat of diesel fuel is modelled and described by Ding, this part of the model will not be adapted [12].

The evaporation process in the cylinder is difficult to measure directly. Differences in evaporation speed and required heat shown by the model are expected to be seen in the experiments from the pressure signal. For instance, the start of combustion is expected to be delayed due to the evaporation time. Adding the heat of vaporization of methanol to the model improves its capability to simulate direct injection of fuel blends.

3.7.1. Spray development

In this section, a general description of fuel spray development is discussed. After injection, the fuel spray undergoes a thermodynamic process in which the fuel starts in the liquid phase and mixes with air. Heat and mass transfer with the cylinder parts and surrounding air occur. Spray development is divided in sub-processes as shown in fig. 3.6.

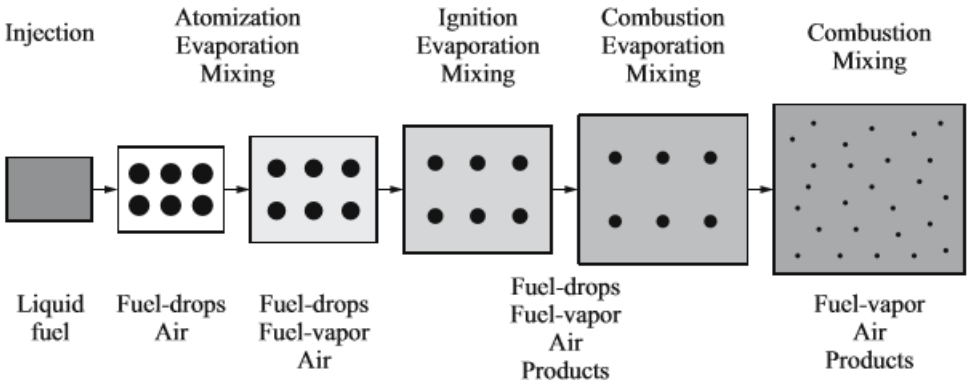

Figure 3.6: Spray development after injection in a combustion engine, taken from Merker et al. [42]

Directly after injection, the fuel breaks up into small droplets in the liquid phase, which is referred to as the spray formation and spray atomization. The small droplets start to heat up due to heat transfer from the gases in the cylinder. The pressure in the cylinder has an important impact on the initial heating period of the liquid droplets. Under constant pressure, the boiling temperature of liquids is a constant value. However, during the compression stroke the pressure rises and this leads to an increase of the boiling temperature of the substance [24].

Once the droplets start to boil, droplet evaporation causes mass transfer from fuel to air. During this process, vapor is flowing into the surrounding gases and forms a combustible mixture. In other words, this is called air entrainment, the mixing of hot air with liquid and vapor fuel. It is important to get the fuel vaporized and to create an ignitable fuel mixture in the cylinder. Furthermore, convective- and radiative heat transfer from the cylinder walls are playing a role in the heating process. Spray formation is considered as an effective measure to control the combustion process in a compression ignited engine [55]. If the air-fuel mixture is lean, combustion might not get started. Rich fuel mixtures lead to hot spots in the cylinder and could lead to local high rates of NO_x formation. Different fuel properties and fuel injector properties have an effect on spray formation in the engine.

During ignition, liquid droplets are still present in the cylinder in which a mixture of stoichiometric gas, fuel vapor and liquid exist. Heat from the flame front evaporates the remaining fuel before its ignition. At the end of combustion, most of the time it is assumed that all the fuel is completely burned and only combustion gas and excess air are present in the cylinder. In a real combustion processes, incomplete combustion decreases the energy released from the injected fuel and the engines efficiency. Chemical components such as CO, unburned hydrocarbons and soot in the exhaust gases are present and indicate whether or not combustion was complete. Usually, incomplete combustion is caused by lack of oxygen [42].

3.7.2. Droplet formation

The injector nozzle is important for droplet formation inside the cylinder. Except for chemical properties, droplet size is dependent on the nozzle diameter, injection pressure and cylinder pressure. These parameters are related to droplet formation in the cylinder, which is described in this section.

After injection, the fuel is still in the liquid phase while breaking up into small droplets. Droplet formation is important for the evaporation process: too large droplets takes to much time to evaporate and can experience wall impingements. A widely used method to describe the mean droplet size in a fuel spray is the sauter mean diameter (SMD). In this thesis, an often described relation in fuel spray modelling for SMD of Hiroyasu is used in the model. These equations are dependent on fuel properties, which are in this thesis variable and expected to make a difference compared to diesel fuel. Several empirical relations for SMD can be found in the paper of Dos Santos et al. [14].

The SMD is the diameter of a droplet with the same volume to surface ratio as the complete polydisperse spray. It can be experimentally measured. The total volume of the fuel injection is the sum of all the droplets in the spray. The relation between evaporation and SMD is that the size of the droplets determines the evaporation rate [55]. Moreover, the combustion efficiency is related to the mixture of air and fuel, which is also dependent on the fuel drop size.

Hiroyasu described the SMD for fuel sprays by empirical correlations as given in eqs. (3.22) and (3.23) [23].

$$SMD_1 = 4.12 d_\mathrm{o} \mathrm{Re}_\mathrm{liq}^{0.12} \mathrm{We}_\mathrm{liq}^{-0.75} \left(\frac{\mu_\mathrm{liq}}{\mu_\mathrm{gas}}\right)^{0.54} \left(\frac{\rho_\mathrm{liq}}{\rho_\mathrm{gas}}\right)^{0.18} \tag{3.22}$$

$$SMD_2 = 0.38 d_\mathrm{o} \mathrm{Re}_\mathrm{liq}^{0.25} \mathrm{We}_\mathrm{liq}^{-0.32} \left(\frac{\mu_\mathrm{liq}}{\mu_\mathrm{gas}}\right)^{0.37} \left(\frac{\rho_\mathrm{liq}}{\rho_\mathrm{gas}}\right)^{-0.47} \tag{3.23}$$

$$SMD = \max\left[SMD_1, SMD_2\right] \tag{3.24}$$

where d_o is the nozzle diameter. Re and We are the Reynolds and Weber number respectively. μ and ρ represent the dynamic viscosity and density in the liquid or gas phase of the fuel. In the model, the highest result of the SMD is chosen for further calculations as can be seen in eq. (3.24). The Reynolds and Weber number are defined in eqs. (3.25) and (3.26).

$$\mathrm{We}_\mathrm{liq} = \frac{v_\mathrm{liq}^2 \cdot d_\mathrm{o} \cdot \rho_\mathrm{liq}}{\sigma_\mathrm{liq}} \tag{3.25}$$

$$\mathrm{Re}_\mathrm{liq} = \frac{v_\mathrm{liq} \cdot d_\mathrm{o} \cdot \rho_\mathrm{liq}}{\mu_\mathrm{liq}} \tag{3.26}$$

An important consequence regarding the SMD approximation is that the droplet size distribution is neglected. Using only the SMD and not the size distributions, important aspects such as droplet deformations and interactions during evaporation are disregarded [22, 52, 55]. Furthermore, diesel and methanol are injected simultaneously. Viscosity and density of both fuels differ, which causes differences between fuel components as shown in table 2.1. The number of droplets of each fuel depends on the ratio on which the fuel is injected and simulated.

When all the droplets are assumed to have the same SMD as diameter, the number of droplets is calculated according to eq. (3.27)

$$N_\mathrm{drop} = \frac{m_\mathrm{liq}}{\frac{\pi}{6} \cdot \rho_\mathrm{liq} \cdot SMD^3} \tag{3.27}$$

The specifications of methanol and diesel are calculated separately. After droplet formation, heat transfer starts to heat up the liquid droplets discussed in section 3.7.3.

3.7.3. Heat transfer

The process of heat transfer to fuel droplets depends on many parameters. To simplify the calculations, the evaporation process is simplified by using assumptions. Droplet evaporation modelling varies in degree of difficulty and detail. Information about the general evaporation process of a droplet in this case is important for this phase in the research.
The evaporation model only calculates the heat transfer process by convection. Radiation is assumed to be small compared to convection and is therefore neglected [5, 55]. Moreover, deformation, collisions and other interactions of droplets during the evaporation process are not taken into consideration. These processes have impact on droplet mass, trajectory and heat transfer. Another impact on the evaporation process is that the temperature and pressure are assumed to be constant in the evaporation model.

Turbulent dispersion by velocity gradients between the in-cylinder gas and droplets results in more diffusion or dispersion. The time of the mixing process between fuel and air by turbulent velocity fluctuations decreases due to turbulent dispersion [5]. Large and small eddies in the fuel spray react to turbulent fluctuations from the in-cylinder gases and depends on the turbulent kinetic energy. This process can be modelled using $\kappa - \epsilon$ models which provide information about the fuel-air interaction by turbulent eddies. Details can be found in Baumgarten [5].

Fuel is directly injected into the cylinder in liquid form by the injection nozzle. Small orifices in the nozzle combined with high injection pressures ensure that the fuel bulk breaks up into small droplets. The droplets are assumed to be equally distributed within the spray. In this way, each droplet undergoes an equal process in the cylinder.

Fuel injection is important to create an equally distributed flammable gas mixture. The heat transfer process is dictated by the effective heat transfer area of the fuel spray and is dependent on the diameter of the fuel droplets. By using the SMD, it is assumed that each droplet has an equal initial droplet diameter. An energy balance for a single droplet is solved to calculate the heat required to evaporate the droplet. The heat balance for a single droplet is described by eq. (3.28) based on the unsteady vaporization theory of Borman [9]. The model is build in the MATLAB Simulink environment.

$$m_{\mathrm{f,liq}} \cdot c_{\mathrm{p,f,liq}} \cdot \frac{\mathrm{d}T_{\mathrm{f,liq}}}{\mathrm{d}t} = \tilde{h}^* \cdot A_0 \cdot \left(T_\infty - T_{\mathrm{liq}}\right) - \dot{m}_{\mathrm{evap}} \cdot h_{\mathrm{fg}} \tag{3.28}$$

where the left hand side is equal to the changes in the energy stored in the liquid droplet. The right hand side of eq. (3.28) is the sum of the convective heat flux in to the droplet and the energy stored in the vapor leaving the droplet. $\tilde{h}^*$ is the corrected convective heat transfer coefficient determined with the Nusselt number in eq. (3.29). The Nusselt number describes the ratio between convective and conductive heat transfer and thus is a dimensionless number. A_0 is the area of the fuel droplet exposed to heat from the cylinder. T_∞ is the cylinder temperature and T_{liq} is the temperature of the droplet. h_{fg} is the difference between liquid and vapor enthalpy of the fuel and the droplet temperature. The driving force for convective heat in this equation is decided by the temperature difference between the droplet and the cylinder air.

$$\mathrm{Nu} = \frac{\tilde{h} \cdot d}{k_{\mathrm{f,gas}}} = 2 + 0.6\mathrm{Re}_{\mathrm{d}}^{1/2} \cdot \mathrm{Pr}^{1/3} \tag{3.29}$$

Equation (3.29) gives the dimensionless Nusselt number, in which Re is the Reynolds number of the droplet and Pr the Prandtl number. Both are dimensionless numbers. d describes the droplet diameter, which is initially equal to SMD and changes during evaporation. The Reynolds number is used to describe the ratio between inertial and viscous forces. The Prandtl number is the dimensionless ratio between kinematic viscosity and thermal diffusity of the surrounding gas shown in eq. (3.30).

$$\mathrm{Pr} = \frac{c_{\mathrm{p,f,v}} \cdot \mu}{k_{\mathrm{f}}} \tag{3.30}$$

The convective heat transfer coefficient must be corrected for high rates of vaporization. Vapor is blowing away from the droplet which affects convection to the surface of the droplet. Vapor will heat

up to the cylinder temperature while leaving the droplet's boundary layer. Bird, Stewart and Lightfoot corrected $\tilde{h}$ for the superheating effect by eq. (3.31) according to Borman [8, 9].

$$\tilde{h}^* = \tilde{h} \cdot Z = \tilde{h} \cdot \frac{z}{e^z - 1} \tag{3.31}$$

$$z = \frac{\dot{m}_{\text{evap}} \cdot c_{\text{p,v}}}{\tilde{h} \cdot A_0} \tag{3.32}$$

where z is dependent on the mass transfer from the droplet to the surroundings, as can be seen in eq. (3.32). $c_{\text{p,v}}$ is the heat capacity of fuel vapor. It can be seen that the convective heat transfer to the droplet is strongly dependent on the vapor mass flow away from the droplet. Therefore, the mass transfer is described in a subsequent relation. Mass transfer is discussed in section 3.7.4.

3.7.4. Mass transfer

The difference between the vapor and cylinder pressure is the driving force for vapor flowing away from the droplet. To describe mass transfer, the Sherwood number (Sh) is used to calculate the mass transfer film coefficient $\tilde{h}_{\text{D}}$, which is actually considered as the Nusselt number for mass transfer. Equation (3.33) shows the equation for the mass transfer film coefficient.

$$\mathrm{Sh} = \frac{\tilde{h_D} \cdot d}{D_{\text{AB}}} = 2 + 0.6 \cdot \mathrm{Re}^{1/2} \cdot \mathrm{Sc}^{1/3} \tag{3.33}$$

where Sc is the Schmidt number, the ratio between momentum and mass diffusity. Moreover, $\tilde{h_D}$ is the mass transfer coefficient and D_{AB} is the binary diffusion coefficient between fuel vapor and air. The mass transfer coefficient is corrected for high vaporization rates. Therefore, as done before while describing the convective heat transfer coefficient, $\tilde{h_D}$ is corrected by Bird, Stewart and Lightfoot according to Borman [8, 9]. The relation is shown in eq. (3.34)

$$\frac{\tilde{h}^*_{\text{D}}}{\tilde{h}_{\text{D}}} = \ln\left(\frac{p - p_{\text{v},\infty}}{p - p_{\text{v},0}}\right) \cdot \left(\frac{p}{p_{\text{v},0} - p_{\text{v},\infty}}\right) \tag{3.34}$$

where p is the cylinder pressure, $p_{\text{v},\infty}$ the vapor pressure in ambient conditions, which is assumed to be zero during this simulation. Assumed is that there exists no fuel vapor far away from the fuel droplet. Thus, there is a strong dependence on the saturated vapor pressure $p_{\text{v},0}$ at the droplet temperature and the cylinder pressure. The difference between the vapor pressure at the droplet surface and vapor pressure at infinity is the driving force for mass transfer. By using eq. (3.34), the mass transfer coefficient is also valid for high rates of vaporization and can be implemented in the relation for the evaporation rate, shown in eq. (3.35). After substituting $\tilde{h_D}$ in eq. (3.33) for $\tilde{h}^*_{\text{D}}$ by eq. (3.34), the vaporization rate described in eq. (3.35) can be written as eq. (3.36).

$$\dot{m}_{\text{evap}} = \tilde{h}_{\text{D}} \cdot A_0 \cdot \left(p_{\text{v},\,0} - p_{\text{v}\,\infty}\right) \tag{3.35}$$

$$\dot{m}_{\text{evap}} = \pi \cdot d \cdot \rho_{\text{f,v}} \cdot \ln\left(\frac{p}{p - p_{\text{v,f},0}}\right) \cdot \mathrm{Sh} \tag{3.36}$$

Note that in eq. (3.36), the vapor pressure and cylinder pressure can not be identical. The mass transfer would in that case be infinitely large. Dividing by zero would lead to an mathematical error and is physically not possible. Mass transfer will be infinity when both pressures are equal. If the vapor pressure is zero at the droplet surface, there will be no mass transfer from the droplet to the surroundings.

The total amount of vaporized fuel mass is equal to the initial droplet mass when the droplet is completely evaporated. In the model, when the droplet is almost evaporated completely, a mathematical error occurs because the droplet diameter is reaching zero. Therefore, the model is limited to a

maximum evaporation rate of 90 [%] based on the diameter of the droplet. At this point, the evaporation and heating processes of diesel and methanol fuel are already described sufficiently to see the differences between them.

3.7.5. Fuel properties

Decane is used in the evaporation model as a diesel surrogate fuel, which shows comparable chemical properties. For decane and methanol, the fuel properties are used from REFPROP. Table 3.2 provides the parameters used in the evaporation models. The parameters are considered to be temperature dependent.

Table 3.2: Fuel properties for methanol and decane used in the evaporation model

Fuel property	**Variable**	
Vapor density	ρ_{gas}	[kgm^{-3}]
Liquid density	ρ_{liq}	[kgm^{-3}]
Liquid surface tension	σ_{liq}	[Nm^{-1}]
Liquid Dynamic viscosity	μ_{liq}	[Pa-s]
Vapor Dynamic viscosity	μ_{gas}	[Pa-s]
Vapor thermal conductivity	$\kappa_{\mathrm{f,gas}}$	[Wm^{-1}K^{-1}]
Liquid thermal conductivity	$\kappa_{\mathrm{f,liq}}$	[Wm^{-1}K^{-1}]
Vapor pressure	$p_{\mathrm{v,0}}$	[Pa]
Binary diffusion coefficient	D_{AB}	[m^{2}s^{-1}]
Vapor heat capacity	$c_{\mathrm{p,f,gas}}$	[Jkg^{-1}K^{-1}]
Liquid heat capacity	$c_{\mathrm{p,f,liq}}$	[Jkg^{-1}K^{-1}]

Each variable shown in table 3.2 is calculated using REFPROP for variable temperatures. However, the binary diffusion coefficient for methanol in air is temperature dependent and is described by Lapuerta et al. by using an empirical equation [35]. The equations for methanol in air (D_{MA}) and diesel in air (D_{DA}) are given in eqs. (3.37) and (3.38).

$$D_{\mathrm{MA}} = \mathrm{e}^{(4.4426 \cdot \ln(\mathrm{T}) - 27.056)} \tag{3.37}$$

$$D_{\mathrm{DA}} = (-0.02513 + T \cdot 0.00013439 + 3.1511 \cdot 10^{-7} \cdot T^2) \cdot 10^{-4}) \tag{3.38}$$

The temperature T in eqs. (3.37) and (3.38) is based on the mean film temperature of the droplets liquid temperature and the environmental temperature of the droplet.

3.7.6. Evaporation rate: d^2-law

This section gives the theoretical background of the evaporation rate analysis of single droplets. Regarding the process of droplet evaporation, two phases can be distinguished. The first phase concerns the heating up period and lasts until the fuel reaches its boiling point. It is possible that the droplet diameter increases during this phase due to a decreased density. The equations for this effect are captured in the model but this phenomena is not observed. After the droplet reaches its boiling point, the droplet diameter starts to decrease more rapidly.

A widely used method for vaporization analysis is the d^2-law, which states that after the droplet's initial heating up period the droplet area decreases linearly in time. The equation for the droplets lifetime known as the d^2-law and is given in eq. (3.39) [60].

$$d^2(t) = d_0^2 - Kt \tag{3.39}$$

where $d(t)$ is the droplet diameter [mm], d_0 is the initial droplet diameter [mm]. K is the evaporation constant [mm^{2}s^{-1}], which is the derivative of the droplet's area after the initial heating period. t is the

time [s].
For methanol and diesel droplets, the evaporation rate is expected to be different. The evaporation is dependent on gas and fuel properties as well. The mean temperature of the droplet and its surrounding gas is calculated to determine the gas properties of fuel droplets.

3.7.7. Heat of vaporization

The heat of vaporization of methanol is for compression ignited engine applications a challenging parameter. The total heat of vaporization required for the evaporation of methanol as a percentage of the lower heating value is equal to 5.4 [%]. Diesel fuel only requires 0.6 [%] of its combustion heat to evaporate the fuel. Clearly, the amount of required energy for evaporation of methanol is relatively much larger compared to diesel fuel, which could lead to longer ignition delays and lower in cylinder temperatures.

The heat of vaporization is calculated with the proposed model in section 3.5. The heat of vaporization is equal to the second term on the right hand side of eq. (3.28). In thermodynamic processes, the latent heat of vaporization is dependent on temperature. In this simulation, the latent heat of vaporization is considered to be a constant. Furthermore, the environmental temperature is not adapted to the heat subtracted from it by evaporation. In the engine, the heat of vaporization to evaporate the droplets causes a decrease of the cylinder's temperature. A constant cylinder temperature means in fact that the available heat in the system is unlimited, which is actually not real in an engine. Where in reality the heat of vaporization of methanol causes a larger temperature drop of the surroundings, now it is constant and therefore the convective heat transfer to the fuel is larger. Another important aspect in this simulation is that the pressure is kept constant. The pressure in the engine is changing in time. The effect of this is not investigated, because it led to numerical errors due to infinite results in the model.

3.8. Single zone model

3.8.1. Heat of vaporization

This section discusses the improvements to the dual fuel single zone model of Lee [37]. The model's capability to perform direct injection engine calculations is improved by implementing the heat of vaporization of methanol. Using the single droplet evaporation and injection model, the heat of vaporization during a closed cylinder cycle is calculated and applied in the single zone model. Adding the methanol heat of vaporization in the model is important due to the increased required energy to vaporize the methanol droplets. Unfortunately, the aim to model the ignition delay effects of methanol has not been reached during this research period.

Ding describes the energy losses required for fuel heat up and evaporation by eq. (3.40). For diesel fuel, the heat of vaporization is already included in the model. Methanol's evaporation heat is also calculated by eq. (3.40) and thus by the method proposed by Ding. The method from Ding is used to verify the method proposed in this thesis. The results are discussed in section 5.2.3

$$\dot{E}_{\mathrm{f}} = \dot{m}_{\mathrm{f}} \cdot \left(h_{\mathrm{f,liquid}} - u_{\mathrm{f}} \right) \tag{3.40}$$

where $\dot{m}_{\mathrm{f}}$ is the fuel injection rate in the single zone model, $h_{\mathrm{f,liquid}}$ the enthalpy of entering fuel and u_{f} the internal energy of fuel vapor. The heat balance for methanol changes to eq. (3.41).

$$m \cdot c_{\mathrm{v}} \cdot \frac{\mathrm{d}T}{\mathrm{d}t} = \dot{Q}_{\mathrm{comb}} - \dot{Q}_{\mathrm{loss}} - p \cdot \frac{\mathrm{d}V}{\mathrm{d}t} + \dot{E}_{\mathrm{f}} \tag{3.41}$$

The calculation of the amount of heat required for evaporation is still dependent on the mass balance in the single zone model. The injection rate, evaporation rate and combustion rate are expected to vary when the methanol/diesel ratio is increased due to the heat of vaporization. In fact, the heat of evaporation calculated for the fuel spray is now located at the position where the fuel is burned according to the single zone model. The effect of the ignition delay is expected to be visible in the

pressure signal, while the model does not calculate the effects captured by the pressure signals. This could lead to model inaccuracies.

Future researchers could make use of the detailed evaporation model to extend the existing model with more detail regarding the ignition delay and heat of vaporization directly after injection.

3.8.2. In-cylinder process

Due to lack of experimental data, the SOC and EOC were assumed in the original model of Lee. Dual fuel experiments will increase the accuracy regarding the combustion duration of the model based on the valve timings of the engine. Taking this into account, the simulation starts at IC and ends at EO according to the engine's specifications.

3.9. Uncertainties

3.9.1. Droplet formation

Droplet formation in the cylinder is difficult to measure. Assumptions are there to simplify the process and these have a significant influence on the results. One of these important assumptions is that collisions between droplets are ignored. Collisions create new, larger droplets and change the evaporation process. Furthermore, it is assumed that all droplets have equal diameters and that the droplets are equally distributed in the fuel spray. Moreover, all the droplets evaporate without any vapour pressure in the cylinder's trapped air. During evaporation, more fuel vapour appears in the air by diffusion, which has impact on the evaporation process.
Although methanol and diesel are miscible up to 3 [%] blended methanol by volume at room temperature, the droplets of a mixture are assumed to be totally immiscible. Therefore, simulations are based on a pure droplet evaporation process, which in real mixtures will be different.

3.9.2. Liquid temperature

The liquid temperature of each droplet is assumed to enter the cylinder at the same in cylinder temperature. In reality, the temperature of the engine changes due to volume changes by the piston movements. Unfortunately, simulations use constant cylinder temperature and pressure. More investigation is required to the effect of pressure and temperature changes during evaporation of droplets.

3.9.3. Air entrainment

After injection, air mixes with the fuel droplets to form a combustible mixture. It is assumed that each droplet receives a sufficient amount of air based on stoichiometric air to fuel ratios. Perfect mixing of fuel and air is assumed. Methanol/diesel blends are expected to increase the fuel flow, which affects the mixing process and local air to fuel ratios. Local lean or rich air/fuel mixtures have impact on the combustion efficiency and formation of exhaust gases.

3.9.4. Evaporation process

Each droplet in the fuel spray develops according a single simulation of the droplet's evaporation. Changes in in-cylinder engine parameters and non evaporated droplets are neglected. Environmental parameters affect the evaporation process of fuel droplets and have effect on the fuel spray development. Moreover, the heat of vaporization for the fuel is assumed to be constant. In reality, the heat of vaporization changes with the temperature.

4

Measurements

This chapter describes the effect of methanol/diesel blends in a diesel engine, which are investigated by doing engine performance experiments. Blends of methanol and diesel of multiple ratios are directly injected in a compression ignited engine using the specially designed dual fuel operation system for the MAN4L20/27. Experiments are executed to investigate the effect of methanol on the heat release parameters and emissions in the diesel engine without adapting the geometric parameters of the engine. Measurements on several parameters are done to provide an insight in the combustion process. After the experiments, the data from the fuel blends are compared to data from F76, which is considered to be the benchmark for this engine.

The maximum reachable percentage of methanol injected depends on the engines capability to ignite the blends. The aim of increasing the methanol volume is to try to find the limits of the engine. This chapter describes the assumptions made for the experiments, discusses the engine parameters and also describes important parameters to monitor during the experiments. Moreover, technical indicators for diesel engine performance are introduced. Measurement results will be used in the single zone model to simulate the heat release process during the closed cylinder process. Moreover, uncertainties regarding diesel engine experiments are discussed. The final section of this chapter discusses the performance and emission analysis of the experiments.

4.1. Assumptions

Assumptions are made to represent complicated processes outside the scope of this research. It is important to be aware of the complex processes without being able to take them into account. For this research, the macro effects of diesel and methanol/diesel blends are investigated.

An assumption regarding the macro effects of methanol/diesel blends is the immiscibility of both components. Miscibility is an issue while blending methanol and diesel without using additives. Assumptions for the measurements simplify the miscibility problem, but these assumptions definitely have an impact on the accuracy of the measurements.

Gases inside the cylinder are assumed to behave as ideal gases, which indicates that the thermodynamic properties are only dependent on temperature fluctuations. Moreover, another assumption is that the fuel spray is perfectly mixed with the air to form a combustible mixture.

Although the blend ratio is composed precisely before the measurement starts, variations occurring in the mixing ratio during the measurement are considerable. Before the measurement starts, the mixture ratio is checked visually to see if the correct methanol/diesel ratio is coming from the tank and enters the suction line of the pump. It is not possible to check whether the correct ratio was flowing through the system beyond the fuel supply pump or not. Assumed is that the ratio did not change in this considerably short time. The fuel supply system is discussed and described schematically in ap-

pendix F.1.

Additional assumptions made for the measurements are listed below.

- Fuel mixtures are stable and perfectly mixed
- The engine room is ventilated sufficiently. Therefore, the temperature of ambient air is unchanged during a measurement grid.

The ambient temperature in noted at the start of each measurement grid.

4.2. Measurement set-up

Measurements will be performed on a MAN 4L20/27 compression ignited engine. Technical specifications of the engine are given in table 4.1. The dual fuel operation system is specially designed for the possibility to operate the engine on fuel blends. The physical engine parameters remained unchanged, except the fuel pipe material, fuel supply pump and the daily supply tank. A complete scheme of the measurement setup is given in fig. F.1.

Cold engine start is done while operating on F76 each day. In that way, the engine heats up and stabilizes its temperatures to reduce unnecessary heat losses during the experiments. The system is designed to switch between blended fuel and pure F76 during engine operation. This is done by controlling the valves manually before and after the measurements. At the end of the experiments, the system is cleaned by operating on F76 for half an hour at least in order to reduce the chance of corrosion on the fuel system and toxic exposure caused by methanol.

Fuel blends are prepared before the start of the measurements. Methanol has a lower density compared to F76 and mixing experiments at small scale proved that the effect of this density could help during the mixing process. Therefore, the inlet of the methanol fuel into the tank is at the bottom of the tank. F76 flows in the tank first during the mixing process. When the right mass of F76 is in the tank, which can be read from the scale, the methanol filling process starts and lasts until the right mixing ratio has been reached. The accuracy of the scale is half a kilogram and is readable per kilogram. At least 700 [kg] of blended fuel is loaded inside the tank, which gives a maximum reading error of 0.14 [%]. The scale has a measuring range of 0-2000 [kg] with an accuracy of 0.05 [%].

Personal protecting gear must be worn during the filling process and while entering the engine room. The personal protecting gear consists of a chemical resistant overall, full face mask and gloves suitable for methanol. Furthermore, experiments with methanol can not be performed without having a proper ventilation system. Mobile ventilators are used to remove methanol vapours from the engine and fuel storage room. Moreover, when entering the engine room it is obligatory to use portable gas detectors to detect formaldehyde. Formaldehyde is a possible reaction product of incomplete methanol combustion at high temperatures and is toxic for human beings. Fixed gas detectors are located in the fuel storage room and engine room to detect possible methanol vapors diffused in the air. Detectors for methanol vapor must be located close to the ground, since methanol vapor has a higher density compared to ambient air.

Performing experiments with methanol is not without risks and should only be done in a controlled laboratory with a sufficient amount of safety measures. More detailed information about safety regarding methanol is provided in the *Methanol safe handling manual* from the Methanol Institute [3].

4.2.1. Engine parameters

Table 4.1 gives the engine parameters which are relevant for the model input and the specifications regarding valve timings. The parameters shown in table 4.1 are not changed for the fuel blend configuration.

Table 4.1: MAN 4L20/27 diesel engine parameters

Parameter	Value	Unit
Engine	MAN 4L20/27	
Stroke (L_S)	0.27	[m]
Bore (D_B)	0.20	[m]
Number of cylinders (i)	4	[-]
Nominal Power (P_b)	340	[kW]
Nominal Torque (M_b)	3247	[Nm]
Connecting rod	0.52	[m]
Start of Injection	4	[degree bTDC]
Inlet valve Closes (IC)	20	[degree aBDC]
Exhaust valve Opens (EO)	300	[degree aBDC]
Nominal speed (N)	1000	[rpm]

In Table 4.1, bTDC means *before top dead centre* and aBDC means *after bottom dead centre* of the piston. These specifications come from the engine's manufacturer. Unfortunately, the nominal power and speed are downgraded due to the age of the engine. The maximum reachable power and speed is 300 [kW] at 950 [rpm] operating on diesel fuel. Adding alcohol will decrease the maximum power due to the decreased lower heating value and the mechanical injector's flow capacity limits.

4.2.2. Measurement grid

Measurements on the diesel engine will be performed following the measurement grid in fig. 4.1. For both power and torque, the measurement points are calculated based on the nominal engine torque.

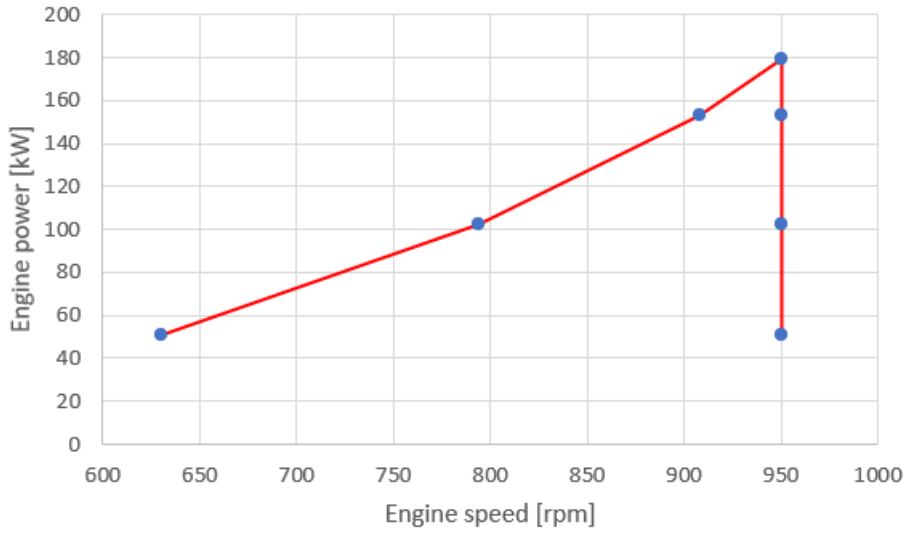

Figure 4.1: Measurement grid for each fuel blend

Different engine speeds and loads are measured along the red line from bottom left to bottom right for each fuel. Going up and down in the engine load prevents the engine from extreme differentials in mechanical and thermal load.

Between each load point, the engine stabilizes for 15 minutes. Temperatures, exhaust gas flows and fuel flow have to stabilize in this period. This reduces the chance of measurement errors and increases the repeatability of the measurements. This process is equal for each measurement point for each fuel. The measurement grid is measured two times for each fuel to prevent measuring errors and increase the repeatability. The mean values of these results are used for the performance anal-

ysis later in this chapter. Detailed information on the complete measurement process is discussed in appendix B.

Only a selection of points from the measurement grid will be used to analyse the in-cylinder combustion, depending on the operating envelope of the engine when injecting methanol/diesel blends. However, the whole grid is important in order to get insight in the engine's performance and emission characteristics for different fuel compositions. A comparison between the fuels is made based on the multiple load points. The calculation of the measurement grid is given in appendix D.

4.3. Performance measurements

The measurements on the engine include pressure, temperature and fuel consumption measurements. In-cylinder pressures correlated to the crank angle are measured by using the Kistler Kibox, which is an engine performance analyser. Properties of the pressure sensor, crank angle adapter and charge amplifier are shown in appendix C. The pressure signal provides valuable information to calculate multiple in-cylinder performance parameters. This section discusses the performance parameters obtained from the measurements.

4.3.1. Mechanical efficiency

The mechanical efficiency is an important parameter for an operating engine, which states the ratio between the effective and indicated work of the engine. Friction of moving parts decrease the mechanical efficiency. The mechanical efficiency of the engine is 100 [%] when all indicated work is converted to effective (brake) work. Equation (4.1) gives the definition of η_m according to Stapersma [53].

$$\eta_\mathrm{m} \overset{\text{def}}{=} \frac{W_\mathrm{e}}{W_\mathrm{i}} \tag{4.1}$$

where η_m is the mechanical efficiency, W_e and W_i are the effective and indicated work respectively. Mechanical losses occur due to friction and are dependent on the engine load and speed. A higher engine speed and load leads to higher mechanical efficiencies since the friction and pump losses decrease relatively to the total indicated work. The mechanical efficiency is always lower than 100 [%] due to these friction and pump losses.

Calculations of the mechanical efficiency are based on a four stroke cycle. Four stroke mechanical efficiencies are higher compared to the mechanical efficiency of only the closed cylinder, since the friction and pump losses are negative and decrease the indicated work.

4.3.2. IMEP

The IMEP is the indicated mean effective pressure in the cylinder, defined as the indicated work divided by the stroke volume. If the pressure during the expansion stroke is equal to the IMEP, then the indicated work would be equal to the current indicated work. The IMEP is also considered as the mean pressure during the expansion stroke [53]. A higher IMEP therefore could lead to higher indicated work and increases the engines efficiency. The calculation of the IMEP is given in eq. (4.2) [53].

$$\mathrm{IMEP} = \frac{W_\mathrm{i}}{V_\mathrm{s}} \tag{4.2}$$

which is actually the ratio between the indicated work and the stroke volume.

The variation of the IMEP gives an indication about the stability of combustion in the cylinders. Therefore, based on the IMEP of 30 cycles, the mean value is calculated. After calculating the standard deviation to the mean of each cycle, the coefficient of variation (COV) is known. The standard deviation and the COV are defined by eq. (4.4).

$$\sigma_n = \sqrt{\frac{\sum_{i=1}^{n} (\mathrm{IMEP_i} - \mathrm{IMEP_{mean}})^2}{n}} \tag{4.3}$$

$$COV = \frac{\sigma}{\mathrm{IMEP_{mean}}} \tag{4.4}$$

where n is the number of the cycles in the statistical window, which is 30. In chapter 5 the results of the mean COV will be analysed for each fuel blend ratio over 41 measured cycles.

4.3.3. Air consumption

The air consumption of the engine is measured by a venturi. The pressure at two locations in the airflow is measured, which gives the amount of airflow entering the engine using Bernoulli's equation. Methanol has a lower stoichiometric air to fuel ratio, implicating that the required air for complete combustion will decrease when the amount of methanol increases.

4.3.4. Fuel consumption

Environmental impact of diesel engines is highly related to the fuel consumption of the engine. During the experiments, the fuel consumption is measured with a flow meter in the fuel supply system. It is however difficult to compare different engines based on fuel consumption in kilograms or liters per unit time. Therefore, defining the specific fuel consumption is a better method to compare engines behaviour. Specific fuel consumption is defined as the ratio between fuel consumption and effective engine power as can be seen in eq. (4.5) [53].

$$sfc = \frac{\dot{m}_\mathrm{f}}{P_\mathrm{b}} \tag{4.5}$$

where sfc is the specific fuel consumption, $\dot{m}_\mathrm{f}$ the measured fuel flow of the engine and P_b the engines brake power.

4.3.5. Exhaust gas temperature

The exhaust gas temperature is measured by using the Testo 350 Analyser with a thermocouple type-K. The gas probe is located at the turbine outlet in the exhaust pipe. The enthalphy of the exhaust gas changes due to the temperature drop in the turbine. Therefore, the absolute effect on the exhaust gas temperatures of methanol/diesel blends compared to F76 is possibly reduced.

4.3.6. Emission measurements

Emissions as NO_x, CO_2, CO, SO_x and O_2 are measured by using the Testo 350 Maritime portable gas analyser. Specifications of the gas analyser are shown in table C.5. All variables are measured in [ppmv] except for oxygen, which is in [vol%].

Unburned hydrocarbons (C_xH_y) are measured by using the Testo 350 gas analyser, which is a different system compared to the Testo 350 Maritime. The gas probes of this system is located at the same location in the exhaust pipe as the Maritime analyser. Measuring these flue gases was not possible with the Maritime analyser. For understanding combustion in an engine, the rate of unburned hydrocarbons is an important parameter. Adding methanol possibly reduces the combustion efficiency in the engine and it will then result in more unburned hydrocarbons in the exhaust gas pipe [29].

At least 15 minutes before the measurements start, the exhaust gas measurement system is turned on to preheat the analyser and the first round of zeroing the sensors is done. Right before the engine is turned on, the sensor is at its desired temperature and needs to be zeroed again to prevent the system from drifting below zero. The complete measurement grid is executed while the Testo is capturing data all the time. Therefore, before the measurements start, the local time on the computers are set equally.

Processing the measurement data is based on the time noted for a specific load point. The result from a specific load point measurement is calculated as a mean value for a time lapse of 60 seconds. This contains 60 data points of a single measurement point. The mean value of these 60 seconds are considered to be representative for the emissions for that specific load point.

4.3.7. Course of the experiments

The aim of the experiments on the diesel engine was to find the physical limits of the methanol ratio in the fuel blends. During the measurements, the methanol rate is increased by 10 [%] based on energy for every new batch. It was found that during the measurements with M10, the engine had no struggles with the methanol addition. The complete measurement grid was measured and gave hope to increase the amount of methanol to 20 [%] by energy. After switching from F76 to M20, the effect of methanol became visible in the pressure signal immediately. At low loads, the engine was unable to maintain the brake power and the ignition in cylinder three and four started to fail. After trying for multiple times at low loads, the engine load was successfully increased to 153 [kW], 950 [rpm]. Decreasing to 100 [kW] immediately caused the engine to switch off again. The result of this is that the M20 experiments are only performed at high loads and high speeds.

4.4. Uncertainties

4.4.1. Fuel flow measurements

Expected is that the fuel flow of two fuels are different, based on the lower heating value and the engines efficiency. The accuracy of the coriolis flow meter used for these experiments is important to keep in mind. The properties of the flow meter are given in table C.4. The coriolis meter is able to measure density, temperature and fuel flow based on a specific vibration of the fuel pipe caused by the fuel flow. Differences in these vibrations could occur when the fuel blend is not mixed homogeneously, these are not known precisely.

4.4.2. Pressure measurements

The pressure sensors are located in a channel connected to the cylinder. In this engine, the sensor is not exactly located at the point of which the channel ends. Therefore, pressure fluctuations in the channel cause a Helmholtz frequency in the pressure signal. The Helmholtz frequency gives large fluctuations at high pressures, which makes the real pressure in the engine uncertain. For after treatment of the pressure signal, a smoothing spline is applied by using the MATLAB curve fitting toolbox.

4.4.3. Exhaust gas emissions

The sulphur and unburned hydrocarbon emissions are difficult to measure. The sulphur content in F76 is too low to measure with a high degree of accuracy. The Testo measurement range is from 100-4000 [ppmv] for sulphur dioxides. Below that limit, the sensor will not be accurate, which reduces the repeatability and accuracy of these measurements. The sulphur content in diesel fuel and methanol is already small.

The unburned hydrocarbons sensor shows a comparable issue with the sulphur dioxide unit. The measurement range lies between 400-4000 [ppmv]. During pure diesel fuel combustion, a diesel engine does not reach those concentrations of unburned hydrocarbons. However, from previous experience it is seen that unburned hydrocarbons condensate to the walls of the gas probe during experiment. Ambient temperatures cool down the gases in the pipe which causes condensation effects. Locally, high concentrations of C_xH_y appear due to condensation, which is not expected. This could results in wrong concentrations being measured by the sensor.

4.5. Performance analysis

In this section, an engine performance analysis is described based on the experimental results from the diesel engine. Based on pressure signal and fuel consumption measurements, the main important parameters of the engine are calculated.

Engine performance analysis is based on multiple measurements on the MAN 4L20/27 diesel engine. Using the Kistler Kibox pressure sensors, the pressure as a function of the crank angle is measured for 41 cycles per measurement point. The measurement grid is shown in fig. 4.1. The results actually have a different order of each measurement point which is shown in table 4.2. Table 4.3 shows the fuel composition in energy, volume and mass percentages.

Table 4.2: Measurement point numbering as shown in figures shown in the performance analysis

Number	Engine speed [rpm]	Engine power [kW]	Engine load [Nm]
1	630	51	775
2	794	102	1230
3	909	153	1612
4	950	51	512
5	950	102	1025
6	950	153	1537
7	950	180	1809

Table 4.3: Methanol volume and mass percentages of prepared blends

Mixture	Energy percentage [%]	Volume percentage [%]	Mass percentage [%]
M10	10	19.9	18.9
M20	20	35.9	34.4

The Kistler Kibox measures the pressure signal as function of the crank angle. Detailed technical specifications of the Kibox are available in appendix C. The TDC of the engine is in the Kibox specified by a TDC-shift with the Kibox software. The TDC-shift is applied to make sure that the crank angle and the pressure signal are correlated. During calibration of the Kibox, a mistake has been made, which shifted the TDC to the wrong position. From the engine parameters, the time of IC is known to occur at 160° bTDC. However, the moment that IC closes in the pressure signal is at 167° bTDC. This location is observed visually by analysing the pressure signal. Therefore, a TDC-shift of 7 °CA is applied to correct the pressure signal measured by the Kibox. In this way, the pV diagram as shown in fig. A.4 has the shape that is expected based on theoretical study [53]. Another parameter to check whether the pressure signal has a correct shape or not is the mechanical efficiency. The area below the pV diagram is equal to the indicated work done by the engine. The ratio between the indicated and effective work of the engine is equal to the mechanical efficiency as proposed in eq. (4.1) and is determined by the engine manufacturer. The mechanical efficiency results are discussed and shown in section 4.5.6. Furthermore, the polytropic constant of the compression stroke gives an indication about the position of the pV diagram. Details on this method are described in appendix A.1.1.

4.5.1. Pressure signal aftertreatment

The pressure signal from the measurements is evaluated in this section. From engine parameters, it is known that fuel injection starts at 4 °CA bTDC. The pressure signal from the Kibox shows that the steep slope of start of combustion (SOC) is located at 11 °CA bTDC in fig. 4.2. Combustion is physically impossible at this moment, because there is still no fuel injection at this point. Another reason why it is clear that the signal needs to be shifted is that the moment of IC is known from the engine manufacturer, which is 160°CA bTDC. The original signal from the Kibox shows that the inlet valve

already closed earlier. Therefore, in order to calculate the correct mechanical efficiency and to have a correct pressure signal in time, the signal is shifted in horizontal direction with +7°CA. This is already mentioned in section 4.5.

The pressure signal shown in fig. 4.2 is measured while operating on F76. It can be seen that the

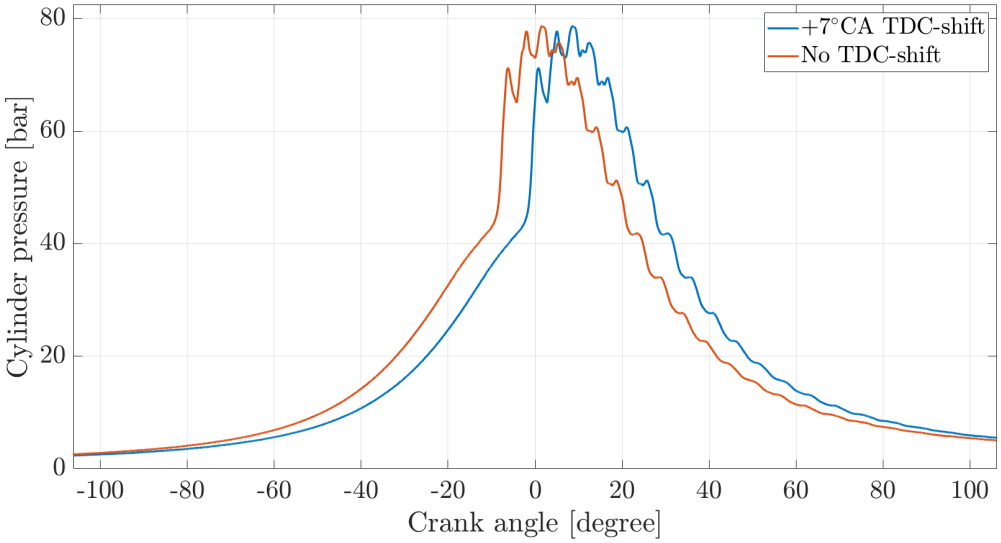

Figure 4.2: Pressure signal with and without TDC-shift

ignition observed from the Kibox was earlier than what would be physically possible. Since no changes have been made to the Kibox between the measurements for all the fuel blends, the TDC-shift is added to each pressure signal. The pressure signals show a signal disturbance at the peak. Typical for the MAN4L20/27, this noise is caused by the position of the pressure sensor. The sensor is located in a tube connected to the cylinder. Pressure fluctuations and air flow inside the tube cause the sensor to detect pressure fluctuations, also known as the Helmholtz frequency. The pressure signal is used for in-cylinder analysis using a single zone model. Numerical solutions of the model deal with extreme fluctuations when experiencing these bad pressure signals. To prevent these fluctuations, the pressure signals have been smoothed by using the CurveFittingToolbox from MATLAB. The new signal is represented in a way that the Helmholtz frequency is filtered out. By smoothing a signal, it is plausible that some information of the signal is filtered out. the smoothing process is inevitable by using the single zone model. Large differentials in the pressure signal cause heavy fluctuations in the heat release signals and they need to be prevented. Figures 4.3a to 4.3c give the result of the smoothing process for a pressure signal from measurements with F76.

Smoothing the signal, as shown in fig. 4.3a removes the Helmholtz frequency from the signal. Nevertheless, it also lowers the maximum pressure of the signal and therefore the heat release development in the single zone model. However, each pressure signal is smoothed in an identical way. By doing the engines performance analysis, the results are based on the rough pressure signals from the engine. The smoothed pressure signal is only used for the single zone model analysis.

4.5.2. Pressure signal comparison

This chapter provides an analysis of the experimental results based on the pressure signal from the engine. During the experiments, multiple measurements are executed which resulted in mean pressure signals. The mean pressure signal shown in this chapter is based on 41 cycles over cylinder two, three and four with a data point on each 0.1 degree crank angle. Unfortunately, cylinder one of the engine has a different fuel injector and cylinder head which affects the combustion. Therefore, results of cylinder one will be discussed separately in the pressure signal analysis.

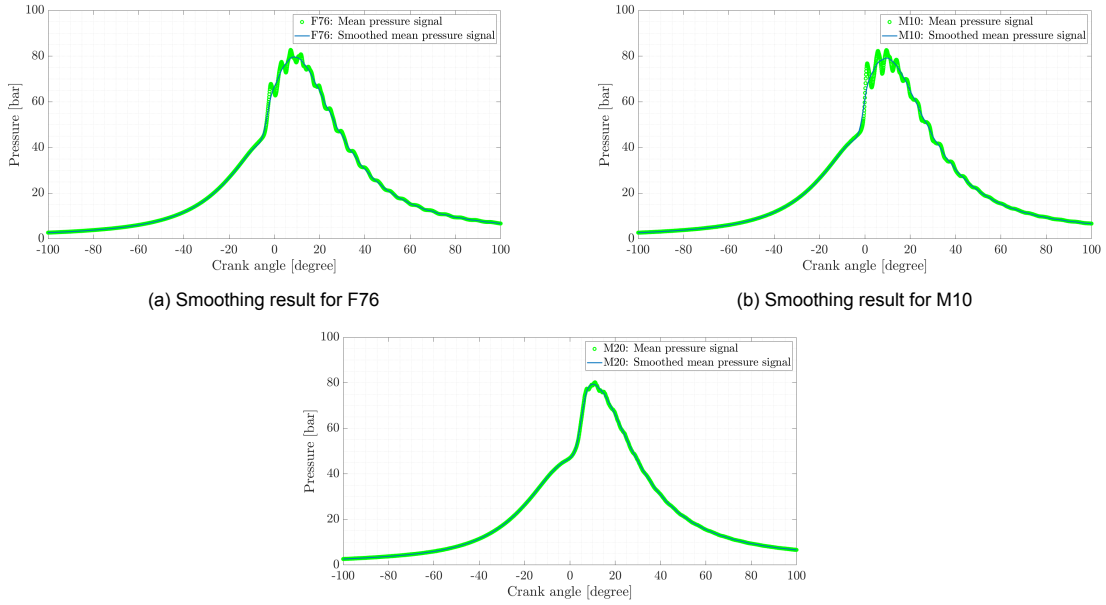

(a) Smoothing result for F76

(b) Smoothing result for M10

(c) Smoothing result for M20

Figure 4.3: Smoothing result for each fuel type for the mean of cylinder two, three and four over 41 cycles and two measurements. Measurementpoint: 950 [rpm], 180 [kW], 1809 [Nm].

Figures 4.4a to 4.4c show the mean pressure signal for each fuel type at 180 [kW] and 950 [rpm]

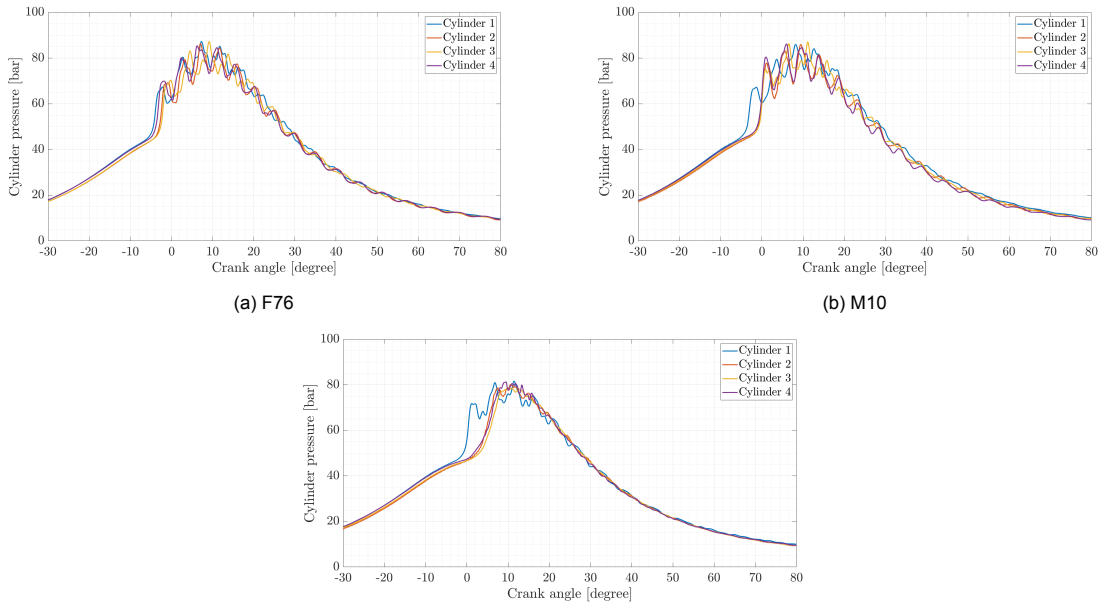

(a) F76

(b) M10

(c) M20

Figure 4.4: Mean pressure signals for each fuel type measured for four cylinders over 41 cycles. Measurementpoint: 950 [rpm], 180 [kW], 1809 [Nm].

for each cylinder. Each signal is the mean pressure signal over 41 cycles. It is shown that cylinder one shows a shorter ignition delay compared to the other cylinders. A higher methanol/diesel ratio increases the differences obtained for cylinder one compared to cylinder two, three and four. The difference is related to the fuel injector, which for cylinder one has other dimensions. The evaluation of the in-cylinder combustion process will be based on the mean of cylinder two, three and four. These

cylinders give a better representation of the complete engine. Raw pressure signals for a single cycle are given in appendix A.

Comparison between figs. 4.4a to 4.4c proofs that the effect of the fuel injector is detectable by increasing methanol/diesel ratio. Eventhough the dimensions of the injector in cylinder one are not known precisely, it seems to have a positive effect on the dual fuel operation on methanol/diesel blends. The vaporization of methanol/diesel blends causes a smaller ignition delay for cylinder one. This indicates that the fuel mixtures are vaporized and mixed with air earlier compared to the fuel in cylinder two, three and four. A shorter ignition delay affects the heat release and temperature levels in the cylinder. Different heat release results are expected between cylinder one and the mean of cylinder two, three and four based on these pressure signals.

Figure 4.5 shows the comparison between the measured fuel types of the mean pressure signals

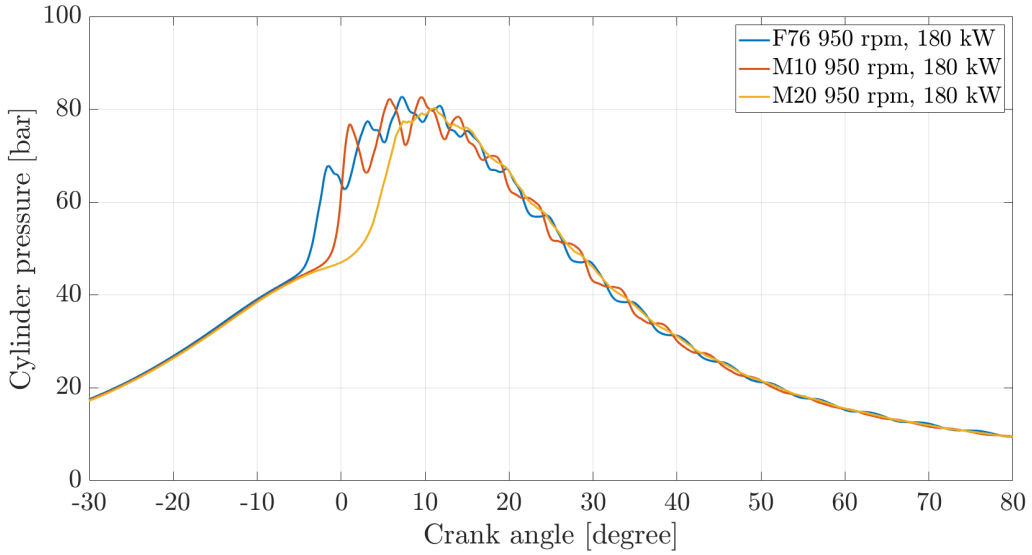

Figure 4.5: Mean pressure signals for F76, M10 and M20 measured at cylinder two, three and four over 41 cycles and two measurements. Measurementpoint: 950 [rpm], 180 [kW], 1809 [Nm].

for cylinder two, three and four at full load. Here, the effect of adapting the fuel blend is shown. The fuel injectors of these cylinders are equal, and thus no large differences between the three cylinders individually have been observed. Pressure signals are taken as a mean of these three cylinders for 41 cycles and two measurements at each measurement point.

M20 shows an ignition delay of almost 8°CA longer compared to F76, as visually obtained from fig. 4.5. The methanol needs more time to evaporate after injection as was already visible for M10. Ignition starts after TDC while injecting M20 due to this large ignition delay. The brake power at the water brake of 180 [kW] was still reached even after the late start of combustion. In the late combustion phase, the mean pressure for M20 is slightly higher compared to M10 and F76. In this phase, the pressure is higher and therefore the late start of combustion is compensated. The heat of vaporization and low cetane number of methanol cause the elongated ignition delay for the methanol/diesel blends. In this way, the fuel vapor has more time to mix with air homogeneously. Therefore, more energy could be released at the same time when ignition starts. Expected is that the premixed combustion heat release rate increases for an increased methanol/diesel ratio.

Remarkable for the M20 pressure signal is that the Helmholtz frequency disappears after averaging out 41 cycles and two measurements. Unfortunately, for single cycles of M20, the Helmholtz frequency still exists. See appendix A for the raw pressure data of a single cycle. The combustion stability of the engine is fluctuating heavily while running on M20. The fluctuations are described by the coefficient of variance, which is observed for the IMEPN and for the maximum pressure per cycle. IMEPN is the indicated mean effective pressure for the complete 4-stroke cycle obtained from the Ki-

box. The COV is the ratio between the standard deviation and the mean of a variable over 30 cycles according to eqs. (4.3) and (4.4). This is calculated for each of the 41 cycles measured.

The COV IMEPN gives an indication about the combustion stability in the engine. In automotive industries, running below a COV of 10% indicates that the engine is running stable [22]. Moreover, a high COV also means that the repeatability of the measurements reduces. The more cycles are measured, the smaller the relative error becomes. For future research, it is advised to increase the number of cycles captured by the Kibox to investigate if this has an impact on the results [33].

Differences in the COV IMEPN shown in figs. 4.6 and 4.7 are mainly caused by varying fuel properties. Variations in the fuel blends could cause an increase in the combustion instability of the engine. Methanol is assumed to be mixed with diesel fuel homogeneously, but the blend ratio could slightly vary during the experiments. Moreover, the lower heating value of methanol has an impact on the required fuel flow into the engine. While the effect of the chemical properties of methanol on the fuel spray is not investigated, the amount and size of the fuel droplets could vary per cycle compared to diesel fuel.

Methanol contains 50 [%] oxygen by molar mass. The higher ratio of methanol increases the amount of oxygen in the cylinder, while the air intake is dependent on the engine and could not be changed in the current setup. Therefore, the fuel/air mixture in the cylinder will be more lean. Lean combustion could affect the combustion stability.

A higher amount of methanol increases the COV for the maximum pressure for each cylinder as

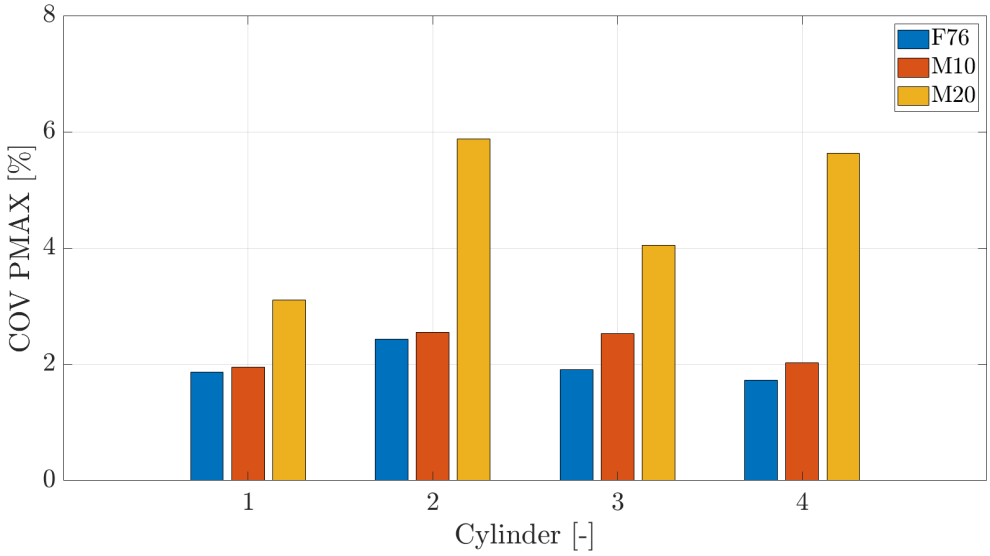

Figure 4.6: Mean COV for maximum pressure for four cylinders. Measurementpoint: 950 [rpm], 180 [kW], 1809 [Nm].

shown in fig. 4.6. Cylinder one has the lowest variation in maximum pressure. Differences in the COV PMAX are caused by the fuel blend. The energy required to evaporate the fuel combined with slight differences of the injected fuel blend results in a varying ignition delay and peak pressure variations. Moreover, the Helmholtz frequency per cycle also has an impact on the maximum pressure. A high COV PMAX indicates that the combustion causes more mechanical load on the cylinders and that the height of the peak pressures is varying more. The COV IMEPN shown in fig. 4.7 for cylinder one is slightly lower for diesel fuel compared to the other cylinders. By adding methanol, the relative difference between the cylinders decreases. In this measurements, cylinder one performs more stable for each fuel compared to cylinder two, three and four. Cylinder one, three and four stay below a COV of 2 [%] while running on M20. Adversely, cylinder two shows a larger deviation in the IMEPN by increasing the amount of methanol while cylinder three and four show a decrease. The large maximum pressure fluctuations from fig. 4.6 obtained for M20 are not shown by the COV IMEPN, which shows smaller values. The result of the COV IMEPN is in line with knowledge obtained from literature, which also

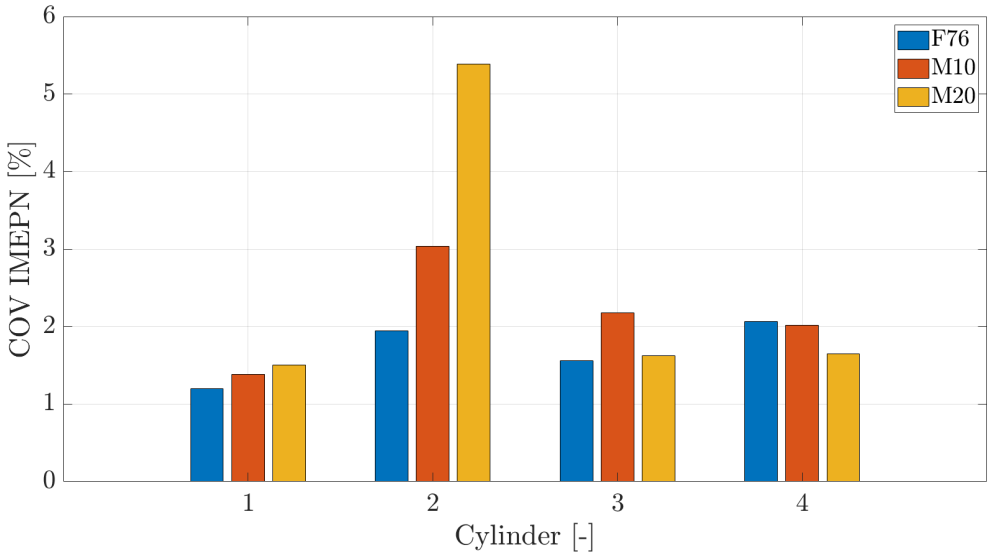

Figure 4.7: Mean COV for IMEPN for four cylinders. Measurementpoint: 950 [rpm], 180 [kW], 1809 [Nm].

mentiones an increase for higher ratio's of methanol injected [29]. However, the large COV IMEPN of cylinder two could be a correction as a reaction to the combustion in cylinder one. The relatively stable combustion in cylinder one compared to the other cylinders requires more research to understand these differences.

4.5.3. Effect of engine speed

The engine speed dictates the time that is available for evaporation before ignition starts. Effects of the engine speed with a constant load of 153 [kW] are shown in fig. 4.8. Three different fuels are presented

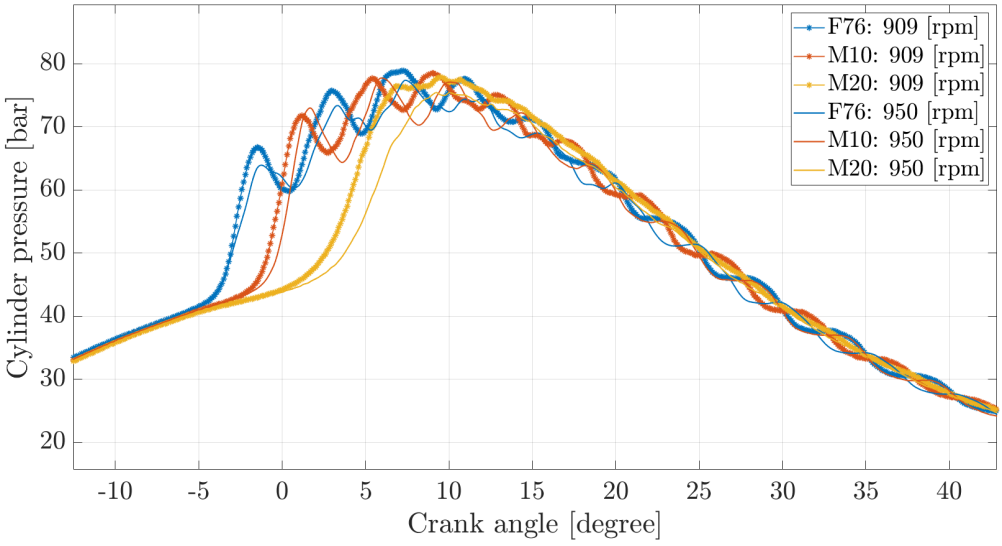

Figure 4.8: Effect of engine speed on pressure at constant load of 153 [kW]

and it can be seen in fig. 4.8 that by running on a lower engine speed the fuel ignites at an earlier crank angle. The effect on the ignition delay for M20 is larger than for F76, since methanol has more time to evaporate properly at lower engine speeds. Higher pressures are obtained while igniting earlier. The air/fuel mixture seems to form a better homogeneous mixture at lower engine speeds. Energy releases

earlier at lower engine speed, which is expected to be visible in the heat release rates.

4.5.4. Combustion duration

Combustion duration in the engine is expected to decrease by using methanol, as obtained from the pressure signal in fig. 4.5. Undesirable auto-ignition properties of methanol mixtures ensure that the ignition delay increases compared to diesel fuel, which is already mentioned while analysing the pressure signals. Again, the important parameters for the elongation of the ignition delay are the low cetane number and the higher heat of vaporization of methanol compared to F76.

The combustion duration is measured by the Kibox, which solves the first law of thermodynamics to calculate the total amount of fuel burned in the engine. AI05 gives the moment in time [°CA] that 5 [%] of the fuel is burned. AI90 is considered as the moment that 90 [%] of total fuel mass is burned according to the Kibox.

Table 4.4 gives AI05, AI50 and AI90. AI50 is the point where 50 [%] of the total injected fuel mass is burned. F76 ignites before TDC, which was expected from normal diesel fuel operation at this engine. F76 has a mean combustion duration of 80°CA. M10 reduced the combustion duration with 3.7°CA, M20 has an almost 12°CA shorter combustion duration compared to F76. Eventhough the ignition delay was much longer for M20, rapid combustion of methanol/diesel blends reduced the total combustion duration. M10 has a relatively small decrease of combustion duration compared to M20. A reason for that small effect is that M10 consists of almost 80 [%] by volume of F76. The majority of F76 in M10 results in a small visible effect of the methanol content.

Table 4.4: Combustion duration measured by the kibox corrected with the 7°CA TDC-shift. 950 [rpm], 180 [kW]

Fuel	AI05 [°CA]	AI50 [°CA]	AI90 [°CA]	AI90-AI05 [°CA]
F76	-3.5	23.0	76.5	80
M10	-0.9	18.9	75.4	76.3
M20	4.4	14.9	72.7	68.3

4.5.5. IMEP

The indicated mean effective pressure of the engine is independent of the load point and engine speed. Comparison between the IMEP of different fuel compositions gives important information about the engine's performance. A high pressure and thus temperature in the cylinder is related to a higher thermodynamic efficiency, which increases the engine efficiency [53].

Figure 4.9 shows the IMEP for each measurement point. The IMEP is calculated for the closed cylinder part of the cycle. For each measurement point, a slight decrease of IMEP is observed for M10 compared to F76. However, adding more methanol leads to an increase of IMEP at high loads. According to literature, it is expected that higher methanol ratios will lead to a lower IMEP and loss of engine power in the end [29]. The high methanol ratio at which this decrease in IMEP is obtained is at high loads not found during this set of experiments.

For this engine, the methanol ratio was already on its physical limit. On low loads operating on M20, the pressure reduced and the engine switched off. This was the moment that the indicated work was not sufficient to meet the required power output. The reason for the insufficient indicated power for low loads is the engine's temperature. Therefore, the evaporation of methanol required too much time to form an ignitable mixture with the air.

4.5.6. Mechanical efficiency

The mechanical efficiency of the engine is dependent on load and speed. Increasing the engine's power and speed will give an increased mechanical efficiency. The relative losses compared to the delivered power are smaller at higher loads, which causes the higher mechanical efficiency. At low loads, friction and for instance pump losses are relatively large compared to the delivered indicated power.

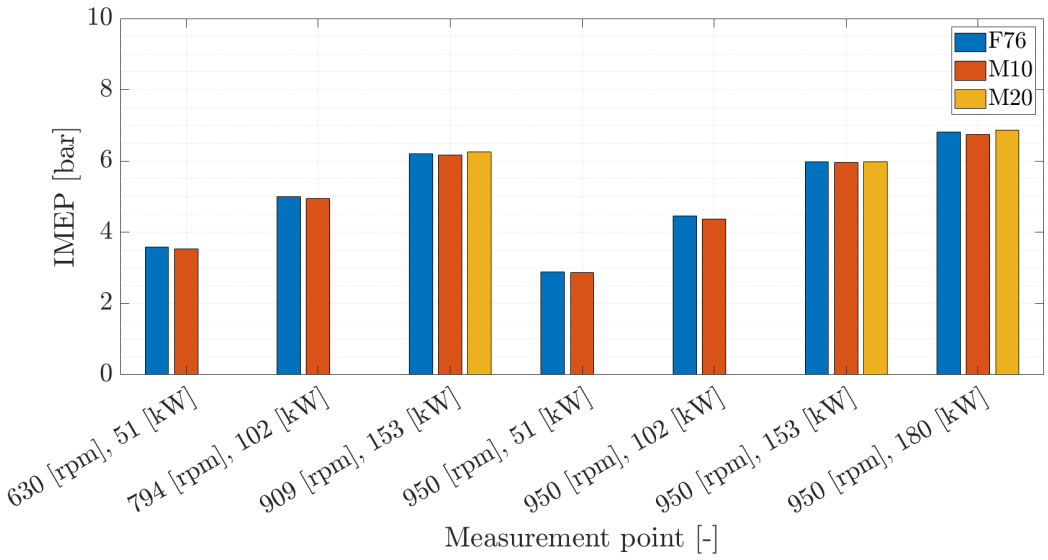

Figure 4.9: Result measurements: IMEP

Figure 4.10 shows the theoretical nominal mechanical efficiency for a typical diesel engine. The charge pressure has influence on the mechanical efficiency of the engine, since a high charge pressure increases the power output of the engine. This engine has a charge pressure of 1.7 [bar] at 180 [kW] during the experiments. The envelope of the current engine starts at its nominal mechanical efficiency of 85 [%] and decreases with the same power related curve as shown in fig. 4.10. Therefore, the mechanical efficiency at low loads decreases rapidly.

Calculated mechanical efficiencies are based on the shifted pressure signal. Full load conditions are not reached and a lower mechanical efficiency is expected at 180 [kW]. Another reason why the mechanical efficiency is lower is because the complete engine cycle is taken into consideration for calculation of the indicated power, thus including pump losses.

Figure 4.11 shows the results for the mechanical efficiency for each measurement point. At each

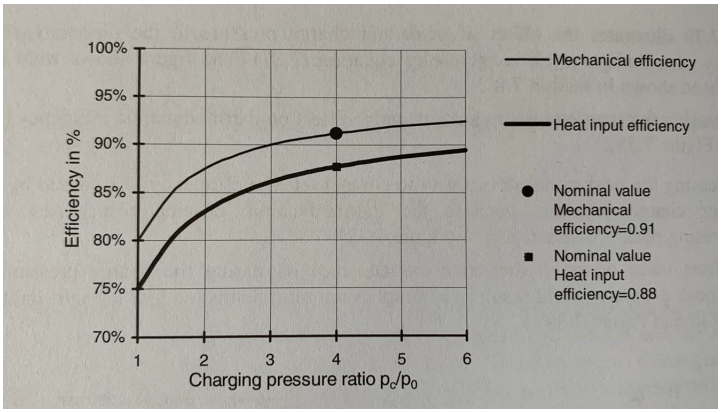

Figure 4.10: Typical mechanical efficiency of a diesel engine as function of the charge pressure, taken from [54]

load point, M10 shows that the mechanical efficiency increases slightly compared to F76. For M10, ignition is closer to TDC. The effective power in each load point is equal, thus the indicated power running on M10 must be lower compared to F76. This is also shown by the IMEP, which is slightly lower for M10 compared to F76. The mechanical efficiency for M20 is comparable to F76. Moreover, the IMEP of M20 was more or less equal to the values shown for F76. Indicated power is dependent on the pressure and volume of the cylinder in time. Therefore, the mean in-cylinder pressure of M20 must

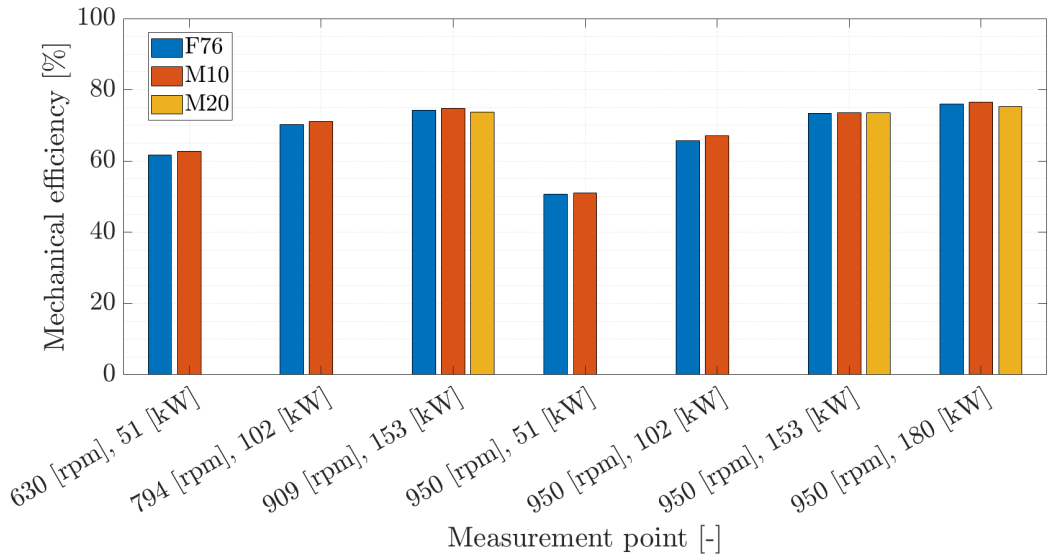

Figure 4.11: Result measurements: Mechanical efficiency [%]

be higher compared to M10 resulting in the higher mechanical efficiencies and IMEP that are obtained. This is a remarkable result in combination with the large ignition delay of M20.

4.5.7. Air consumption

Figure 4.12 shows the measured air excess ratio for all measurement points. The air excess ratio is

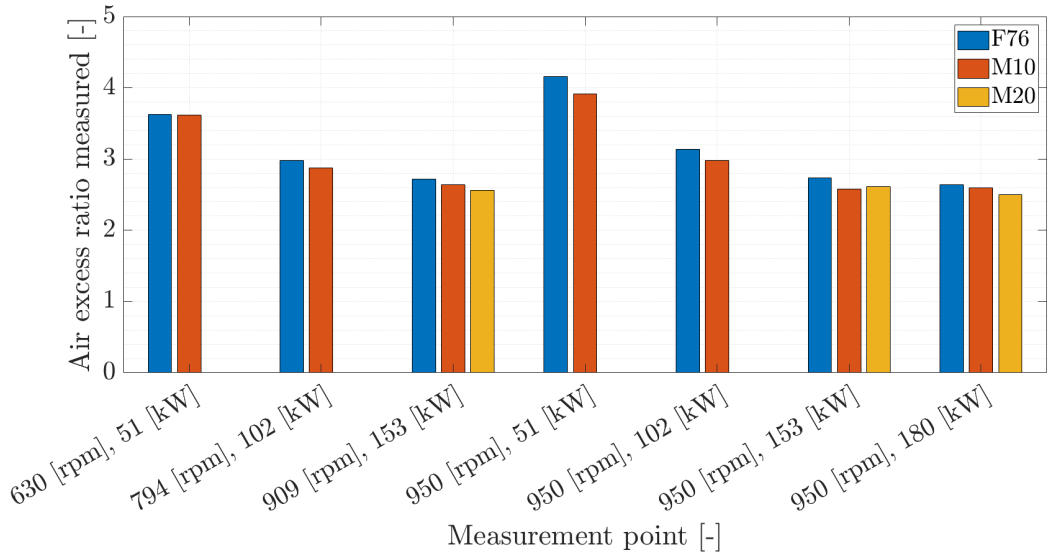

Figure 4.12: Result measurements: Air excess ratio [-]

the ratio between the measured AFR and the stoichiometric AFR. Observed is that the air excess ratio decreases when alcohol content increases, while the stoichiometric AFR of methanol is much lower compared to diesel fuel. The required stoichiometric AFR of M10 and M20 are calculated and shown in table 2.2. The measurement results show that the air consumption in kilograms per cycle of the engine is almost stable: only a small decrease of 2.9 [%] in air consumption is observed at 180 [kW] for M20 compared to F76. On the other hand, the fuel consumption increases with 23 [%] at 180 [kW] for running on M20. A decreased air excess ratio normally results in higher in cylinder temperatures

due to the rich air/fuel mixture in the cylinder [53].

The turbine of the engine depends on the engine speed and exhaust gas flow and could not manually be adapted to the requirements of the injected fuel. The result of this is that the engine barely changes the amount of supplied air, while the stoichiometric AFR and the fuel consumption do change. The almost constant air flow and increased fuel consumption seems to cancel each effect out. Expected was a large increase in air excess ratio due to the low stoichiometric AFR of methanol compared to F76. The fuel consumption results are discussed in section 4.5.8.

4.5.8. Fuel consumption

During the experiments, fuel consumption is measured with a flow meter. The lower heating value of methanol is much lower compared to F76 as shown in table 2.1. Reaching the same load point of the engine is only possible by increasing the fuel flow to the cylinder. An increase of fuel flow and specific fuel consumption were expected.

Figure 4.13 shows that the fuel consumption increases with higher methanol/diesel ratio. Each

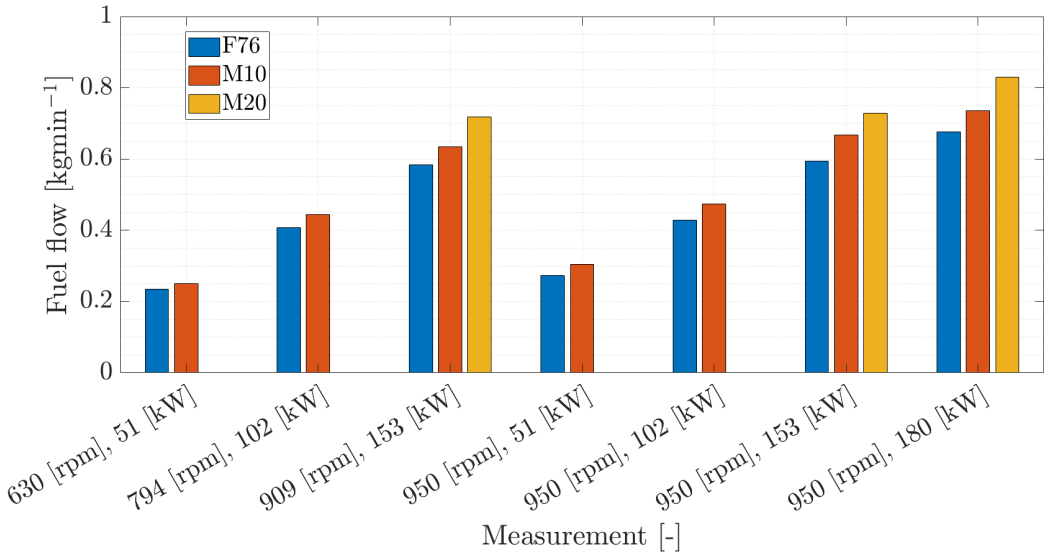

Figure 4.13: Result measurements: Fuel flow [kgmin^{-1}]

measurement point shows an increase in fuel consumption of 23 [%] while running on M20. Running on M20 at full load shows a higher fuel consumption compared to the expectation. The increase of fuel consumption based on the lower heating value was 22.0 [%] assuming constant efficiency. Engine efficiency decreased slightly for M20, resulting in a larger increase of fuel consumption. For M10, a fuel consumption increase of 8.5 [%] for 909 [rpm] is observed. This is less than the expected increase of 11 [%] based on lower heating value. The engine efficiency at this measurement point has increased by 2.3 [%] relatively compared to F76. The real fuel consumption of the engine is lower than the presented values in fig. 4.13. Fuel leakages are not taken into account by forming this values. Measuring the fuel leakage flow was impossible due to safety measures regarding toxic methanol vapor and its products. However, the fuel leakages are expected to be equal for each measurement point for each fuel and are expected to be negligible compared to the total fuel consumption. The fuel flow meter influences the results too. When the methanol/diesel blend is not mixed well, the density measured by the flow meter varies. Therefore, fluctuations in the measured fuel flow could appear. Those fluctuations were not noticed while analysing the data, but it can be a systematic error.

Evaluating engine performance is difficult when comparing results from different engines. Comparing exhaust gas parameters of different engines is mostly done by looking at specific parameters. A general applied parameter is the specific fuel consumption, which gives the fuel consumption in grams

per kilowatt per hour. Diesel engines usually operate most efficient at 80 [%] of the nominal engine load. For this engine, the nominal load specified by the manufacturer is not reached. Flow capacity limits of the mechanical injectors make it impossible to reach the nominal engine load with a high percentage of methanol in the fuel blends. Moreover, the time required to evaporate the methanol also affects the nominal engine load. The lower specified nominal load point from fig. 4.1 is around 60% of the nominal engine load in normal diesel operation. The low energy density of methanol decreased the maximum reachable power of the engine. Results for the specific fuel consumption are shown in fig. 4.14.

At low loads, the specific fuel consumption is higher compared to high loads. Methanol addition

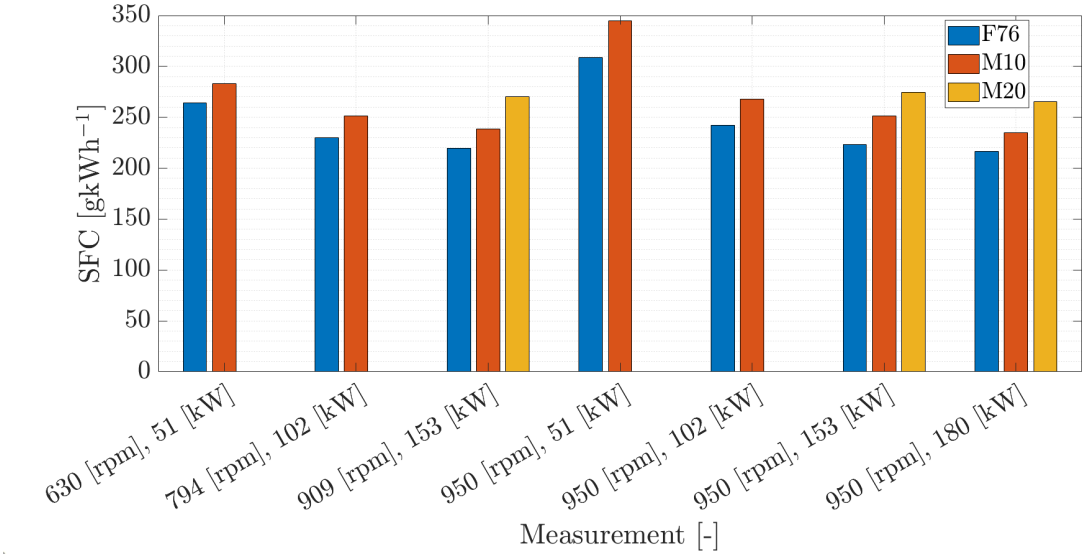

Figure 4.14: Result measurements: SFC [gkWh^{-1}]

to diesel fuel increases the specific fuel consumption of the engine with almost the same ratio as the fuel flow in fig. 4.13. Higher engine loads have a lower specific fuel consumption as expected from eq. (2.11). The same trend for the specific fuel consumption is observed compared to the fuel consumption in fig. 4.13: the specific fuel consumption of methanol/diesel blends is higher compared to F76.

4.5.9. Engine efficiency

The engine efficiency, also known as the brake thermal efficiency, is defined by the brake power measured on the engine shaft divided by the total energy injected by fuel. Each fuel type has its own lower heating value, which is included in this calculation. Therefore, the efficiency is calculated based on each fuel's lower heating value shown in table 2.2.

In section 4.5.8, it is concluded that the addition of methanol to diesel fuel increases the fuel consumption of the engine. The brake power per measurement point remained constant. Figure 4.15 shows that running on M20 leads to a decrease of the engine efficiency of 0.1 [%] at full load and 0.25 [%] at 153 [kW] and 950 [rpm]. M10 shows an increase in engine efficiency at five measurement points. At full load, M10 shows an increase of 0.84 [%] compared to F76.

Four times more energy is required to evaporate methanol compared to diesel fuel. Inherent to the heat of vaporization is the ignition delay. The combination of these two factors related to methanol could reduce the engine's efficiency. Preheating the methanol or adapting the injection timing could decrease the ignition delay and increase the brake thermal efficiency of the engine [55]. It must be noted that preheating methanol is challenging regarding the safety and its low boiling point. Methanol needs time to evaporate, injecting the fuel blend earlier gives the fuel more time to evaporate and could result in earlier SOC. Earlier start of combustion for high rates of methanol could increase the

mechanical efficiency and IMEP. While having earlier SOC running on M20, the engine is expected to operate more smoothly since ignition is closer to TDC. This will eventually lead to higher pressures and temperatures, which could change the mechanical and thermal loads as well as formation of harmful emissions.

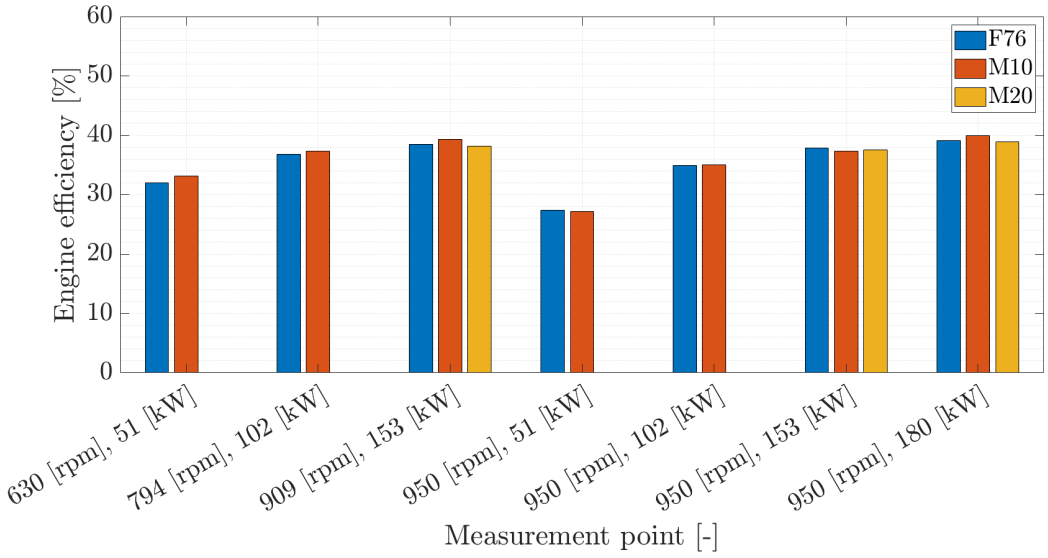

Figure 4.15: Result measurements: Engine efficiency [%]

4.5.10. Exhaust gas temperature

The exhaust gas temperature provides information about the combustion process. The temperature sensor is located behind the turbine. Energy from the exhaust gases is used by the turbine to drive the compressor. Therefore, temperatures of the exhaust gas at the outlet of the turbine are much lower compared to temperatures directly measured at the cylinder exhaust valve. However, a comparison between exhaust gas temperatures for different fuels can be made. In general, higher engine loads result in a higher exhaust gas temperature. More heat is released in the cylinder, which results in more indicated work. This is also visible in the exhaust gas temperature.

The measurements show that the air excess ratio reduced by an increased methanol/diesel ratio. This indicates that the air/fuel mixture became richer and contained relatively more fuel. Experiments show that the exhaust gas temperature slightly decreased by operating on higher alcohol content. It is questionable whether these temperatures provide a sufficient amount of information. One of the reasons is the position of the temperature sensor, which is not directly behind the exhaust valve. As a result, heat loss effects and the turbine have already decreased the temperature of the exhaust gases, which reduces reliability of the result. Furthermore, the accuracy of the sensor could influence the results, since the difference between the measured temperatures is not significantly large. However, it seems that the temperature appears to decrease a few degrees by increasing the blend ratio.

4.5.11. Discussion

This chapter provided a performance analysis of the experiments done on the MAN4L20/27 diesel engine. Firstly, the pressure signals for different cylinders and fuels were analysed. The fuel injector of cylinder one has a positive effect on the combustion of methanol/diesel blends. Generally, the effect of the heat of vaporization and low cetane number of methanol were observed. Higher methanol/diesel ratio's cause an ignition delay up to 8°CA longer compared to F76. Secondly, measurements obtained by the Kibox gave insight in the combustion duration of the measured fuel compositions. The combustion duration seems to decrease up to 12.7°CA for M20 compared to F76. The engine remained its

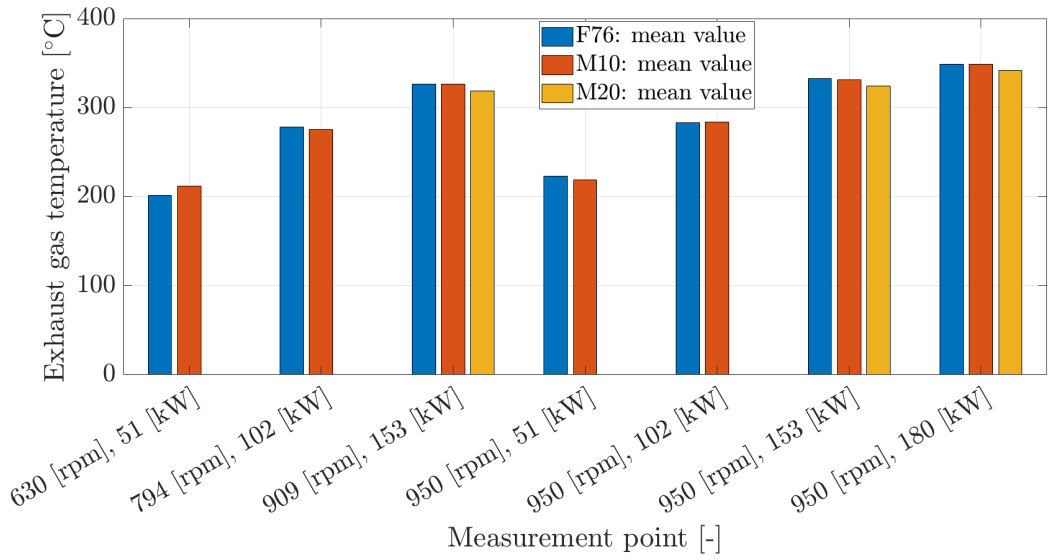

Figure 4.16: Result measurements: Exhaust gas temperature [°C]

brake power at the measurement points which were measured and thus shows only small differences in IMEP and mechanical efficiency. Furthermore, the air excess ratio decreased for running on M20 compared to F76. Less air could lead to rich fuel/air mixtures and thus to high combustion temperatures. Fuel consumption increased with 23 [%] for M20 compared to F76, which was expected from the lower heating values combined with the decreased engine efficiency. Finally, a plausible exhaust gas temperature decrease for methanol is observed. It must be noted that the exhaust gas temperatures are measured at the turbine outlet and already lost much of its initial enthalpy.

Different options are available to increase the engine performance running on methanol/diesel blends. Firstly, the temperature of the fuel injected could be increased. Total heat required to vaporize the fuel will be lower. However, methanol has a low boiling point and safety measures must be taken into account. More research on this is required before implementing this solution. Secondly, the time of injection should be shifted to give the methanol more time to evaporate. Expected is that the injection timing will affect the engines efficiency in a positive way. Furthermore, the size of the fuel droplets must be smaller compared to diesel fuel. In this way, the effective heat exchanging area of the fuel spray is increased resulting in higher evaporation rates. This could improve the operating envelope of the current dual fuel engine setup.

4.6. Emission analysis

This chapter analyses the the emissions measured by the Testo 350 (Maritime) gas analyser. Exhaust gas components are measured in parts per million volume [ppmv] in dry air. This is not a unit for exhaust gas emission comparisons between multiple engines. Therefore, the emissions are converted to specific power based units given in [g(kWh)$^{-1}$]. In this way, the unit does not contain more information then necessary and it is comparable to literature. Except for the oxygen emissions, all the presented emissions are given in [g(kWh)$^{-1}$]. Derived from unit conversion equations proposed in Stapersma, the specific emissions of each substance can be calculated by using eqs. (4.6) and (4.7) [53].

$$\mathrm{per_j} = \frac{\mathrm{ppmv_j^{dry}}}{10^3} \cdot \left(\lambda_{\mathrm{tot}} \cdot \sigma_{\mathrm{da}} + 1 - \frac{1}{2} \cdot \frac{\mathrm{M_{H2O}}}{\mathrm{M_H}} \cdot \mathrm{x_H^f} \right) \tag{4.6}$$

$$\mathrm{spe_j} = \frac{\mathrm{ppmv_j^{dry}}}{10^6} \cdot \frac{\rho_{\mathrm{j}}^{\mathrm{nom}}}{\rho_{\mathrm{g}}^{\mathrm{nom}}} \cdot \left(\lambda_{\mathrm{tot}} \cdot \sigma_{\mathrm{da}} + 1 - \frac{1}{2} \cdot \frac{\mathrm{M_{H2O}}}{\mathrm{M_H}} \cdot \mathrm{x_H^f} \right) \cdot \mathrm{sfc} \tag{4.7}$$

where per_j is the pollutant emission ratio of specific exhaust gas j in [gkg^{-1}]. Moreover, $\mathrm{ppmv_j^{dry}}$ is the measured concentration of the exhaust gas for dry air. $\mathrm{spe_j}$ is the specific emission of a measured exhaust gas. For both equations, the measurements are based on dry air. Also the normal densities of the exhaust gases ($\rho_{\mathrm{j}}^{\mathrm{nom}}$ and $\rho_{\mathrm{g}}^{\mathrm{nom}}$) are important for the specific emission calculations. Those values are taken from Stapersma [53].

4.6.1. Emission measurement accuracy

To get an indication for the expected exhaust gas emissions beforehand, the emissions resulting from complete combustion can be calculated before running the engine. Stapersma analysed the emissions for diesel fuel and proposed the equations for complete combustion of a fuel for given carbon, hydrogen and sulphur content [51]. The equation to calculate the amount of emissions per kilogram of fuel is shown in eq. (4.8).

$$\mathrm{mr_{CO_2}^{g-out}} = \frac{\mathrm{M_{CO_2}}}{\mathrm{M_C}} \cdot \mathrm{x_C^f} \tag{4.8}$$

Because complete combustion is assumed, only CO_2 can be calculated based on this method. The other measured parameters can not be compared to the theoretical values from these equations. CO is measured in the exhaust gases, which indicates that combustion in the engine is not complete. Also unburned hydrocarbons indicate whether combustion is complete or not. Therefore, the measured CO_2 emissions will be lower compared to the calculated values based on complete combustion. To check whether the emission analyser measures the right values, the calculated and theoretical values of carbon dioxide are compared in table 4.5.

According to Stapersma, the air excess ratio is calculated based on O_2 and CO_2 emissions. By using this method, an indication about the accuracy of the emission results can be obtained. Based on fuel consumption and air intake measurements, the air excess ratio is calculated in eq. (4.9). Based on CO_2, O_2 measurements, dry air properties and the fuel properties, the air excess ratio is calculated according to eqs. (4.10) and (4.11) [52].

$$\lambda_{\mathrm{measured}} = \frac{\mathrm{afr_{tot}}}{\sigma} \tag{4.9}$$

$$\lambda_{\mathrm{CO_2}} = \frac{\mathrm{M_{da}}}{\sigma_{\mathrm{da}}} \cdot \left(\frac{1}{\mathrm{y_{CO_2}^{da-out}}} \cdot \frac{\mathrm{x_C^f}}{\mathrm{M_c}} + \frac{1}{4} \cdot \frac{\mathrm{x_H^f}}{\mathrm{M_H}} \right) \tag{4.10}$$

$$\lambda_{\mathrm{O_2}} = \frac{\mathrm{y_{o_2}^{da-in}} - \mathrm{y_{o_2}^{da-out}} \cdot \frac{1}{4} \cdot \frac{\mathrm{x_H^f}}{\mathrm{M_H}} \cdot \frac{\mathrm{M_{da}}}{\sigma_{\mathrm{da}}}}{\mathrm{y_{O_2}^{da-in}} - \mathrm{y_{O_2}^{da-out}}} \tag{4.11}$$

where y gives the volumetric concentration of the measured gas in dry air and dry exhaust gas. The concentration oxygen in air is considered to be 21 [%]. The molar mass of dry air is 28.96 [kgmol^{-1}]. The results of the air excess ratios are shown in table 4.5. Based on these air excess ratios, the specific emissions for CO_2 are calculated. Fuel properties determine the maximum exhaust of the carbon dioxide emissions per kilogram fuel based on fuel consumption.

It is visible that the CO_2 emissions based on oxygen and the measured values are lower compared

Table 4.5: CO_2 exhaust gas emission concentration calculated with the air excess ratio based on CO_2 and O_2 emissions and from air and fuel consumption measurements. Measurement point: F76, 950 [rpm], 180 [kW]

Parameter	λ [-]	$\mathrm{per}_{\mathrm{CO_2,theory}}$ [gkg^{-1}]	$\mathrm{per}_{\mathrm{CO_2,measured}}$ [gkg^{-1}]	Rel. Difference [%]
CO_2	2.92	3170	3209	1.3
O_2	2.51	3170	2756	-15
Measured	2.62	3170	2877	-10

to the theoretical maximum emissions. One of the reasons for this is that incomplete combustion results in CO and unburned hydrocarbon emissions. However, these concentrations are not large enough to compensate the 15 [%] difference between theory and measurements based on oxygen shown in table 4.5. Moreover, the gas analyser has a tolerance of ± 2 [%].

The measured air excess ratio in table 4.5 shows a relative difference of 10 [%] to carbon dioxide exhaust emissions from theory. One of the reasons why this is happening because of the loss of fuel by fuel leakages. As already mentioned, the fuel leakages could not be measured. The amount of injected fuel is in reality thus smaller as has been measured. The measured air excess ratio is larger as in reality. Therefore, the difference between measurements and theoretical calculations increases.

It is hard to determine which value is actually the correct one. Varying results are obtained by looking at different parameters. The emission results analysed in this chapter are based on the measured air excess ratio. Not all the measurement points are evaluated in this chapter.
It is observed that after the emission calculation for each load point, a measuring error of the same size occured. Therefore, it is assumed that the difference between theory and practice is a systematic error. The relative differences between fuels at varying load points are comparable while dealing with a systematic error. However, the absolute value of the emissions could be higher.

4.6.2. NO_x and SO_2 emissions

Nitrogen oxides are considered to be harmful gases for the atmosphere and human bodies. Nowadays, reducing these emissions is of importance. The effect of methanol compared to F76 on the specific NO_x emissions is shown in fig. 4.17. The NO_x emissions measured contain components of NO and NO_2.

Figure 4.17 shows that the use of M20 reduces the nitrogen oxide emissions with 10.6 [%] at 180 [kW], 950 [rpm]. By running on a low load of 51 [kW] and 950 [rpm], using M10 shows a reduction of 14.2 [%] compared to F76. Each measurement point shows a reduction of NO_x of at least 2.9 [%] when running on methanol/diesel blends.
The reason why methanol reduces these toxic emissions is the cooling effect by the heat of vaporization. As been discussed in section 2.6.1, NO_x formation is dependent on time, temperature, oxygen and nitrogen available. The ignition delay caused by the low cetane number and heat of vaporization leads to a decrease of the in-cylinder temperature, which is obtained from the exhaust gas temperature. According to section 4.5.4, the combustion duration of methanol/diesel blends is shorter which indicates a reduced residence time at high temperatures.

The load points of 153 [kW] show more NO_x emissions for M20 compared to M10. An explanation is that the oxygen in methanol has participated in the combustion process [19, 48] . At specific points in the cylinder, higher temperatures can be reached which increases the formation of nitrogen oxides. Late ignition of M20 as shown in the pressure signal in fig. 4.5, creates a high heat release rate at the start of combustion causing high combustion temperatures.

A reduction of NO_x emissions was expected based on the lower exhaust gas temperatures measured for methanol/diesel blends. Unfortunately, literature shows divergent results for NO_x emissions. Dierickx mentioned an average decrease of 60 [%] of NO emissions for dual fuel operation with a substitution ratio of 70 [%] [11]. Sayin et al. and Jamrozik et al. concluded an increase in NO_x emissions for methanol/diesel blends [29, 48]. Equations and fuel properties shown for calculations of the specific

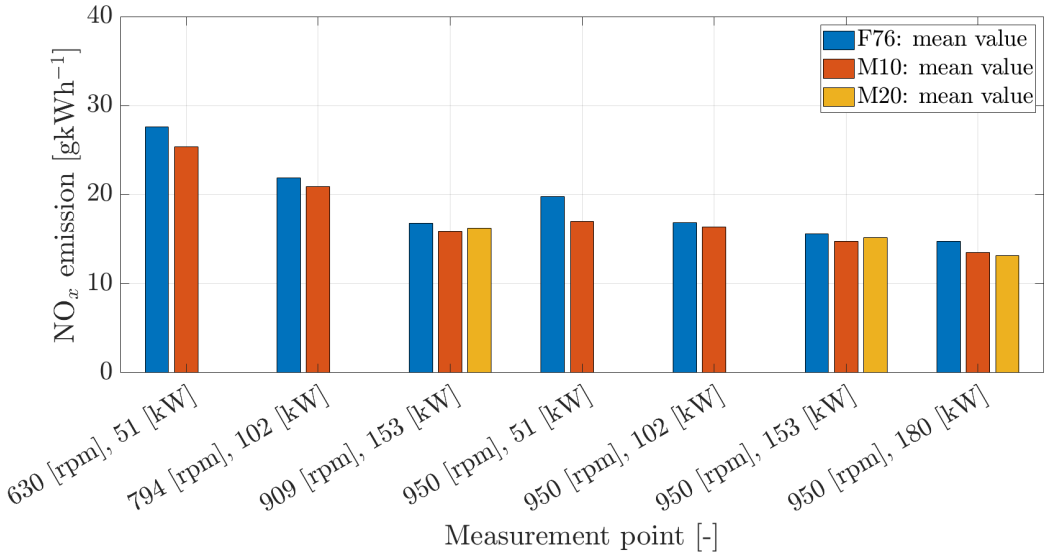

Figure 4.17: Result measurements: NO_x emissions

emissions are not shown in these papers. Choosing the correct stoichiometric air/fuel ratio and air excess ratio has an impact on specific emission calculations. For these calculations, the blend properties given in table 2.2 are used.

Sulphur content in diesel fuels is already low because of the strict emission regulation areas. According to its specifications, the emission measurement equipment is not suitable for measuring SO_2 emissions for fuels than contain less than 0.5 [%] sulphur. The sulphur content of F76 is lower than that limit. Adding methanol will only decrease the total sulphur content, because methanol does not contain it. Besides, results for this measurements were between 0-100 [ppmv], which is outside the measurement range of the sensor shown in appendix C. Therefore, the SO_2 emission measurement is irrelevant for this analysis.

4.6.3. CO and CO_2 emissions

Carbon monoxide emissions only exist if incomplete combustion took place. For a well operating engine, the CO emissions are usually low. The results for CO emissions are given in fig. 4.18. As expected, the specific CO emissions are relatively low compared to other exhaust gases. Methanol/diesel blends decrease the CO exhaust gas emissions which implements that the combustion process is more complete. More oxygen is available in the fuel, which could lead to increased combustion performance. Moreover, the oxygen content in methanol helps the CO to convert to CO_2 by contribution of the extra available oxygen to the combustion process. The carbon content in the fuel blends decreases for high methanol rates. This also leads to a decrease of the carbon monoxide. At 950 [rpm], 51 [kW], CO emissions show an increase. For both fuels measured in this point, the emissions were relatively high compared to the other load points.

CO_2 is one of the greenhouse gases that much maritime companies are trying to reduce. Methanol has a low carbon content which could help to decrease the carbon dioxide emissions. Beforehand, the expectation for CO_2 emissions was that it would decrease with an increased methanol/diesel ratio. Carbon content of methanol is much lower compared to F76 and automatically decreases the total injected carbon molecules per kilogram of blended fuel. Table 4.6 shows the total amount of carbon injected per hour in the engine based on fuel flow measurements. As can be seen, the total mass of carbon per kilogram fuel decreases when the methanol percentage increases. However, the fuel consumption of the engine increases due to the lower heating value of methanol. Taking fuel consumption into account, the total amount of carbon injected per hour only decreases by 1.7 [%] by injecting M20.

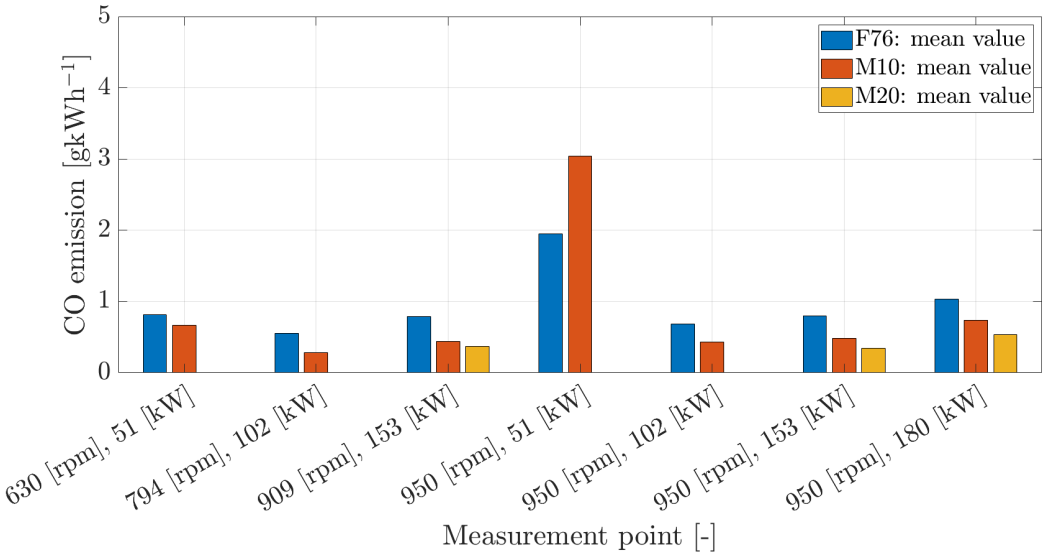

Figure 4.18: Result measurements: CO emissions

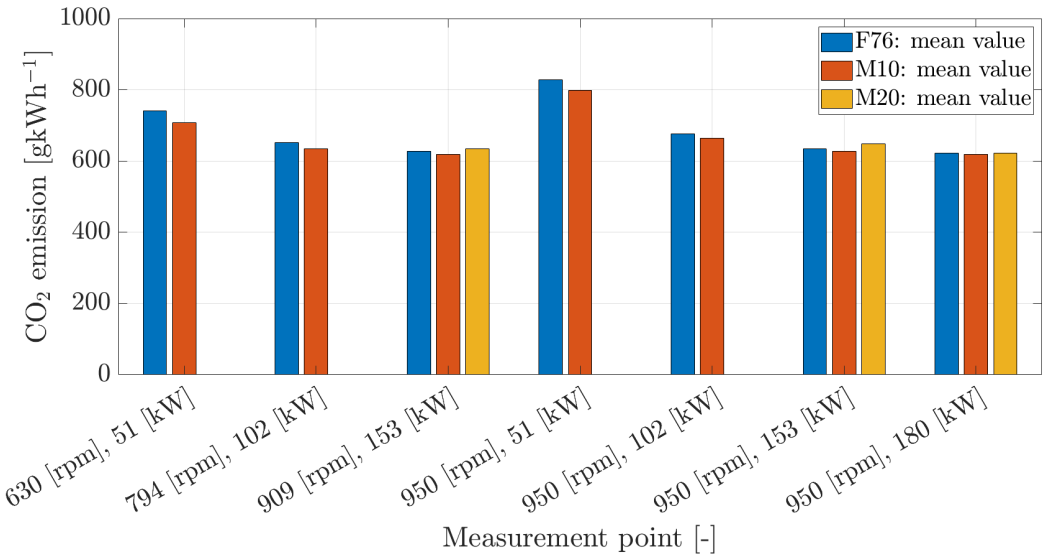

Figure 4.19: Result measurements: CO_2 emissions

Figure 4.19 shows the measurement results of carbon dioxide emissions. Using M10 shows a

Table 4.6: Carbon content per prepared blend, fuel flow per cycle based on 950 [rpm], 180 [kW]

Mixture	Mass percentage [%]	Fuel flow [kgh^{-1}]	Carbon flow [kgh^{-1}]
F76	86.6	40.68	35.2
M10	77.3	43.92	33.95
M20	69.7	49.68	34.62

slight reduction of 4.5 [%] at 630 [rpm] and 0.4 [%] at full load at 950 [rpm]. The use of M20 shows an increase in CO_2 emissions compared to M10, which was already expected by the amount of carbon injected based on the fuel consumption shown in table 4.6. Compared to F76, the emissions increase for 153 [kW] at both measured engine speeds. Only a small decrease 0.1 [g(kWh)$^{-1}$] is observed at

full load.

The total carbon flow is reduced by injecting the M20 fuel. A reason for the only small decrease of carbon dioxide emissions is that the oxygen content of methanol participates in the combustion process [48]. During combustion, the oxygen releases and is available directly for combustion compared to oxygen in the air. This phenomena is also related to the CO exhaust gas emissions, where a decrease was observed by using methanol/diesel blends indicating that the combustion process is more complete.

Another important parameter which has a large impact on the CO_2 emissions is the engines efficiency. Based on the results shown in fig. 4.15, the engine efficiency decreases with 0.1 [%] at full load conditions. Fuel consumption increases because more energy is needed for the required power output. Lower engine efficiency causes the fuel consumption to increase faster compared to the expectation based on the ratio between lower heating value of methanol and diesel.

Based on these results, it is not proven that the reduction of carbon dioxide is worth the investment in using methanol/diesel blends without adapting the engines parameters. The reduction of CO_2 is too low to meet the IMO requirements of a 50 [%] reduction in 2050 by only changing the conventional diesel fuel by methanol/diesel blends. However, the capability to produce methanol as a renewable fuel creates opportunities for methanol as an alternative fuel to conventional diesel fuel.

4.6.4. O_2 emissions

Data obtained about oxygen emissions give an indication about the combustion process. The more oxygen in the exhaust gases the less is used for combustion. Due to methanol addition to the fuel, more oxygen is injected into the cylinder. It is expected that this oxygen participates in the combustion process. Therefore, less oxygen from air is required.

The air excess ratio measured from air and fuel consumption, shown in fig. 4.12, decreases when methanol/diesel blends are used. Oxygen content in methanol is a possible reason why this is measured which has a lower stoichiometric air to fuel ratio. Moreover, the amount of fuel injected increased with higher methanol/diesel ratio's. Therefore the air to fuel ratio decreases, which means that the air excess ratio decreases too. Observed is that the O_2 emissions decrease by using M10 fuel. The main reason for this is the decreased air excess ratio, which automatically means that less oxygen enters the cylinder. In an improved scenario, the turbine capacity of the engine would have been changed to supply the exact amount of air required for combustion of methanol/diesel blends.

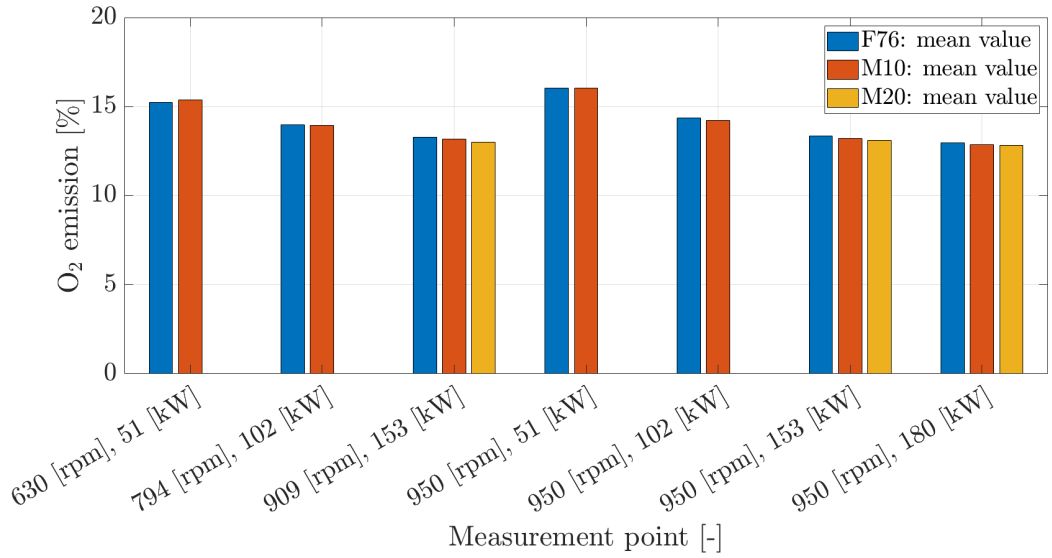

Figure 4.20: Result measurements: Engine efficiency [%]

4.6.5. Unburned hydrocarbons

This section discusses the unburned hydrocarbon measurements. Measurements are performed multiple times to check the repeatability of the measurements. It was for now concluded that the unburned hydrocarbon measurements are not repeatable. Different values per measurement point show an increase in C_xH_y independent of the load points during the day. The mean values of the C_xH_y measurements are given in fig. 4.21.

obtained from the results in fig. 4.21, the unburned hydrocarbon emissions increase by inject-

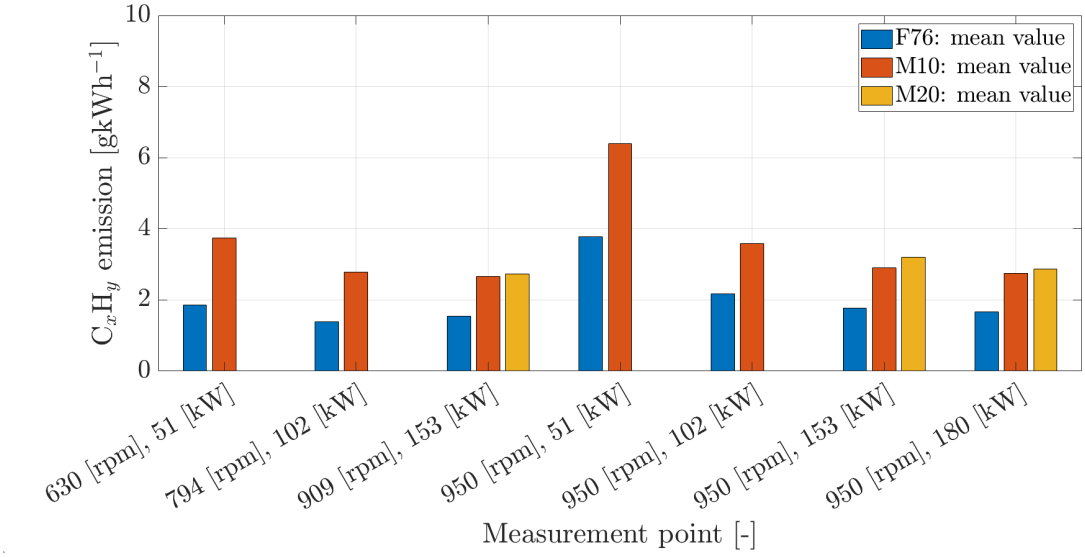

Figure 4.21: Result measurements: Unburned hydrocarbons emissions

ing methanol/diesel blends. However, as discussed earlier in section 4.4.3, the measurements were expected to be not representive. A reason for the high variation in the measurement data is that the exhaust gas hose was not heated, which normally should have been done. The effect is that unburned hydrocarbons could condensate against the hose walls and this causes measurement errors. This could declare the increase in concentration particles during the day. Another reason for the fluctuations is that the measured values were low in the sensors measurement range. The accuracy of the sensor was $\pm$400 [ppmv] while the sensor measured a maximum of 600 [ppmv]. Nevertheless, an increase of unburned hydrocarbons was expected based on literature [29]. The measurements show an increase when more methanol is injected.

4.6.6. Discussion

Emissions for F76, M10 and M20 are measured using the Testo 350 gas analyser. First of all, comparisons between the methanol/diesel blends and F76 showed that the specific NO_x emissions reduced for each measurement point between 2.9 and 14.2 [%]. Methanol's cooling effect and the short period of high temperature lead to this reduction. Secondly, the effect on the carbon dioxide emissions was small. The increased fuel consumption and thus number of carbon atoms injected reduces the effect of the low carbon content in methanol. Despite of the already low carbon monoxide emissions, in general the CO_2 emissions reduced by methanol/diesel blends compared to F76. The increased fuel consumption leads to an increase in oxygen consumption. The oxygen concentration in the exhaust gases decreased with 1 [%] at full load. Unburned hydrocarbons and sulphur dioxide measurements are considered to be unreliable. The measuring range of the sensors and low emission concentrations are the most important reasons for the inconsistent results for unburned hydrocarbons and sulphur dioxide.

Unburned hydrocarbons need to be measured again in future research. The effect of methanol

on the rate of unburned hydrocarbons is important to understand regarding the combustion efficiency. Correct measurements will provide a view on the completeness of the combustion process. Emissions of SO_2 were expected to be negligible. The sulphur content of F76 is low and methanol does not contain sulphur.

5 Analysis

This chapter describes the results of the injection, evaporation and single zone model. Each model is validated based on experimental values and connected to the single zone model. Effects of different fuel types are compared by the model's results. Moreover, section 5.4 discusses the effect of a different fuel injector on the combustion process.

5.1. Injection model analysis

This section provides the analysis of the mechanical injector model from Zeng [63]. A way to tune the model in order to match experimental data is described first. Secondly, the injection rate for the fuel blends is presented. The injected fuel flow is used for the fuel spray calculation.

5.1.1. Injection model results

Results from the injection model are used in the calculation of the fuel spray heat of evaporation. The injected volume flow into the cylinder is the most important result calculated by this model. The main goal of calculating the injection rate is to simulate the injected fuel in a proper way.

In order to get the right fuel flow into the cylinder, the model results are matched to experimental data. Adapting the model to the different fuels is done by adjusting the viscosity and density values according to table 2.2. The tuning parameter used to match the model output to experimental data is the nozzle discharge coefficient. From literature, as shown in fig. 3.5, it is known that the discharge coefficient must be lower than 0.8 [45]. However, for this model, the discharge coefficient was higher in order to reach the desirable fuel flows compared to the experimental data. The main reason for the high discharge coefficient is related to the lack of knowledge on the injector parameters, which are not exactly known. Therefore, spring constants and diameters are assumed, which affects the model's accuracy. More research into the injector parameters and required pressures and resistances in the system is needed to model the injector more accurate.

Density and viscosity changes of the fuel were insufficient to keep the discharge coefficient below unity. In order to simulate the right fuel flow for the methanol/diesel blends, the calculation of the fuel rack position is adjusted. The fuel flow running on methanol/diesel blends increases for a given load. Therefore, the relation between the effective power and fuel rack position changes along with this. Based on engine data, the fuel flow is known for the maximum fuel rack position. Based on a linear relation between power and measured fuel consumption for M10 and M20, the fuel rack position is calculated. In this case, assumed is that the efficiency at each measurement point from table 4.2 is equal. The equations for the fuel rack positions for different fuels are given in eqs. (5.1) to (5.3).

Table 5.1: Injection model tuning parameter: nozzle discharge coefficients at different engine load and speed per fuel

Fuel	Engine speed [rpm]	Engine Load [kW]	Discharge coefficient [-]
F76	909	153	0.85
F76	950	153	0.86
F76	950	180	0.91
M10	909	153	0.95
M10	950	153	0.99
M10	950	180	1
M20	909	153	0.94
M20	950	153	0.94
M20	950	180	0.98

$$\mathrm{RACK}_{\mathrm{F76}} = 5.95 \cdot 10^{-2} \cdot P + 5.28 \tag{5.1}$$

$$\mathrm{RACK}_{\mathrm{M10}} = 5.25 \cdot 10^{-2} \cdot P + 6.28 \tag{5.2}$$

$$\mathrm{RACK}_{\mathrm{M20}} = 7.69 \cdot 10^{-2} \cdot P + 4.07 \tag{5.3}$$

where P is the brake power of the engine. The fuel rack position varies from zero to 28 [mm] and per fuel type dependent on the measured effective power and fuel consumption. The position of the fuel rack is now determined for each fuel type more accurately. Discharge coefficients used to tune the model remain high compared to fig. 3.5. Despite of many assumptions, the model is able to simulate the correct amount of injected fuel flow into the engine. Table 5.1 shows the used nozzle discharge coefficients to tune the model to experimental values.

The comparison between the fuel injection from the model and the experiments is shown in table 5.2. Using the discharge coefficient, the fuel injection from the model is tuned to the experimental data as shown in table 5.2. The amount of fuel injected simulated by the model does not differ more than 2 [%] from the experimental data. The differences are sufficient for this research, because the aim for using this model is to simulate the correct amount of fuel injected.

The differences in efficiency are visible in the discharge coefficients of M10 between 909 and 950 [rpm] at 153 [kW]. The efficiency at 153 [kW], 909 [rpm] is almost 3 [%] higher compared to the same load point at 950 [rpm], which is shown in fig. 4.15. The fuel consumption is lower when having higher efficiencies at the same load point. This leads to the difference in discharge coefficients for two different engine speeds and same loads running on M10 fuel.

Table 5.2: Injection model versus experimental values: injected fuel volume

Fuel	Speed [rpm]	Load [kW]	Model [10^{-6} m^3]	Exp. [10^{-6} m^3]	Rel. difference [%]
F76	909	153	0.3742	0.3780	1.0
F76	950	153	0.3678	0.3691	0.4
F76	950	180	0.4195	0.4213	0.4
M10	909	153	0.4120	0.4141	0.5
M10	950	153	0.4127	0.4170	1.0
M10	950	180	0.4540	0.4450	2.0
M20	909	153	0.4723	0.4711	0.3
M20	950	153	0.4577	0.4583	0.1
M20	950	180	0.5209	0.5192	0.3

The results from the injection model are shown in figs. 5.1a to 5.1c. The injection starts at 4°CA bTDC for each cycle. For high load, it is shown that injection takes more time what comes with a higher

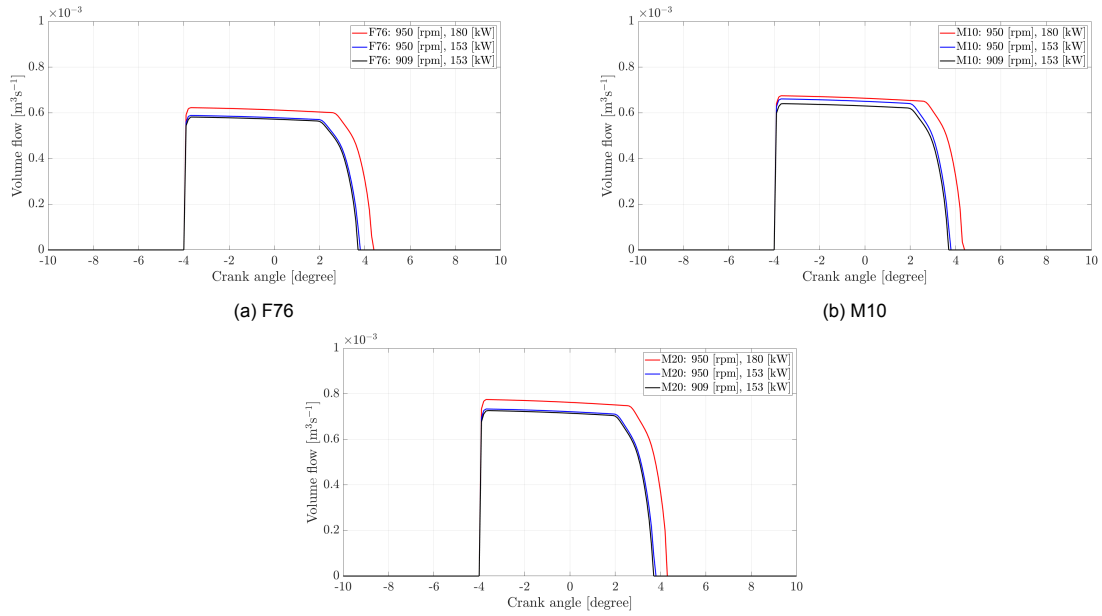

(a) F76

(b) M10

(c) M20

Figure 5.1: Fuel injection rate calculated by the injection model for each fuel type at three measurement points

injection rate. This effect was expected because the fuel injection is load dependent. Signals shown in figs. 5.1a to 5.1c are implemented in the calculation of the heat of vaporization of the fuel spray.

5.1.2. Discussion

The results from the injection model are discussed in this chapter. It is proven that the model is able to predict the fuel flow injected dependent on the fuel rack position and engine load. Assumptions of injector parameters and unknown density and viscous effects during the injection process cause that the model is tuned with surreal tuning values. The fuel rack position is determined for each type of fuel by a linear relation between fuel consumption and engine load. Tuning is done by using the discharge coefficient of the injector nozzle with values smaller or equal to one. For this thesis, the results are sufficient to simulate the fuel injection rate.

More research to the viscosity and density effects in mechanical injectors could help to understand the faced tuning problems in this model. Another way to improve this model's accuracy is to implement the physical properties of the fuel injector. For this model, detailed data is unknown.

5.2. Vaporization model analysis

This section discusses the results from the evaporation model built for methanol and diesel fuel. Diesel fuel is represented as decane, which shows comparable properties compared to diesel. Moreover, chemical properties of decane were available from REFPROP and experimental data is obtained from literature. At first, the model is verified by comparing modelling results and experimental data for decane and methanol. After that, simulation results are presented. In the end, the connection between the evaporation model, injection model and single zone model is described and the results are shown.

5.2.1. Validation

This section describes the model validation of the single droplet evaporation model for methanol and decane fuel. Validation is done by simulating equal environmental parameters as was found in literature written by Miller et al. [43]. Figure 5.2 shows the experimental and modelling results for decane coming

from literature and the result from the developed evaporation model based on Borman et al. [9]. The experimental initial droplet diameter was equal to 2 [mm]. During evaporation, the droplet diameter decreases because the droplet loses mass. In the figure, the droplet initial diameter is 2 [mm] and the environmental air temperature is 1000 [K] at atmospheric pressure. Moreover, the initial Reynolds number is equal to 17. The evaporation model shows that it produces comparable results to the rapid

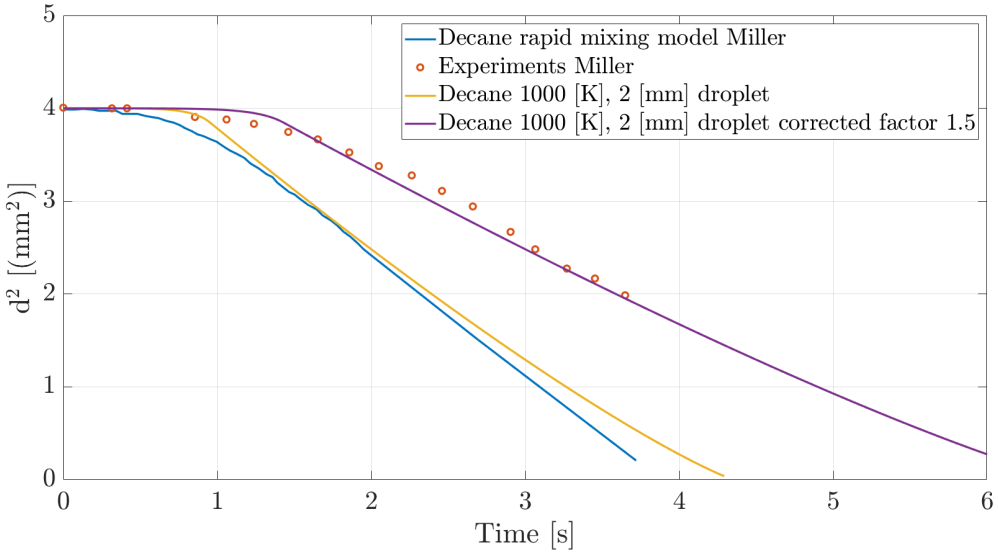

Figure 5.2: Verification of the droplet evaporation model for decane. Experimental data taken from Miller et al. [43]

mixing model of Miller et al. [43]. The initial heating period of the droplet is defined as the time before the droplet reaches its boiling point. After reaching the boiling point, the droplet's area decreases linearly in time. In the model, assumed is that conductivity is infinite, which results in a smaller heating up period of the droplet. The diameter's slope after the initial heating period is comparable to the experimental data. A multiplication factor of 1.5 can be applied to the model in order to match it with the experimental data.

In a diesel fuel spray, droplet diameters are much smaller compared to the validation data. The model must be matched to experimental values to be sure that the model is giving the correct results. Therefore, a dimensional analysis of the parameters involved in the droplet's initial heating period is performed. The dimensionless number describes the relation between the droplet diameter and the heating period. Furthermore, the dimensionless number could be used to fit the model to experimental data for different start diameters.

The initial heating up period of a fuel droplet depends on multiple parameters. The most relevant parameters are considered to be as follows: k_f, ρ_f, d_0, T_d and t. The initial heating period of the droplet is dependent on the droplet's diameter. Due to temperature differences in and outside the droplet, a temperature gradient appears as a function of the distance into the droplet. Moreover, the density and diameter of the droplet determine the volume of the droplet to be heated. Using these parameters, a dimensionless number is derived from these parameters. The number gives a description of the relation between the droplet's heating time and diameter. Note that there are multiple dimensionless numbers possible to describe this relation when using other variables. The parameters involved in this number shown in eq. (5.4) are seen as the most important involved during the initial heating period of the droplet. The result of the dimensionless analysis is shown in eq. (5.4). The complete determination of eq. (5.4) is discussed in appendix E.

$$t_\mathrm{h} \propto \left(\frac{\rho_\mathrm{f} \cdot d^4}{k_\mathrm{f} \cdot T_d}\right)^{\frac{1}{3}} \tag{5.4}$$

where t_h is the time that represents the initial heating period of the droplet, ρ_f the fuel density, d the droplet diameter, k_f the conductive heat transfer coefficient of the droplet fuel and finally T_d the droplet temperature. The time for heating up the droplets is written as shown in eq. (5.5).

$$t_c = 1 + (t_0 - 1) \cdot \left(\frac{d}{d_0}\right)^{\frac{4}{3}} \tag{5.5}$$

where t_0 is the correction factor of 1.5 applied to the rapid mixing model shown in fig. 5.2. t_c represents the correction factor applied to the time. d_0 is the droplet diameter of 2 [mm] used in the verification of the model. The theoretical range of this scaling process is $1 < t_c < \infty$. However, when d_0 increases, the droplet diameter is too large to be interesting for this research. The value of t_c can not be lower than unity, because the temperature inside the droplet can not be higher than the environmental temperature in the diesel engine. The scaling factor t_c from eq. (5.5) is considered as a correction factor to the time vector in the model in order to represent results that are comparable to the results of the experiments at a given initial droplet diameter. The results are shown in table 5.3.

Table 5.3: Correction factor evaporation model for different initial droplet diameter

Initial diameter [μm]	**Correction factor (t_c) [-]**
1	1.0000
10	1.0004
20	1.0011
50	1.0036
100	1.0092
500	1.0788
2000	1.5000

Table 5.3 shows the correction factors to the model of Borman for decane. It is shown that according to this method, the effect of infinite conductivity to the initial heating period of small droplets is negligible compared to applying finite conduction in the model. Conductive heat transfer always exists in the fuel droplets, but the effect of conductivity strongly decreases when having small droplet diameters.

For a liquid sphere undergoing convective heat transfer from its surroundings, the Biot number (Bi) determines if the temperature gradients in the droplet are negligible. This is the case when Bi is smaller than 0.1, as shown in eq. (5.6) [9, 44].

$$\mathrm{Bi} = \frac{\tilde{h} \cdot d}{k_s} \leq 0.1 \tag{5.6}$$

For a typical diesel fuel droplet of 10 [μm], the Biot number is $7.7 \cdot 10^{-3}$. Implicating that for droplets inside the diesel engine the thermal conductivity and thermal gradient effects can be ignored. This is also in line with the data shown in table 5.3. This data also shows that the model results in an almost negligible correction factor to the heating period of the droplet at droplet sizes smaller than 100 [μm].

The model for methanol evaporation is equal to the decane model, except for the fuel properties. The results for methanol are validated on experimental data for methanol vaporization. The experimental results shown in fig. 5.3 are measured by using a furnace with a methanol droplet in it. The droplet diameter change during evaporation is monitored by using a high speed camera [59]. Not all parameters regarding the experimental setup are given in literature. Lack of knowledge about the experiments found in literature gives an uncertainty for comparison with the models. For future research, it is recommended to perform fuel droplet evaporation experiments. In that way, all variables and environmental factors during the experiments are known, which prevents uncertainties for the authors.

The velocity and maximum temperature of the droplet have a large impact on the evaporation results. Since authors of literature including experimental results do not always mention the surrounding

air velocity, it was set on zero in the model for methanol validation. However, the droplet velocity is in the simulations not equal to zero, because it is injected in the engine with a certain speed. Adapting the droplet velocity results in a faster evaporation rate. Velocity is defined in the Reynolds number, which has an impact on the convective heat transfer coefficient. The relation between the velocity and convective heat transfer coefficient is described by the Nusselt number as shown in eq. (3.29).

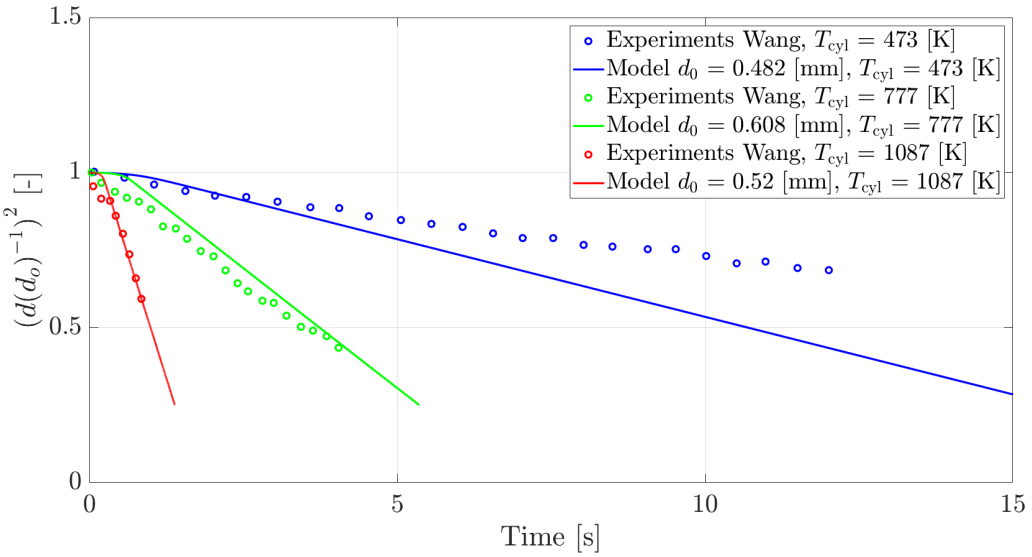

Figure 5.3: Validation for the model simulating evaporation of methanol compared to experiments executed by Wang et al. [59]

Figure 5.3 shows the evaporation time and the dimensionless diameter of the droplets for different starting diameters and environmental temperatures. The model simulates the evaporation rate at constant cylinder temperature. The correction factor applied to the evaporation model for decane, as shown in eq. (5.5), could not be used for the methanol model. The correction factor for decane is not sufficient for simulating the correct evaporation time of methanol droplets. Therefore, eq. (5.5) is adapted to apply it to the model of methanol and is shown in eq. (5.7).

$$t_{c,m} = \text{constant} + (t_0 - 1) \cdot \left(\frac{d}{d_0}\right)^{\frac{4}{3}} \tag{5.7}$$

where $t_{c,m}$ is the correction factor for the heating period of methanol evaporation. This parameter is used as a tuning parameter to match the model with experimental data. Tuning for methanol is done by adapting the value of constant in eq. (5.7) to 10. The assumption that the infinite conductivity effects are captured by the dimensionless number are not valid for the methanol model. The effect of the dimensionless number applied to methanol is small compared to the number applied to the evaporation of decane.

At lower environmental temperatures it is expected that the heating period of the droplets increases due to a smaller temperature difference between the droplet and surrounding air. As a result, the temperature gradient inside the droplet is smaller. Therefore, lower environmental temperatures leads to larger correction factors for infinite conductivity models applied to methanol evaporation. More specific research to this topic is needed to understand the in-depth principles of methanol evaporation. A disadvantage for this analysis is that experimental data on methanol evaporation is rare.

The results from the model are matched with the experimental results for sufficient large environmental temperatures for engine applications. According to former single zone model results by running on diesel fuel, the temperature is expected to be around 700 [K] at the moment of ignition. Therefore, the inaccurate results on the environmental temperature of 473 [K] are less of importance for the

evaporation of methanol in the diesel engine.

5.2.2. Droplet size variation

Multiple droplet sizes appear in a diesel engine. In the fuel spray, the droplet size distribution is variable due to droplet interactions and the evaporation process. Therefore, the evaporation processes of droplets start at different initial droplet sizes. The effects of different initial droplet sizes are shown by simulations of the model. The injection speed is set as a constant and is seen as a mean spray velocity of 100 [ms^{-1}] based on an typical initial injection speed of 200 [ms−1] [9]. This value varies for each injector and engine and is hard to measure directly. Since the spray dynamics are not taken into account, a mean value is taken. This parameters have an influence on the fuel spray and its physical and thermodynamic processes.

For methanol, the settings of the model are crucial for in simulations of the evaporation process. If methanol is limited to the boiling point, the droplet diameter decreases as shown in fig. 5.5. Less time is needed to evaporate a decane droplet compared to methanol, which is shown in fig. 5.4. In

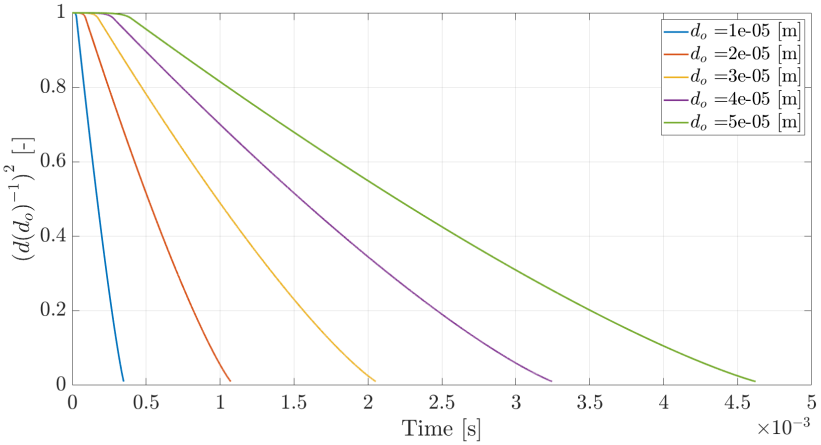

Figure 5.4: Diesel: Dimensionless droplet diameter at constant temperature and pressure of 700 [K] and 1 [bar] respectively, for a variable initial droplet diameter. Injection speed is set to 100 [ms^{-1}]

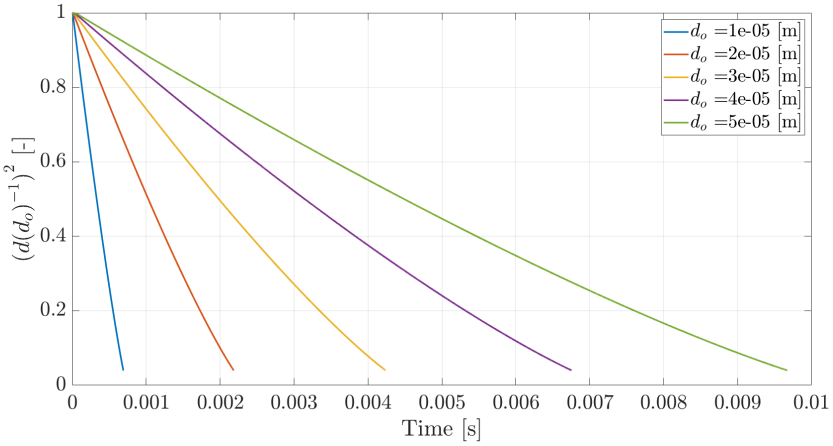

Figure 5.5: Methanol: Dimensionless droplet diameter at constant temperature and pressure of 700 [K] and 1 [bar] respectively, for a variable initial droplet diameter. Injection speed is set to 100 [ms^{-1}]

figs. 5.4 and 5.5, it is shown that the evaporation time of methanol is almost two times less compared to decane. The figures show that the heating period of decane is larger compared to methanol, caused

by the higher boiling point. Important to notice is that the decrease in droplet diameter does not follow the d^2-law exactly caused by the injection speed. When giving the droplets a velocity, the Reynolds number of the droplet varies during the evaporation process.

The initial heating period of methanol is faster due to the lower boiling point compared to decane. The slow evaporation rate of methanol after the initial heating period is related to the energy required to evaporate the fuel. The evaporation process takes more time due to this high heat of vaporization, which is not in advantage of the current diesel engine setup. The large heat of vaporization leads to a larger temperature decrease of the surrounding air in the cylinder compared to diesel fuel. Figures 5.6

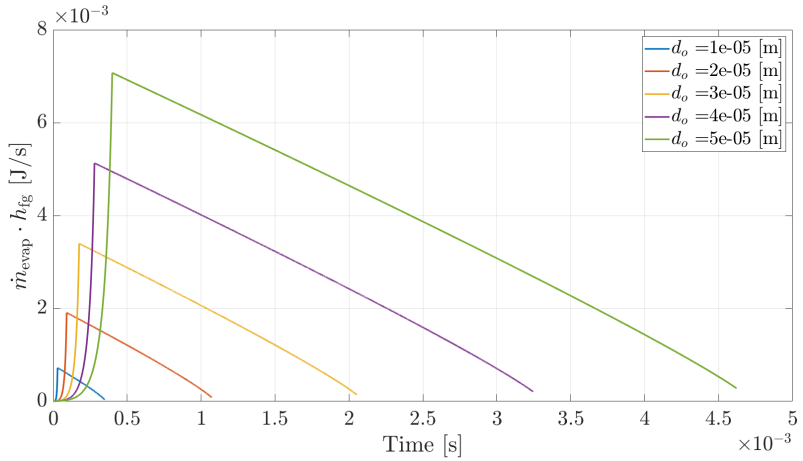

Figure 5.6: Diesel: Heat of vaporization at constant temperature and pressure of 700 [K] and 1 [bar] respectively, for a variable droplet diameter. Injection speed is set to 100 [ms^{-1}]

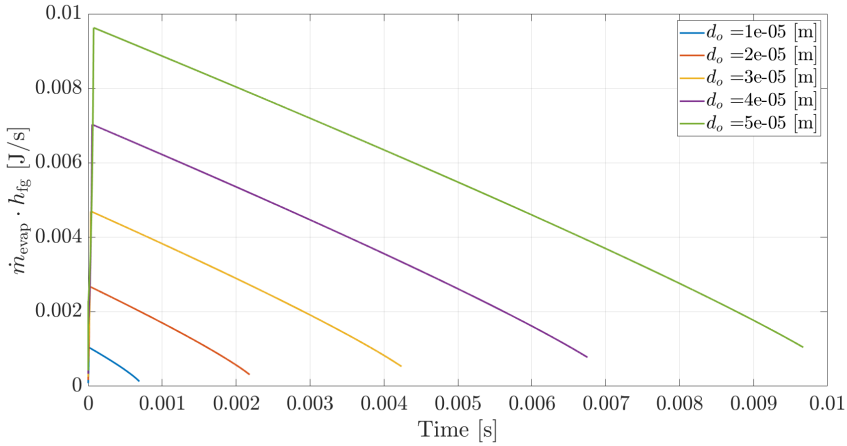

Figure 5.7: Methanol: Heat of vaporization at constant temperature and pressure of 700 [K] and 1 [bar] respectively, for a variable droplet diameter. Injection speed is set to 100 [ms^{-1}]

and 5.7 show the heat required for evaporation for decane and methanol for varying droplet sizes. At first, during the initial heating period the rate of heat supplied to the droplet increases. After the moment that the boiling point is reached, the droplets start to vaporize and the diameters start to decrease. This causes the effective heat exchanging area of the droplet to decrease too. The total heat of vaporization and convective heat needed to evaporate the outer layer of the droplet also decreases due to the smaller droplet area.

The total heat required to vaporize the droplets of methanol is larger compared to decane, which could also be seen in the fuel specifications in table 2.1. This envelope is important for implementation of the methanol evaporation heat in the single zone model. The total evaporation heat does not only

consist of the heat of vaporization. The surrounding air in the cylinder is also affected by the convective heat subtracted by the fuel droplets, resulting in a temperature drop. Figures 5.8 and 5.9 show

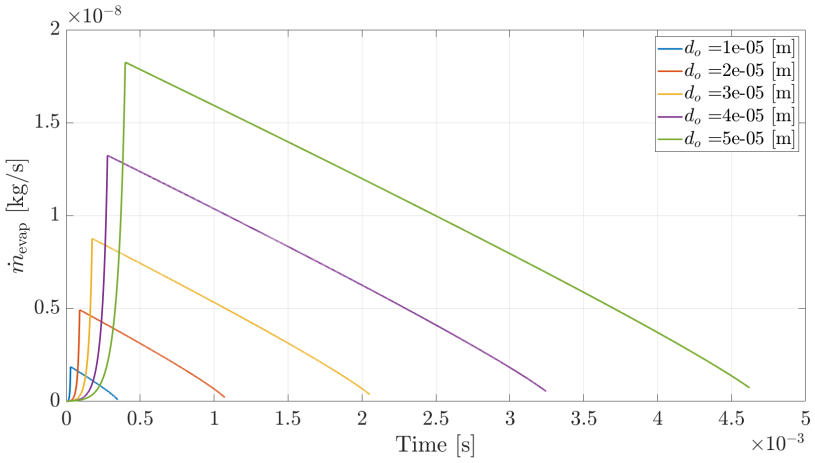

Figure 5.8: Diesel: Evaporation rate at constant temperature and pressure of 700 [K] and 1 [bar] respectively, for a variable droplet diameter. Injection speed is set to 100 [ms^{-1}]

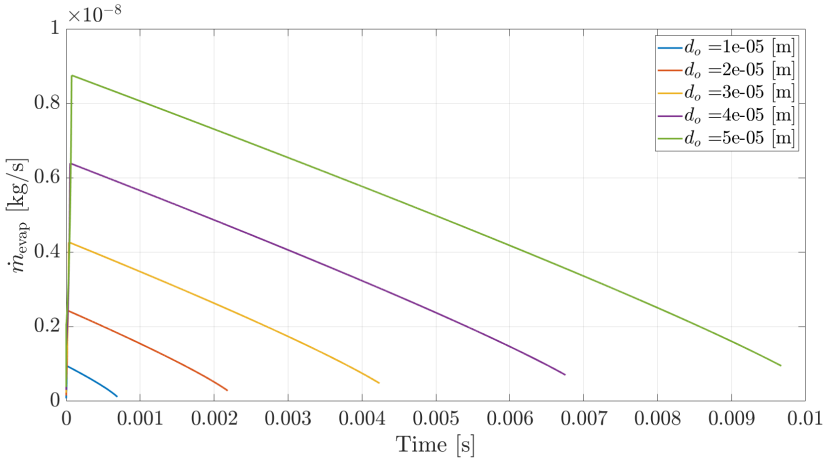

Figure 5.9: Methanol: Evaporation rate at constant temperature and pressure of 700 [K] and 1 [bar] respectively, for a variable droplet diameter. Injection speed is set to 100 [ms^{-1}]

the evaporation rates of methanol and decane. The evaporation rate of methanol is slower compared to decane. The slow evaporation rate is a trade off between the boiling point and the heat of vaporization for each different alcohol. For methanol, the heat of vaporization is large enough to keep the evaporation rate relatively low compared to decane.

The sum of the heat of vaporization and the convective heat transfer of methanol is used to calculate the evaporation heat for the fuel spray. From the evaporation model results, it is expected that the amount of energy required to evaporate methanol is larger compared to diesel fuel. Moreover, the evaporation time of methanol droplets is longer due to the higher latent heat of vaporization.

5.2.3. Model connection: heat of vaporization of a fuel spray

During fuel injection, the fuel droplets enter the cylinder and each droplet undergoes its own evaporation process. For implementation of this method, some important assumptions are made to simplify the calculation of the fuel spray. In reality, the fuel spray has multiple different sub processes and droplet interactions appear. For instance, turbulence effects in the spray are neglected. Moreover, vapor in

the cylinder does not affect the vaporization process of other droplets. Droplets are also assumed to consist of pure fuel components.

For this calculation method, the evaporation process of the droplet is pre-calculated by the evaporation model. The heat of vaporization of each droplet is calculated at a constant cylinder temperature of 700 [K] at an atmospheric pressure. The temperature is assumed based on pure diesel fuel simulations. Moreover, it is assumed that the droplets do not influence each others evaporation process and the infinite vapor pressure in the cylinder is zero. The evaporation model simulation is stopped at the point where 90% of the droplet's mass is evaporated. Otherwise, the evaporation rate reaches infinity, which causes numerical problems.

The injection model provides the injection rate of the fuel into the cylinder, which is multiplied by an assumed number of droplets per time step as calculated in eq. (3.27). The number of droplets per time step are depending on the assumed droplet size. After injection, fuel droplets break up into smaller droplets as discussed in section 3.7.1. This fuel atomization phase is neglected by assuming a SMD for each droplet. The SMD is explained in section 3.7.2. There are multiple equations that can be used to determine the droplet size inside the fuel spray. However, the equations used are based on diesel fuel and require information about the injector nozzle. For methanol, specific equations to determine the SMD are not found in literature. Since the spray behaviour can not be measured in the current experimental setup, it is unknown how the fuel injectors will react to methanol/diesel blends. The effect of viscosity and density of alcohol fuels on fuel sprays still needs to be investigated. Therefore, the assumption for the initial droplet size is based on typical values for diesel fuel [9].

The droplet size is used to tune the results for evaporation losses and to see the effect of different droplet sizes in the fuel spray. Figure 5.10 gives the heat of evaporation of methanol calculated by the energy losses due to evaporation by the equation of Ding in eq. (3.40). The spray calculation from the evaporation model for different droplet sizes are compared to the result calculated by Ding [12].

Figure 5.10 shows that the droplet diameter of 25 [μm] gives the best representation of evapora-

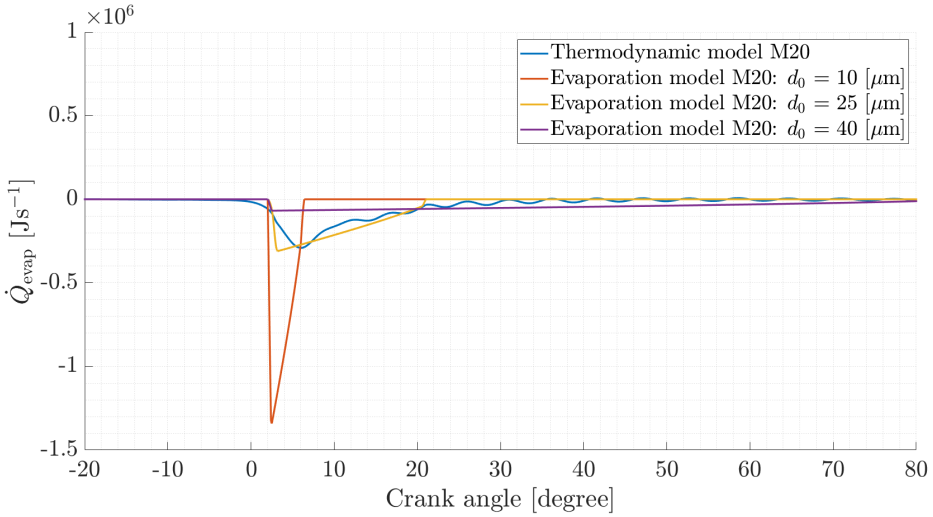

Figure 5.10: Evaporation heat calculated by thermodynamic relation proposed by Ding compared to the spray calculation based on the evaporation model.

tion heat compared to Ding's method. One of the disadvantages of the model is that the mass balance in the single zone model is still the driving parameter for calculation of the total heat of vaporization of the fuel. Therefore, as can be seen, evaporation losses are not directly measured after the start of injection. The evaporation heat is shifted to the right position in the model where combustion starts. This is also related to the fact that the combustion reaction rate is equal to the evaporation rate in the model. Since the evaporation rate of methanol is lower compared to diesel fuel, neglecting the dwelling

time of fuel droplets may not be valid in the dual fuel single zone model.

In fig. 5.10, the effect of the droplet size is indicated. By decreasing the droplet diameter, the effective heat exchanging area of the fuel spray increases. More heat is transferred to the droplets directly after injection and evaporation rates increase. By using a larger droplet diameter, the evaporation rate is lower compared to the smaller diameters. The evaporation process for large droplets does not match with the combustion rate. This result shows that the droplet size influences the evaporation speed. One of the main problems in the current experimental diesel engine setup with methanol is the evaporation time. This is shown while conducting the experiments, where the engine was not able to run on M20 at low loads. The temperature of the engine is too low to evaporate the methanol droplets completely, resulting in misfires due to slow evaporation.

5.2.4. Discussion

The results of the evaporation model described in this chapter are divergent. Decane evaporation is corrected by a relatively small dimensionless number to match experimental values. The modelling results of methanol deviate more compared to the experimental results. The time to evaporate methanol droplets is longer compared to decane. For the current experimental diesel engine setup, this could be a problem for large amounts of methanol. Without adjusting the current setup, large amounts of methanol could lead to bad combustion properties.

An assumption for the mean droplet size based on diesel fuel is applied due to lack of experimental values regarding methanol droplet sizes in a diesel engine. Moreover, the droplet size is used to match the model results to the method of Ding [12]. The results for the different droplet sizes is as expected: smaller droplets evaporate faster.

The proposed method to take the evaporation heat of methanol into account needs improvement during future research. A disadvantage of the proposed method to calculate the heat of vaporization of methanol is that the evaporation process is still dependent on the combustion rate from the single zone model. The ignition delay can not be described well by using this method. Neglecting the dwelling time of fuel droplets does not seem to be valid for injecting methanol droplets, due to the longer evaporation times. Another point of improvement required is the fuel spray calculation. In this research, a simplified sum of fuel droplets based on the injection rate is used to calculate the evaporation heat. Droplet interactions and environmental changes in the fuel spray must be taken into account to gain clear insights in this process. By using a detailed fuel spray model combined with a ignition delay calculation, it is expected that the simulations will be more accurate. Implementation of this detailed sub models in the single zone model could provide better in-cylinder information for dual fuel operation. To verify the models, recommended is to conduct experiments on fuel spray behaviour of dual fuel engines.

5.3. Single zone model analysis

Until now, the single zone model did not contain information regarding the evaporation heat of methanol. The results from the evaporation model provide a first insight in the effect of methanol in the cylinder. By means of the heat release calculations based on the measured pressure signals, important parameters from the single zone model for each fuel are compared. Among other things, an important parameter regarding diesel engine combustion is heat release, which is the amount of heat released from burned fuel. Moreover, temperature is important with reference to emissions and thermal load of the engine. The reaction coordinate, which is the normalised burned fuel mass, gives an indication about the start of combustion and whether the model calculates the correct values based on measured fuel consumption or not.

After analysing the pressure signal of each cylinder, differences are obtained between cylinder one and cylinder two, three and four. The results of the pressure signals are described in section 4.5.2. Cylinder one has a different fuel injector compared to the other cylinders. The effect of different fuel

injectors is expected to be visible in the heat release analysis. The mean pressure of cylinder two, three and four is used in the analysis of the single zone model to be representive for the engine. However, the differences obtained for the different cylinders are described in a complementary section. This chapter provides an analysis of the results from the single zone model, including the effects of different engine speeds, cylinder comparisons and a sensitivity analysis.

5.3.1. Heat release

The heat release rate provides important information about the combustion envelope. The way that heat is released has impact on the engines efficiency. Heat release is divided in three phases: premixed combustion, diffusive combustion and late combustion. Premixed combustion is characterized by the steep peak at the start of combustion. Fuel vapor starts to ignite and releases immediately much of its total heat. High heat release ratios cause the temperature to rise quickly, which increases formation of harmful emissions as NO_x. After the premixed combustion, remaining fuel burns during the diffusive combustion, which is normally less impulsive. Sometimes, late combustion takes place where the remaining fuel is burned.

A comparison between the $GAHRR$ of the experiments with F76 and methanol/diesel blends is given in fig. 5.11 for the mean of cylinder two, three and four. F76, M10 and M20 show different heat

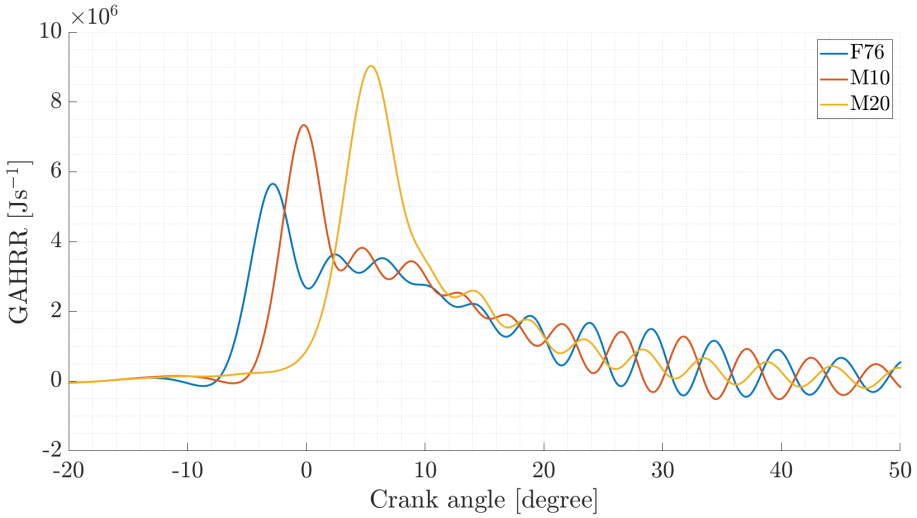

Figure 5.11: $GAHRR$: F76, M10 and M20. 950 [rpm], 180 [kW] for the mean of cylinder two, three and four.

release rates. For F76, the premixed combustion phase is shown before TDC. Ignition starts as expected before TDC for diesel operation. The premixed combustion is followed by a strong diffusive combustion from 0 to 20 °CA. Late combustion is shown in the last part of the heat release, which is only a small part for F76 combustion.

M10 has an ignition delay caused by the evaporation heat and bad ignition properties of methanol. However, fuel in the cylinder has more time to form a combustible air/fuel mixture resulting in a larger premixed combustion peak. More fuel burns simultaneously after ignition, resulting in large heat release rates. Pressure in the cylinder is increased close to TDC by compression and ignition, resulting in higher temperatures. The diffusive combustion is short compared to diesel fuel, since a larger percentage of the fuel is burned during the premixed combustion.

Heat release for M20 has a different shape compared to F76, which was expected according to literature [29]. Heat release from M20 features itself by the large and delayed premixed combustion peak. The evaporation heat and bad ignition properties of methanol causes the fuel to ignite after TDC. Clearly, almost all of the total heat is burned during the premixed combustion. Diffusive combustion is only detected in a short period between 9 and 12°CA. Heat release rates as been seen for M20 have a large ignition delay resulting in steep heat release rates after combustion starts. During this

short period, temperatures increase to high maximum values. Thermal loads and formation of harmful emissions could increase during this period of high temperatures. The total time of high temperatures is short due to the decreased combustion duration, which is shown in fig. 5.12.

The methanol/diesel blends in general show a larger premixed combustion heat release rate compared to F76. Diffusive combustion has a shorter time period and ignition delay increases with increasing methanol ratio. High heat release rates increase the mechanical load on the engine and could result in high temperatures and NO_x formation. The largest heat release ratio is seen by M20, where 35 [%] of volume methanol is injected. An increase of the methanol ratio decreases the combustion duration according to the heat release curves. At high methanol ratio's, the premixed combustion phase is dominant and the heat release rate hardly has a diffusive combustion phase.

Measurement results found in literature showed that the heat release rate increased up to a volumetric alcohol rate of 25 [%] [29]. Heat release curves from M20 simulations shown comparable shapes. Since the experimental setup of the engine in literature is different from the current experimental setup, heat release rates could decrease at higher volumetric ratios. The experiments done on the MAN 4L20/27 were limited to M20 due to a technical failure of the power supply safety switch. Therefore, increasing the methanol ratio to find the limit of the engine was not possible. Besides, the moment that this decrease in heat release occurs is engine dependent. Running on M20, ignition was not possible for low engine loads, which is in that case comparable to literature.

The heat release rate has influence on the engines efficiency. For efficient engine operation, the ignition should take place close to TDC to indicate maximum work during the expansion stroke. When having a large ignition delay as shown by M20, the piston already moves in downwards direction without being pushed by the in-cylinder pressure. The crank angles without combustion aTDC are considered as an efficiency loss. However, the engine efficiency of M20 was hardly affected by the late ignition and even improved with 0.1 [%] compared to F76, as shown in fig. 4.15.

5.3.2. Temperature

The temperature calculated by the single zone model is the mean cylinder temperature. The mean temperature does not provide information about the local hot and cold area's in the cylinder. Temperature is an important indicator for the formation of harmful emissions. The mean in cylinder temperature can provide first information about the in cylinder temperature differences. For F76, M10 and M20 the in cylinder temperatures are compared at full load for the mean of cylinder two, three and four. The results are shown in fig. 5.12.

F76 compared to the methanol/diesel blends shows that the mean maximum temperature of F76

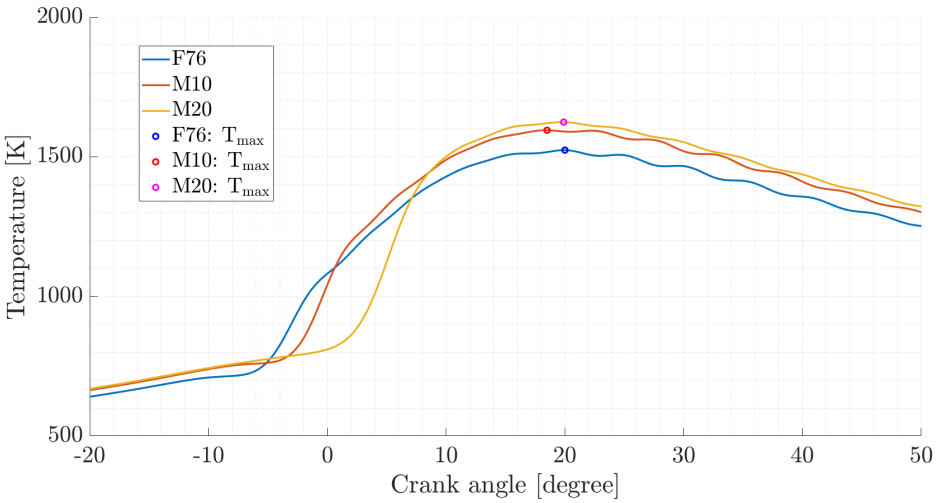

Figure 5.12: Temperature: F76, M10 and M20. 950 [rpm], 180 [kW] for the mean of cylinder two, three and four.

is lower. Ignition delay of F76 is shorter and the temperature rise is starting directly after injection. The temperature increases fastest after ignition, which is related to the heat release curve in fig. 5.11. Premixed combustion of F76 releases the most heat to the system with a temperature rise as a result. M10 ignites later in the cycle and immediately reaches higher temperatures after ignition compared to F76. The maximum mean temperature rises up to 1600 [K]. The cooling effect of methanol is visible during the ignition delay of M10. Despite of the cooling effect, the temperature rises rapidly due to the high heat release rate. The air/fuel mixture has had much time to mix to a combustible mixture and ignites mostly in the premixed combustion. High temperatures appears and the mean temperature during the diffusive combustion phase is around 90 [K] higher compared to F76.

M20 shows the largest cooling effect of methanol. Ignition of M20 is after TDC and the cylinder temperature is up to 7°CA aTDC at a lower point compared to F76. Temperature rises quickly due to the large heat release in the premixed combustion phase. Moreover, fast combustion in a short period increases the temperature significantly even though the late ignition. M20 shows a maximum mean temperature of 1625 [K], which is higher than M10 and F76.

Maximum in-cylinder temperatures are shown in fig. 5.12 for the different fuels. Running on M20 increases the maximum in cylinder temperature with 100 [K]. The position in time of the maximum temperature occurs 0.1°CA earlier for M20 at 19.9°CA after TDC compared to F76. M10 reaches its maximum temperature fastest at 18.5°CA after TDC. The rapid combustion and high heat release curves for methanol/diesel blends ensures that the maximum temperature is reached at a comparable time as F76 does. Furthermore, the mean temperature in the cylinder is correlated to NO_x formation. Not only temperature, also the residence time at high temperatures affects the NO_x formation during a cycle. From the NO_x results, it is shown that the measured specific emissions of NO_x decreased by injecting methanol. Although the mean temperature of the methanol/diesel blends was significantly higher according to the model, the total time at high temperatures to form NO_x was shorter compared to F76.

With the current engine and model setup, the residence time at high temperatures is relatively low for methanol/diesel blends compared to F76. Improving the fuel injectors and adapting the injection timing has the result that the evaporation process of methanol will be more efficient. Start of combustion will be earlier and the cylinder volume at that time is smaller. However, assuming that the heat release curve for methanol remains in its current shape, it is plausible to result in higher temperatures. The formation of NO_x is important to monitor when improving the injectors of the engine.

Important to note from these temperature results is the difference in experimental and model results. The high in-cylinder temperature regarding methanol/diesel blends was not expected according to literature and experiments [11, 29]. Some parameters in the model might not be described well for methanol, which could cause these differences. One of these parameters are the Woschni parameters. The heat exchange parameters of Woschni are widely used for diesel fuel, but the effect for dual fuel operation is not investigated in this research. Moreover, the residual exhaust gas composition have an impact at the mean temperature. Furthermore, the ignition delay is not described properly in the model, while the pressure signal does contain this information. This leads to a mismatch between the calculations and the physical information from the pressure signal. The TDC-shift has a large effect on the model results, which is discussed in section 5.6. Finally, exhaust gas temperatures appear to be lower according to the experiments, which makes it questionable whether these calculated temperatures are correct or not.

According to the model, the mean temperature is higher for higher methanol ratio's for the mean of cylinder two, three and four. This result is counter intuitive compared to the experiments of the exhaust gases. Cylinder one, which has a different fuel injector, has other ignition properties compared to cylinder two, three and four as shown in section 4.5.2. The pressure signal is the input of the model and could influence the model's results. Therefore, the results of the different cylinders are analysed in section 5.4. The combustion in cylinder one might be more representative for dual fuel operation in a compression ignited engine.

5.3.3. Reaction Coordinate

The reaction coordinate calculated in the single zone model is the ratio between the burned and total injected fuel. When the RCO reaches unity, all the fuel injected is burned. From the RCO, start of combustion is visible at the point where the curve intersects the x-axis. Comparison between the measurement data from the Kibox and the model results give an indication about the accuracy of the model. Figure 5.13 gives the RCO for the different measured fuels. The RCO for the fuel blends is calculated separately for methanol and F76. The RCO's of F76 and methanol are shown independently for the blended fuels and are the mean of cylinder two, three and four. Figure 5.13 gives the RCO of both fuel components to give insight in the model's inaccuracies. Resulting RCO figures in this thesis are represented as the mean RCO for both fuels. Note that the underlying differences as shown in fig. 5.13 are still there in that results.

According to the Kibox, 5 [%] of the fuel injected was burned at -3.5°CA aTDC, which is considered

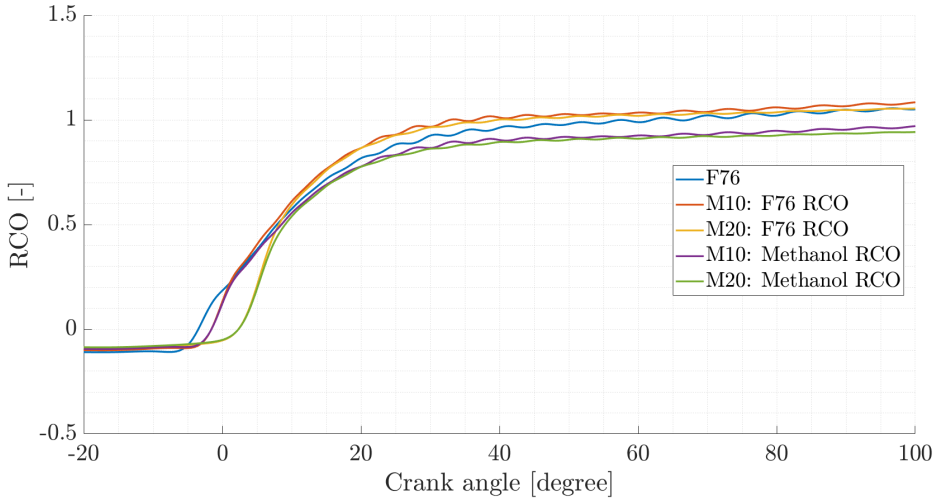

Figure 5.13: RCO for F76, M10 and M20. 950 [rpm], 180 [kW]

as start of combustion. From the model, the RCO crosses the x-axis at -3.5°CA aTDC for F76, which is equal as expected from the Kibox. The Kibox results show that the end of combustion is located at 76.5°CA, which is 90 [%] of total fuel burned. The model gives that 90 [%] of the burned fuel is reached at 28°CA. The total combustion duration of the single zone model is 73.5°CA for F76. The diffusive and late combustion phase elapse slow for F76 according to the model. The last 10 [%] of the fuel is burned during 42°CA. At the end of the simulation, the model has a RCO of 1.06 [-]. This implicates that the total fuel burned is larger than the actual injected fuel.

Combustion duration is defined equal to the values from the Kibox, which is between 5 and 90 [%] of total combustion.The start of combustion for M10 from the Kibox is located at 0.9°CA bTDC. According to the model, start of combustion is located at -1.6°CA aTDC, which is 0.7°CA earlier compared to the Kibox. The combustion duration of M10 is 69.8°CA, indicating a decrease of 3.7°CA compared to F76. The combustion duration of M20 is 5°CA shorter compared to M10. The start of combustion for M20 differs 2.1°CA between the model and the Kibox and starts 2.3°CA aTDC.

Observed is that the total combustion duration of the model is different from the Kibox's results. Reason for this is that the Kibox does not take heat losses into account. The Kibox calculates the NAHRR and ignores heat losses to the cylinder walls. Nevertheless, the results from the Kibox and the model should give the same trends for combustion duration. Combustion duration reduces by methanol/diesel blends, which is shown by the Kibox and the model as well.

The RCO of each fuel could not reach unity in the same simulation. This is a inaccuracy caused by a combination of several factors in the experiments and from the model. During experiments, a delay between the combustion process and data capturing could appear. Inaccuracies for the position

of the pressure signal are expected to be small, but small differences could result in large fluctuations in the model. Moreover, the fuel blend composition was not visible after the fuel pump. Fluctuations in the mixture composition are not excluded. One of the models possible shortcomings is the heat loss calculation by Woschni. The parameters used for Woschni are based on diesel fuel, while methanol probably has different heat loss characteristics. Separate fuels are defined for the heat release calculation with only one mean Woschni calculation. Another reason is that the fuels heat release properties are calculated separately. Furthermore, incomplete combustion could be a result of the bad auto ignition properties of methanol. The increase in measured unburned hydrocarbons could be an indication of incomplete combustion. Despite of that, it is hard to measure the combustion efficiency and it is not sure that the result of the unburned hydrocarbon measurement is reliable. In case of a decreased combustion efficiency, the RCO of the fuel components could be lower than unity.

The RCO is strongly dependent on the TDC-shift applied to the pressure signal. Before SOC, the RCO is -0.1 [-], which is not real. According to literature, the RCO should be zero before injection starts [22, 51]. Between SOI and SOC, the RCO should be negative due to fuel evaporation. An increased methanol/diesel ratio was expected to increase the negative RCO between SOI and SOC. The method to calculate the methanol and diesel combustion could be insufficient for heat release analysis of diesel methanol mixtures. A new method must be found to fix these problems. One of the options is to use mean values for the fuel parameters in the model, instead of parallel combustion of two components. The assumption of miscibility is stronger while using the mean parameters for the fuel's energy, stoichiometric air to fuel ratio and reaction coordinates.

5.4. Cylinder performance comparison

This section provides a comparison between cylinder one and the other cylinders of the engine. The effect of the different fuel injector of cylinder one is analysed by using the single zone model. The differences are discussed with the analyses of the GAHRR, temperature and RCO. To keep the overview in the report, appendix H shows the separated cylinder heat release comparisons per fuel. References to these figures are done, however the signals shown in figs. H.1a, H.1b, H.2a, H.2b, H.3a and H.3b contain the same information as the figures in appendix H. Pressure signals per cylinder are shown in appendix A.

5.4.1. Cylinder comparison: F76

F76 is the fuel normally used in the diesel engine. Noticed from the raw pressure signals shown in appendix A, cylinder one has a slightly earlier ignition compared to the other three cylinders. Heat release comparison in fig. 5.14a shows that the premixed combustion phase in cylinder one has a lower heat release rate compared to the mean of cylinder two, three and four. However, the higher heat release rate in the diffusive combustion phase causes the temperature of cylinder one to be higher for this load point, which is indicated by fig. 5.14b. Differences in the RCO are hardly obtained between the different cylinders, except for the ignition timing visible in fig. 5.14c. For F76, operating with different fuel injectors does not seem to have a large impact on the engines performance. It must be noted that the pressure signal of F76 is smoothed to reduce differentials in the signal. The smoothing process could cause inaccuracies in the heat release rates shown by the single zone model.

5.4.2. Cylinder comparison: M10

According to the single cycle pressure signals shown in appendix A, measurements show that the ignition time of cylinder one is earlier compared to the other three cylinders. By means of the parameters from the single zone model, the effect of the earlier start of combustion is analysed for M10.

Cylinder one shows an earlier and a lower heat release peak in fig. 5.15a. The diffusive combustion phase is longer compared to the mean of cylinder two, three and four. The remaining energy in the fuel which is not burned in the premixed phase, is burned more smoothly in the diffusive phase. Lower heat release rates are expected to result in lower in-cylinder temperatures. This is indicated by

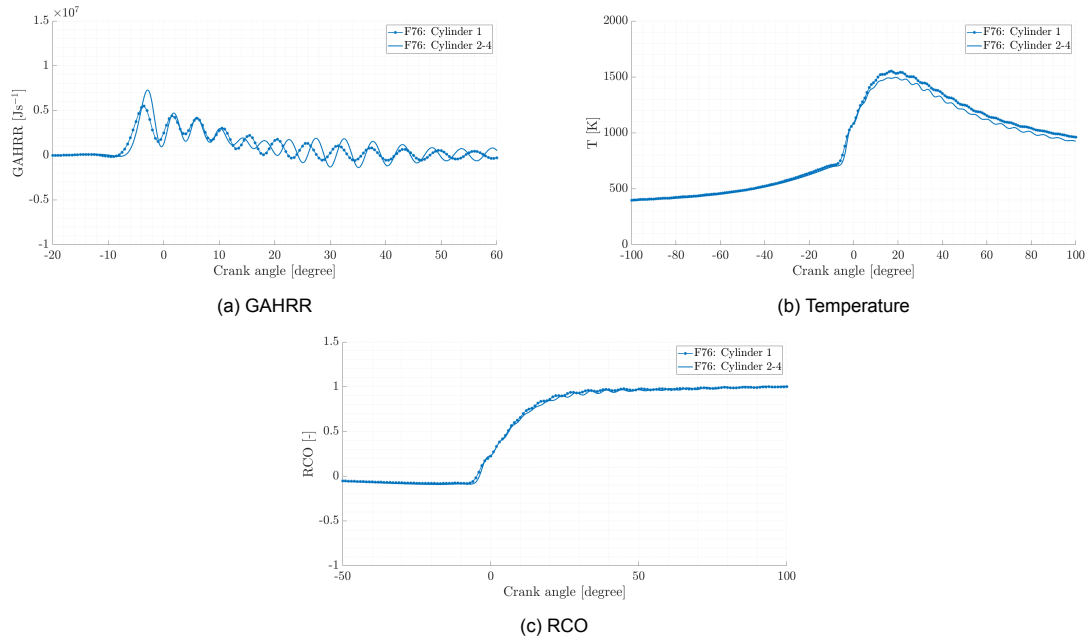

(a) GAHRR

(b) Temperature

(c) RCO

Figure 5.14: F76: : Cylinder one vs. the mean of cylinder two, three and four of single zone model results at 909 [rpm], 153 [kW]

fig. 5.15b. Temperature starts to rise first for cylinder one and the smooth diffusive heat release causes the temperature to rise less quickly compared to the temperature obtained for the mean of cylinder two, three and four. The RCO in fig. 5.15c shows that during the high heat release peak for cylinder two, three and four it overtakes the RCO of cylinder one. This is a sign of a higher combustion rate in the premixed combustion phase.

The ignition delay is important for the combustion process in a compression ignited engine. An increased ignitiond delay gives fuel more time to mix with air and results often in high heat release rates [53]. Lower heat release rates with a wide diffusive combustion phase operate more smoothly, which decreases the thermal load on the engine. Cylinder one shows the most desirable combustion properties for operating on M10 blends compared to the mean of cylinder two, three and four.

5.4.3. Cylinder comparison: M20

Figure 5.16a shows the heat release rates for M20 at 909 [rpm], 153 [kW] for the different cylinders. The shorter ignition delay for cylinder one has a large effect on the heat release rate. Methanol is not evaporated completely, which decreases the heat release rate in the premixed combustion. Diffusive combustion only appears in cylinder one. Late start of combustion in the mean of cylinder two, three and four gives the methanol more time to evaporate and mix with air. The late ignition causes a large heat release rate in the premixed combustion and almost burns all the fuel available in this phase.

The differences in heat release between the cylinders are comparable as seen by M10. A large ignition delay leads to high heat release rates and thus high thermal loads. The maximum temperature as shown in fig. 5.16b is lower for cylinder one. Also the RCO of M20 is comparable to the effect seen by M10. After the premixed combustion of cylinder one, the RCO in fig. 5.16c is overtaken by the mean of cylinder two, three and four due to its high premixed combustion heat release rate. The time the fuel has to mix with air and to evaporate before ignition mainly causes the effect of a short combustion duration. Cylinder one ignites earlier compared to the mean of cylinder two, three and four. This results in smooth heat release rates and lower temperatures. In this way, thermal load and formation of harmfull emissions could reduce. At low loads, cylinder two, three and four showed difficulties to ignite. The fuel injector of cylinder one is expected to increase the operating envelope of the engine on methanol/diesel blends if it is installed at all the cylinders of the engine.

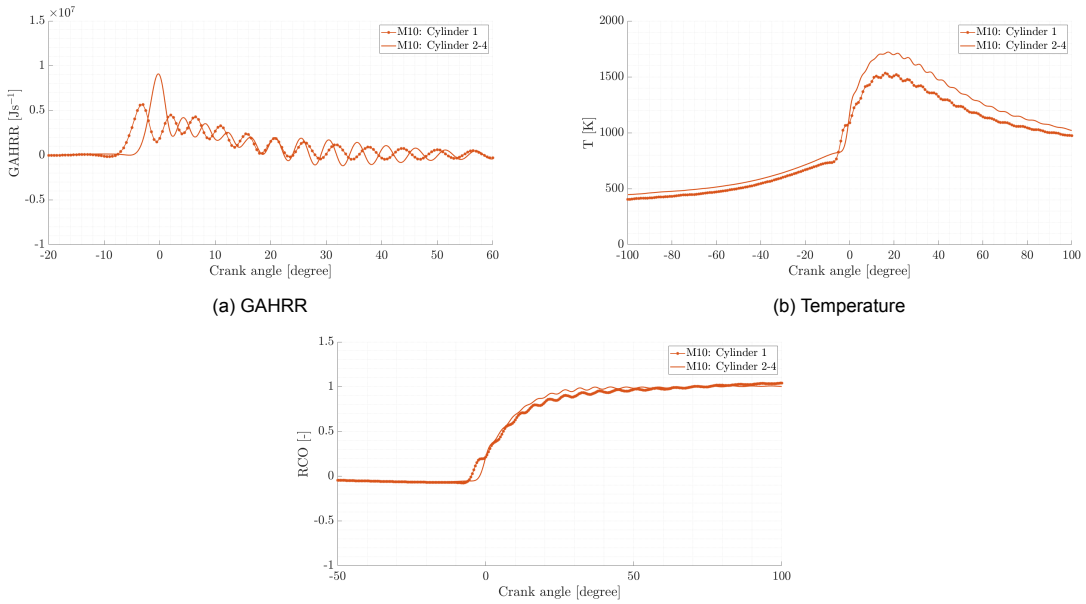

(a) GAHRR

(b) Temperature

(c) RCO

Figure 5.15: M10: : Cylinder one vs. the mean of cylinder two, three and four of single zone model results at 909 [rpm], 153 [kW]

5.4.4. Cylinder comparison

The heat release rate shown by cylinder one hardly shows differences with the mean of cylinder two, three and four when burning F76. An increased methanol/diesel ratio changes the shape of the heat release. Cylinder one structurally ignites earlier compared to the mean of cylinder two, three and four. Increasing the methanol ratio, lower heat release rates and temperatures are obtained for cylinder one. Fuel has less time to evaporate and to mix with air, resulting in a lower premixed combustion phase in cylinder one. Although the ignition delay in cylinder one increases for higher methanol/diesel ratios, it shows better performance compared to the mean of cylinder two, three and four. By increasing the methanol/diesel ratio, the diffusive combustion phase seems to disappear for the mean of cylinder two, three and four. High combustion rates are obtained after ignition during premixed combustion, resulting in higher temperatures and formation of harmful emissions.

For dual fuel operation at this diesel engine setup, it is shown that the fuel injector has impact on the combustion parameters in the engine. The combustion process in cylinder one has more desirable results compared to the mean of cylinder two, three and four. Lower temperatures and smoother heat release rates are obtained for operation on methanol/diesel blends in cylinder one. Implementing these injectors in cylinder two, three and four could improve the engines operating envelope for dual fuel combustion and decrease the formation of harmful emissions.

5.5. Effect of engine speed

The experiments include measurements at varying engine speeds with equal loads. A comparison of the effect of engine speed at constant loads is done for the pressure signal in fig. 4.8 for cylinder two, three and four. The single zone model could provide information about the temperature and heat release. The results for the temperature and $GAHRR$ for different engine speeds at 153 [kW] are shown in figs. 5.17 and 5.18.

For each fuel, the mean temperature in the cylinder increases when running at lower speed. Reason for the increase of temperature at lower engine speed is the time available for the fuel to evaporate. At lower engine speeds, fuel has more time per crank angle to evaporate and to mix with air. As a result, the ignition delay for M10 and M20 has decreased at a lower engine speed. A verification

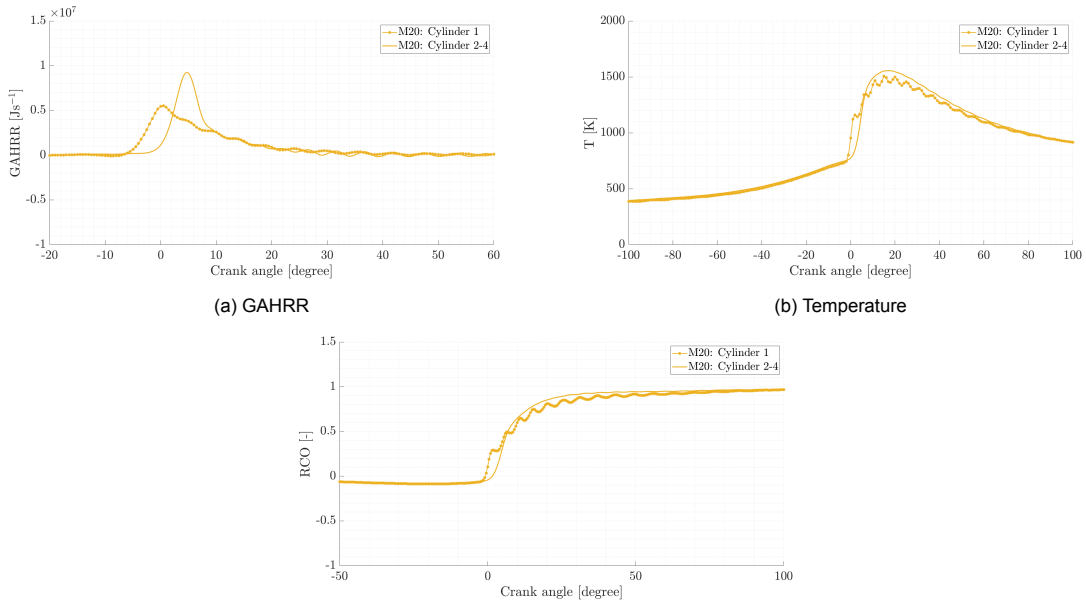

(a) GAHRR

(b) Temperature

(c) RCO

Figure 5.16: M20: : Cylinder one vs. the mean of cylinder two, three and four of single zone model results at 909 [rpm], 153 [kW]

for this result is the experimental result of NO_x emissions. Figure 4.17 shows the results measured at the engine. The specific NO_x emissions were 7.2 [%] higher at 909 [rpm] compared to the same load at 950 [rpm] for F76. For M10 and M20, the NO_x emissions decreased with 6.9 and 6.7 [%] respectively at higher engine speed with equal load. NO_x formation is highly dependent on temperature in the cylinder and is higher at lower engine speeds according to the experiments. The single zone model gives a larger temperature for lower engine speed. Related to the NO_x emissions and exhaust gas temperatures discussed in section 4.5, this is what was expected.

A result observed in c5.17 is that the temperature of M10 at 909 [rpm] is higher compared to M20. For 950 [rpm], the temperature of M20 is higher compared to M10. Experiments on the exhaust gases in fig. 4.16 showed that the exhaust gas temperature of M20 decreased compared to F76 and M10 for each load point. This is an indication that there could be a mismatch between the real and modelled process.

The $GAHRR$ for 909 and 950 [rpm] at 153 [kW] results are shown in fig. 5.18. As expected from the pressure signals shown in fig. 4.8, the heat release peak occurs earlier during the cycle. Except for M10, where ignition starts a crank angle degree earlier, the premixed combustion peak is higher at 950 [rpm] compared to 909 [rpm]. A higher heat release implies a larger mechanical load on the piston and cylinder walls. For M20, the diffusive combustion phase has almost disappeared compared to F76. Obviously, the general shape of the heat release remains comparable for the different engine speeds.

Earlier start of combustion for methanol/diesel blends has a positive effect. From fig. 4.15, the differences in efficiency at varying engine speeds are compared. The engine efficiency at 909 [rpm], 153 [kW] increased with 1.7 [%] for F76 compared to the same load at 950 [rpm]. For M10 and M20, the engine efficiency increased with 5.1 and 1.5 [%] respectively. This supports the fact that more available time to evaporate fuel increases the engine efficiency.

Lower engine speeds are reaching higher efficiencies, although it results in higher NO_x and in general to larger heat release peaks. However, the model does not calculate an increased heat release rate for M10 at 909 [rpm]. This is not what is expected, since the fuel has more time to evaporate and to form a combustible mixture. Earlier ignition for M10 has the disadvantage that the gap to TDC increases. This could reduce the maximum heat release rate for this fuel.

A trade off between exhaust gas emissions, in-cylinder temperatures and engine efficiency must

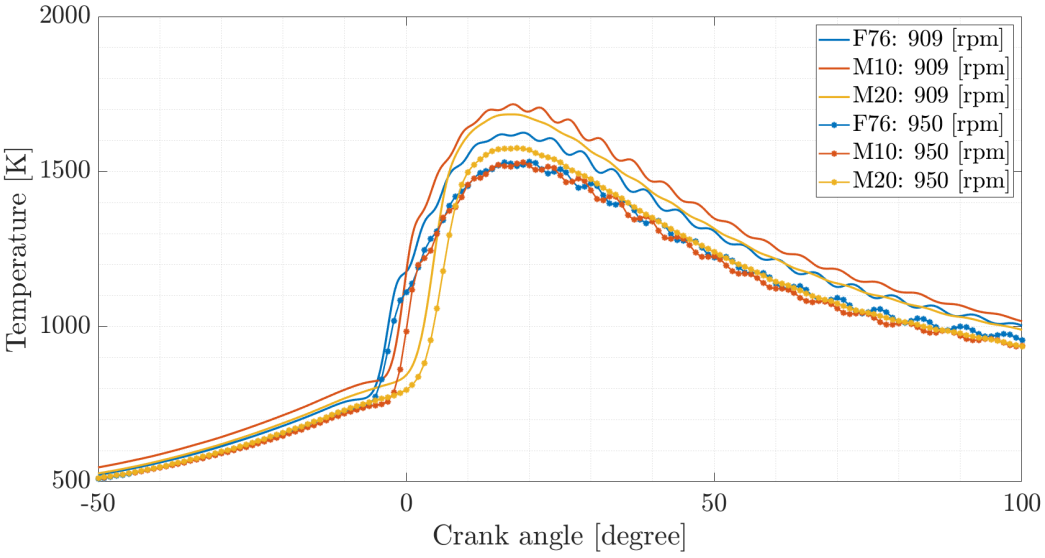

Figure 5.17: Effect of engine speed on in-cylinder temperatures at 153 [kW]

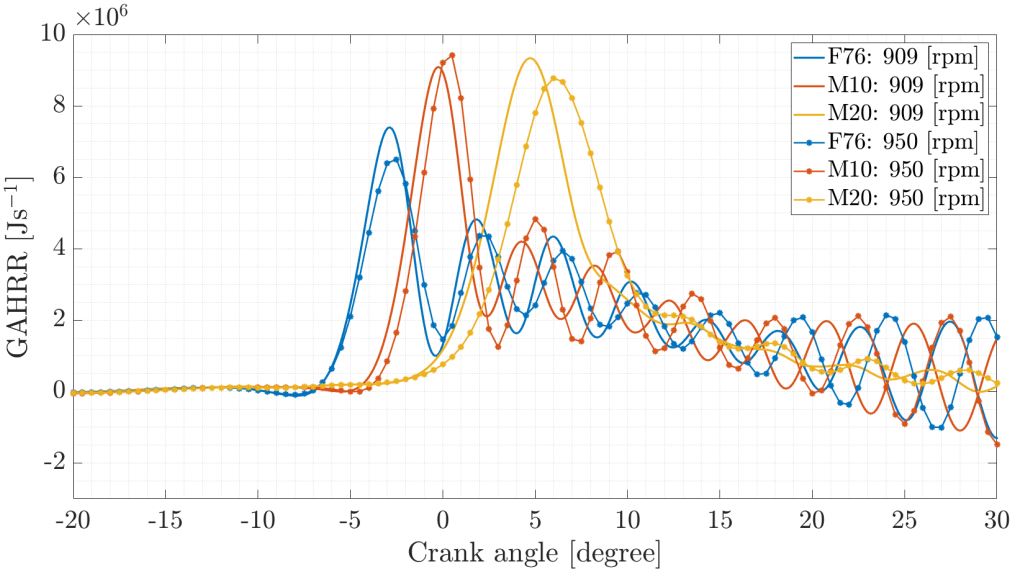

Figure 5.18: Effect of engine speed on GAHRR at 153 [kW]

be made in order to improve the dual fuel performance. Giving fuel more time to evaporate increases the efficiency, but also increases the NOx emissions. Experiments with injection timings can improve the insight in dual fuel engine performance of the current engine setup.

5.6. Model sensitivity

The model is highly sensitive for certain input parameters. Section 5.3 discussed the model results with the implemented TDC-shift of 7°CA. In this chapter, the model's sensitivity to the TDC-shift is discussed by changing the TDC shift according to the value found in literature, which was 0.7°CA [12]. Moreover, to represent the physical properties of the model right, the model is tuned by changing the Woschni heat loss parameters. The heat losses are predicted by the assumed temperatures for the cylinder wall, piston and cylinder head. Moreover, Woschni constant C_1, which is in fact a multiplier for the heat losses, is used for lifting the RCO to unity.

The model has to be tuned for each TDC-shift by the Woschni parameters. Each fuel has its own

parameters, which shows that the heat losses are varying by different fuels. Most important for tuning the model was the RCO, which is zero before SOI and must reach unity at the end of the cycle in case of complete combustion. The Woschni parameters implemented per fuel are shown in table 5.4.

Table 5.4: Woschni tuning parameters for a TDC-shift of 0.7°CA

Fuel	T_{piston} [K]	T_{wall} [K]	$T_{\text{cyl.head}}$ [K]	C_1
F76	600	400	580	450
M10	650	400	650	520
M20	650	400	650	620

Table 5.4 shows that the heat loss parameters are higher when increasing the methanol rate. Knowledge about the heat losses regarding methanol combustion in a diesel engine is limited. The effect of heat losses is therefore expected to be seen in the engine by adapting the fuel injected.

The results from the tuned model with a TDC-shift of 0.7°CA are shown in figs. 5.19 to 5.21. As can be seen from the GAHRR in fig. 5.19, the negative dip before crossing the zero line for methanol/diesel blends is increased due to the large heat of vaporization. More energy to evaporate the fuel is required which decreases the in-cylinder temperature before ignition. This is visible in fig. 5.20, where methanol/diesel blends have a larger temperature drop and a large ignition delay caused by the evaporation time. The relative temperature differences for the different fuels are comparable to the results shown for a TDC-shift of 7°CA in fig. 5.12. The mean maximum temperature of M20 is now almost 200 [K] higher compared to F76. The residence time of M20 at high temperature is again the lowest, which has impact on the NO_x formation.

Important for the combustion process is the RCO calculated by the model. The 0.7°CA TDC-shift

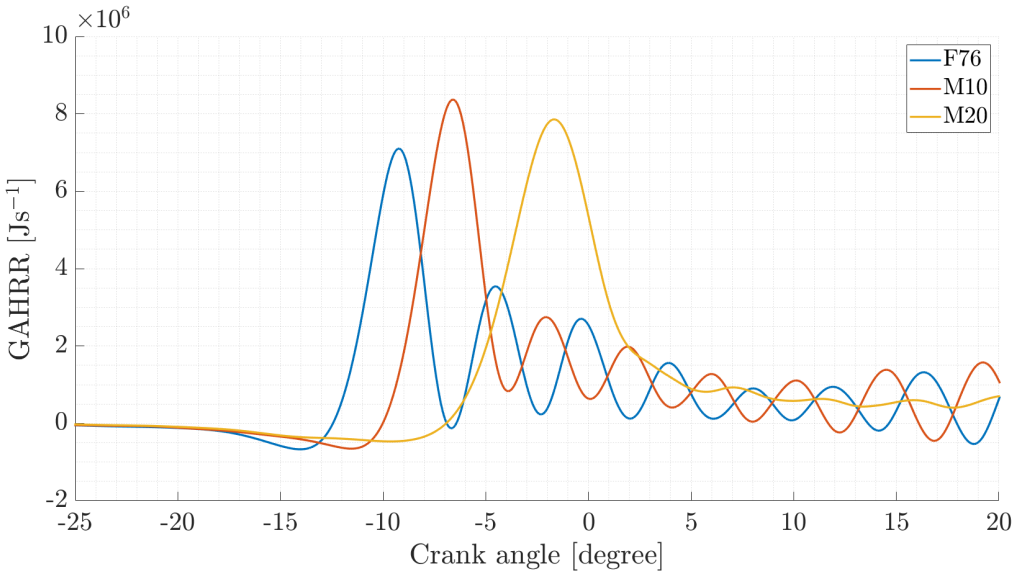

Figure 5.19: GAHRR with a TDC shift of 0.7 °CA for 909 [rpm] at 153 [kW]

shows a different RCO from the previous shift of 7°CA. Highlighting the moment of the start of combustion, it is not at the correct position according to the injection timing of the engine. The negative part of the RCO shows the evaporation losses by fuel and it starts from zero, which is improved compared to the original shift. It still is not real what is shown by this signal, even with the correct shape. Comparison between the fuels shows that the start of combustion is delayed with methanol combustion.

A critical review of this signal and simultaneously comparison with the heat release signal provides more in-dept information about the RCO. The GAHRR creates the expectation that behind the point where the diffusive combustion phase has finished, most of the fuel must be burned. Looking at

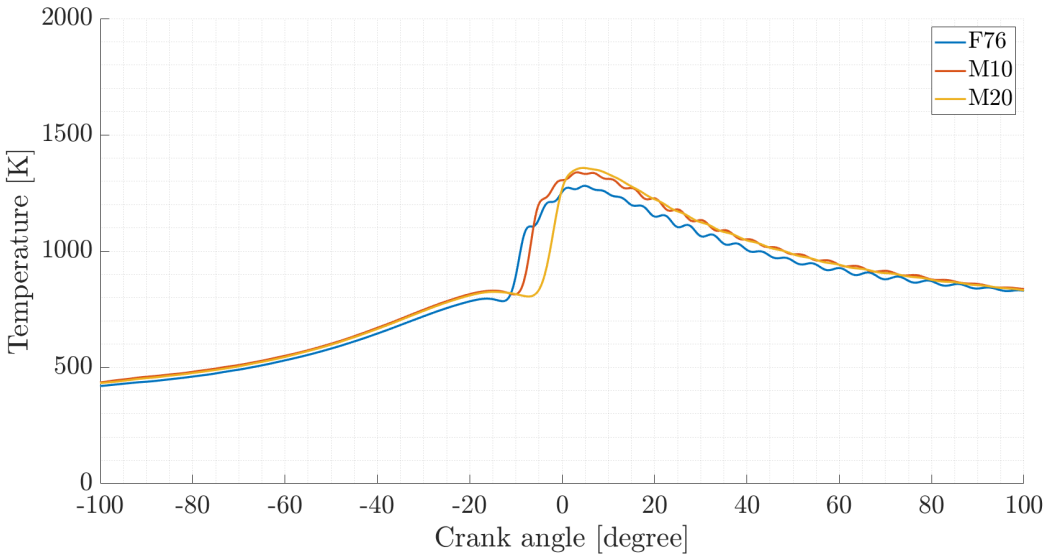

Figure 5.20: Temperature with a TDC shift of 0.7 °CA for 909 [rpm] at 153 [kW]

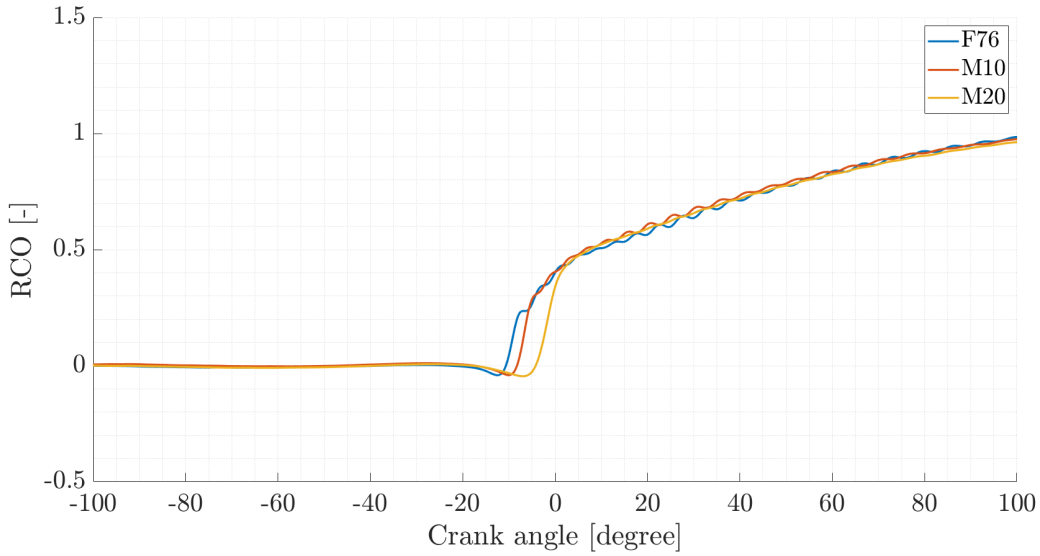

Figure 5.21: RCO with a TDC shift of 0.7 °CA for 909 [rpm] at 153 [kW]

the crank angle of 10 degrees for each fuel, most of the heat is already released. The RCO shows that only 50 [%] of the fuel is burned, which does not match the expectation. It takes 100 degrees for each fuel to reach the 100 [%] fuel burned, which is too long for a diesel engine to operate efficiently. The RCO based on the 7°CA TDC shift has a different trend and shows that when combustion starts, the fuel immediately burns significantly faster. Late combustion also appears but is a small part of the complete process. Although the shape of the 7°CA shifted RCO is below zero before injection, the overall shape seems more reliable.

Another analysis about the accuracy of the model can be executed based on indicated power calculated and measured. The indicated power measured is dependent on the load from the water brake and the position of the pressure signal compared to the crank angle. For this analysis, the 7°CA TDC shift is considered as the correct position for the pressure signal. The indicated power calculated based on this position is therefore used for this comparison.

The difference between measured and modelled indicated power for the closed cycle is up to

Table 5.5: Indicated power closed cycle: Model versus measurement comparison at 909 [rpm], 153 [kW]

Fuel	P_i, measured [kW]	$P_{i,model}$, 0.7°CA TDC-shift [kW]	$P_{i,model}$, 7°CA TDC-shift [kW]
F76	52.2	24.8	48.9
M10	53.3	25.1	48.8
M20	53.9	26.4	49.5

8.4 [%] for M10 with a TDC-shift of 7°CA. An explanation for this difference is the smoothing process, where the peak pressures are lower compared to the original signals. The indicated work reduces since this is dependent on the pressure in the cylinder and the volume change per time step. Relative differences for a shift of 0.7°CA are more than 50 [%] between the measured and modelled result. This is an indication that the model result accuracy is highly dependent on the TDC-shift and gives unreal values for a small shift.

5.6.1. Discussion on single zone model

This section discusses the results from the single zone model. Results from the model are highly dependent on the TDC-shift applied to the pressure signal. The shift of 7°CA is considered as the physically correct one.

After analysing the single zone model results, the shape of the heat release parameters seems to be reliable. The peak heat release values are dependent on the TDC-shift, but the general shape of the signals of the fuel mixtures are equal for each shift analysed.

Differences between the fuels are observed. First, the heat release of the methanol/diesel blends compared to F76 changes. M20 shows that the premixed combustion phase is dominant. The diffusive combustion phase decreases by burning a higher amount of methanol compared to F76. However, the current calculation of the heat release rate leads to physically unreal results in the heat release rate and in the RCO for both TDC-shifts. Moreover, the temperature calculated by the model for each TDC-shift seems to be unreal. Experiments have shown that the exhaust gas temperature seems to be lower, which is not calculated by the model.

The calculated indicated power by the model gives an indication about the right position of the pressure signal and the calculations of the model. Based on the indicated power, it indicates that the 7°CA TDC-shift is at least close to the real position of the TDC. A disadvantage of the large TDC-shift is that the combustion process is calculated less accurate with negative burned fuel mass. A compromising result must be found between the model's accuracy and results.

The single zone model works with the measured pressure signal as an input. Based on this signal, the heat release is directly calculated with only a negligible time delay between the signal and physical process happening in the cylinder. The pressure signal already contains valuable information regarding the evaporation process. In reality, the evaporation process takes place between SOI and SOC. In the model, the so called dwelling time between injection and ignition is ignored. This results in inaccurate heat release shapes, too high temperatures and RCO's with negative mass in the cylinder. Observed is that the shape of the model results is more as expected while hardly shifting the measured pressure signal. In this case, the model's calculations based on diesel fuel seems to work, but due to the pressure signal it shows the evaporation effects by accident at the expected position. The shape obtained for small shifts is deceiving, because the combustion rate is already positive in this phase before injection. Although the shape of the signals seems to improve for the small shift, the physical meaning is not realistic.

The current dual fuel single zone model could not calculate the evaporation losses in the correct way. The main reason is that the pressure signal and its physical details are not evaluated in the model in the same order. A distinction between injected mass, evaporated mass and burned mass is needed to eliminate these wrong calculations. The best solution to implement this is by introducing a new zone

in the model including these distinctions. In this way, ignition delay can be implemented. Moreover, the heat release rate calculation can be improved by using the blend properties instead of separate fuel combustion. The pressure signal helps providing information regarding the evaporation time and the combustion process.

The results of this model show that the general processes are calculated in a proper way. Unfortunately, the calculations are highly dependent on the position of the pressure signal and are influenced by the ignition delay caused by methanol.

Cylinder one contains a different fuel injector. Based on the heat release comparison between cylinder one and the mean of cylinder two, three and four, it is shown that cylinder one shows better performance on methanol/diesel blends. Cylinder one shows a shorter ignition delay indicating that the evaporation process develops more efficiently. Methanol vapor has less time form an ignitable mixture with air, which causes a lower heat release rate. A decreased temperature is observed, which means that the thermal load for cylinder one is lower. Lower temperatures were expected according to literature and experiments [11, 29]. The RCO is equal from 10°CA for cylinder two, three and four. The RCO shown for cylinder one has a constant lower value for M20. The large ignition delay for three cylinders causes rapid combustion for the M20 blend.

The results for cylinder one are more in line with the expectations on beforehand. This analysis shows that the fuel injector of cylinder one shows better ignition properties for methanol/diesel blends in this dual fuel compression ignited engine. The droplets formed in cylinder one are expected to be smaller because of the improved evaporation process. The effective heat transfer area of the fuel spray is larger when having smaller droplets. In that way, heat transfer to the fuel bulk improves, resulting in smaller evaporation times and earlier ignition. Due to earlier ignition, the mean temperature in the engine seems to reduce. Using the injector of cylinder one for dual fuel operation in all cylinders could result in a lower amount of harmful emissions and lower thermal loads on the engine. Optimizing the process for the complete engine could result in a decrease of NO_x formation. Moreover, higher engine efficiencies could be reached operating on methanol/diesel blends due to the shorter ignition delay of cylinder one. Research to the properties of this injector is highly recommended for future dual fuel operation in a compression ignited engine.

6

Conclusions and recommendations

Reducing the use of fossil fuel is a major goal for governments worldwide. Alternative fuels such as methanol could be used without adapting existing engines on board of ships. Methanol is blended with diesel fuel at multiple ratios to investigate the effect of this fuel at the combustion parameters and harmful emissions in and from a diesel engine. The MAN4L20/27 diesel engine itself is not adapted for methanol operation. By in-cylinder and exhaust gas emission measurements, the effect of methanol/diesel blends on the in-cylinder parameters is investigated. Combustion in the cylinder is investigated by an adapted version of the dual fuel single zone model of Lee. The heat of vaporization of methanol is added by building a single droplet evaporation model and calculating the heat of vaporization of a fuel spray with the help of an fuel injection model. In the end, it can be determined whether the model describes the physical heat release phenomena in a sufficient way by comparing it to literature and expectations. This chapter first discusses the conclusions regarding the experiments. Second, the modelling results are concluded. Finally, recommendations aiming for model improvement and methanol-diesel operation are proposed.

6.1. Conclusions

6.1.1. Experiments

Chemical properties of fuel have an impact on the performance and exhaust gases from an engine. Diesel and methanol differ from each other in multiple ways. First of all, methanol contains more than 50 [%] less energy per kilogram, which is denoted by the lower heating value. Combined with a four times higher heat of evaporation and a cetane number of 4, compression ignition of methanol is challenging. A decreased dynamic viscosity of methanol compared to F76 has an impact on fuel lubricated high pressure fuel pumps for the long term. Moreover, methanol contains less carbon but includes oxygen which could contribute to the combustion process.

The chemical properties of methanol causes differences in the in-cylinder combustion process of methanol/diesel blends. The relevant parameters to study the differences with F76 are the in-cylinder pressure, fuel consumption, heat release rate, temperature and reaction coordinate. The pressure and fuel consumption are measured by experiments, while the resulting parameters are calculated based on the pressure signal. Gaining the pressure signal and fuel consumption of the engine by experiments allows the researcher to examine the in-cylinder parameters.

Important conclusions regarding experiments with methanol must be made based on safety considerations. Methanol produces toxic gases for human being. During experiments, sufficient air ventilation systems must be used in order to prevent toxic gases to enter the laboratory. Moreover, protective gear as overalls, gloves and full face gas masks are required while working with methanol to protect the body from methanol exposure.

In-cylinder pressure measurements are performed on a diesel engine to compare the performance of F76 to methanol/diesel blends. Four different cylinders are measured resulting in differences between cylinder one and cylinder two, three and four. The injector design of cylinder one is the only difference, which caused cylinder one to show better performance on methanol/diesel blends. Lower coefficients of variance were found for cylinder one compared to cylinder two, three and four, indicating a more stable combustion in cylinder one. Increasing the methanol/diesel ratio results in higher coefficients of variance for IMEP and maximum pressure for each cylinder.

During experiments, the engine is not able to maintain its operation envelope from a methanol ratio of 20 [%]. At low loads, the engines temperature seems to be too low in order to vaporize the methanol in the engine. For M20, operation below 153 [kW] resulted in an engine failure due to failed ignition in the cylinders.

Analysis based on the mean value of cylinder two, three and four shows an elongated ignition delay up to 8°CA for M20. Furthermore, combustion duration seems to decrease significantly with 12.7°CA according to the Kibox, while the engine efficiency remained almost constant for M20. It was shown that the IMEP and mechanical efficiency showed only small deviations for methanol operation.

Fuel consumption measurements showed that the lower heating value of methanol causes the fuel consumption to increase with almost an equal rate as expected up to 23 [%] for M20. The air excess ratio decreased due to increased fuel flow and a lower stoichiometric air to fuel ratio of methanol blends. The absolute air flow into the engine was almost unchanged for each load point since the turbine settings were unadapted. Finally, the exhaust gas temperature for methanol/diesel blends seems to decrease up to three degrees after the turbine, indicating a lower in-cylinder temperature.

The effect on exhaust gas emissions of F76 compared to methanol blends is investigated by measurements using the Testo 350 gas analyser. NO_x emissions decreased with 2.9 up to 14.2 [%] by using methanol compared to F76. The short combustion time and the cooling effect caused by evaporation of methanol are responsible for this difference. The carbon dioxide emissions slightly reduce by running on M10 since less carbon is injected in the engine. However, increasing the methanol ratio causes no reduction and even an increase of CO_2 emissions for M20 compared to F76. More complete combustion may have been observed by the lower CO emissions of methanol blends. The oxygen content of methanol contributes to the combustion resulting in a plausible increased combustion efficiency. The oxygen concentration in the exhaust gases showed a decrease of 1 [%] compared to diesel fuel, which is not considerably large.

Measurements on sulphur dioxide and unburned hydrocarbons are performed. The sulphur dioxide emissions were not reliable. However, the sulphur content in F76 is already low and methanol does not contain any sulphur. These emissions are not concerning for these measurements due to the already low concentrations. Unburned hydrocarbons seems to be unreliable due to the sensors accuracy. The measurements showed an increase in volumetric concentration during the day. Since it was expected that the unburned hydrocarbons would increase by injecting methanol, the results may still indicate a slight increase in unburned hydrocarbon emissions.

6.1.2. Modelling

This section discusses the conclusions regarding the model performance and results. A critical analysis is done to investigate whether the model is functioning properly. Starting with the injection model, followed by the evaporation model. Finally, the results of the adapted dual fuel model are evaluated.

After improvements of the injection model, it is able to calculate the right amount of fuel injected after tuning it with the discharge coefficient. A new relation between fuel consumption and fuel rack position is determined for methanol operation and has positive effect on the model's results. The discharge coefficient is still high due to assumptions for the injector dimensions and forces in the system. For this research, the fuel flow was considered as most important parameter and was represented sufficiently by the injection model.

The evaporation model is validated by literature for decane and methanol. Decane was used as a surrogate fuel for diesel to compare methanol to diesel. Methanol needs two times more time to

evaporate compared to diesel fuel. A correction factor for conductivity effects in the heat up period is proposed which seems to be valid for decane. Methanol evaporation required a larger correction factor to meet experimental values indicating that the effect of conductivity for methanol evaporation seems to be larger. Moreover, the heat of vaporization of methanol can be tuned by the droplet size to get the evaporation heat as input for the single zone model.

The combustion rate is still the driving force of the single zone model. The spray heat of vaporization is dependent on injected mass and evaporated mass of fuel dictated by the combustion rate. Therefore, the single zone model found its limit in capturing the evaporation heat losses directly after injection at the right position of the pressure signal. The expected negative heat release phase due to evaporation is not measured accurately due to the mismatch between pressure signal and evaporation calculation. Inaccurate results are obtained in the heat release where it crosses the zero line before injection, which was not according to expectations. Moreover, the RCO is continuously -0.1 before ignition, which is physically not possible. Some physical processes in the model need improvement to capture the ignition delay in the model. On the other hand, measurement errors could also be the reason for inaccurate results obtained by the model.

A sensitivity analysis showed that the single zone model is highly dependent on the position of the pressure signal. A small TDC-shift of 0.7°CA instead of the correct TDC-shift of 7°CA leads to decreased indicated power compared to the experiments. The small TDC-shift gives combined with heat loss calibration the right signal shapes according to expectations. Unfortunately, the ignition timing and time of heat release are unreal compared to the physical parameters of the engine.

The main conclusion regarding the working principles and capability of the single zone model to simulate direct injected methanol/diesel blends is that it shows unreal results at multiple points. First, nonphysical results are obtained for the ignition timing with a TDC-shift of 7°CA. Second, the evaporation process should be directly after injection, which is not captured within this model. Also the higher temperatures of the methanol blends compared to F76 are questionable, since the experiments resulted in lower exhaust gas temperatures. Finally, the RCO is negative before injection starts implicating a negative fuel mass in the cylinder. However, an advantage of the model is that the overall shape of the heat release rates of the different fuel types could be compared to each other.

Heat release analysis based on the mean of cylinder two, three and four for different fuel blends has shown that methanol blends appears to have a strong premixed combustion phase and a weakened diffusive combustion phase. According to the model, the strong premixed combustion results in higher mean temperatures. Temperatures are rising fast during the premixed combustion phase, since the fuel/air mixture has had much time to mix homogeneously. The combustion duration seems to decrease by using methanol blends.

Cylinder one shows different combustion behaviour compared to the mean of cylinder two, three and four. The fuel injector has a positive effect on the combustion process, resulting in more smooth heat release curves for methanol operation. Lower peak heat release values were obtained and the in-cylinder temperatures were lower compared to the mean of cylinder two, three and four. The heat release and RCO indicate that the SOC was earlier compared to cylinder two, three and four. Because methanol is expected to have a cooling effect and experiments showed a lower exhaust gas temperature, results for dual fuel combustion in cylinder one were more in line with expectations.

6.2. Recommendations

This section gives recommendations based on experiences during this research. The topics proposed are aiming on improvements for future research. A distinction between the experiments and models is made. First, recommendations regarding the experiments are provided. Finally, the model recommendations are proposed to increase its value in future research.

6.2.1. Experiments

Recommendations regarding the experiments and experimental results are proposed in this section.

- The pressure signal has been shifted with 7°CA, which is normally too much. For future experiments, it is recommended to carefully calibrate the Kibox and perform more checks to make sure that the position of TDC is defined correctly.
- Methanol and diesel fuel are immiscible. During experiments, assumed is that the fuel mixtures were blended homogeneous. Large fluctuations are obtained running on the methanol blends. Emulsifiers could increase the mixtures stability and prevents undesirable impurities in the methanol to diesel ratio. Doetjes investigated the stability of methanol blends for selected emulsifiers and proved that a stable mixture could be obtained [13]. The effect of mixtures including emulsifiers on the combustion stability can be investigated by using these stable blends.
- The diesel engine has operated on methanol blends without adapting the technical parameters of the engine. The injector design of the engine has an impact on the evaporation process of the fuel droplets. Cylinder one showed more desirable combustion performance on methanol/diesel blends compared to cylinder two, three and four. Research to the properties of this injector, combined with experiments on ignition timing are recommended to improve the dual fuel performance of this engine.
- Awareness of toxic gases is required while working with methanol. Exhaust gas measurements including aldehyde measurements gives an insight in the formation of these gases. Aldehydes are a feasible danger for methanol operation. Moreover, the measurements of unburned hydrocarbons are recommended to be performed by using heated hoses.
- Reliability and repeatability of the experiments could be improved by increasing the measured cycles in the Kibox. Coefficients of variance will vary when taking more cycles into account.

6.2.2. Modelling

The modelling recommendations are given in this section.

- The injection model is able to simulate the correct amount of fuel injected into the cylinder. However, some parameters are recommended to get improvement. First of all, knowledge about the physical parameters of the fuel injectors could increase the model's accuracy. Furthermore, the bulk modulus of diesel fuel should be changed to the value of methanol/diesel mixtures. Implementing these values are expected to solve the problem of the high discharge coefficients in the nozzle.
- Conductive heat transfer is not modelled in the evaporation model. The differences between experimental and the modelling results were mainly caused by this simplification. A more detailed evaporation model is obtained by adding conductivity effects to the model.
- The spray calculation is based on the injection model and the evaporation process of a single droplet with constant environmental parameters. In the engine, the temperature and pressure are variable and affect the evaporation process of the droplets. Moreover, the initial conditions of droplets at the start of injection varies due to the pressure and temperature fluctuations in the engine. A detailed spray model including these effects improves the capability to calculate the evaporation heat of methanol/diesel blend more accurately. Moreover, recommended is to do experiments to investigate the effect to fuel sprays of methanol blends compared to diesel fuel. In this way, the models could be validated to experimental data.
- Regarding the proposed dual fuel single zone model and its adaptions for liquid methanol fuel, the following should be taken into account for future projects. Evaporation losses are not modelled as desired, because the assumption of zero dwelling time seems to be invalid for dual fuel combustion with methanol. The heat of vaporization added by the evaporation model is still dependent on the burned mass, which does not give a proper representation of the evaporation losses in time. Higher accuracy is reachable by improving the representation of the physical processes such as early heat release, negative RCO and ignition timings in the model. Improved results can be obtained by adding a second zone to the model with a distinction between the injected,

evaporated and burned mass of fuel.

- The single zone model calculates the GAHRR by dividing it in the diesel and methanol part with separate combustion. Since droplets in reality are not strictly separate from each other, the calculation of the GAHRR could influence the model results. The effect of separated fuel properties in the model can be investigated by calculating the methanol blends as a single fuel with mean blend properties.
- Heat losses to cylinder wall, piston head and cylinder head are modelled according to Woschni. For diesel fuel, the heat transfer coefficient proposed by Woschni is widely adopted. After calibration of the model with these parameters, the values for methanol blends increased compared to diesel. The balance between radiation and convection of methanol is not investigated. Therefore, it is recommended to investigate the heat exchange of methanol to the cylinder and to adjust the heat exchange model in the dual fuel model.
- Cylinder two, three and four are taken as mean value to represent the engines behaviour. However, the combustion stability of the engine decreased while operating on methanol/diesel blends. The ignition time and peak pressures per cylinder are varying much due to the increased instability. Moreover, the performance of cylinder one was different from cylinder two, three and four. For future analysis on compression ignited engines, it is recommended that when high COV values are observed, performing an in-cylinder analysis for each cylinder individually could lead to more detailed results.

Bibliography

[1] Avinash Kumar Agarwal, Nikhil Sharma, Akhilendra Pratap Singh, Vikram Kumar, Dev Prakash Satsangi, and Chetankumar Patel. Adaptation of methanol-dodecanol-diesel blend in diesel genset engine. *Journal of Energy Resources Technology, Transactions of the ASME*, 141(10): 1–9, 2019. ISSN 15288994. doi: 10.1115/1.4043390.

[2] I. Ali and M. A. Basit. Significance of hydrogen content in fuel combustion. *International Journal of Hydrogen Energy*, 18(12):1009–1011, 1993. ISSN 03603199. doi: 10.1016/0360-3199(93)90083-M.

[3] Alliance Consulting International. Methanol Safe Handling Manual. *Methanol Institute*, (October):1–37, 2008. URL http://biodiesel.org/docs/ffs-methanol/methanol-safe-handling-fact-sheets-oct-2008.pdf?sfvrsn=6.

[4] Karin Andersson and Carlos Márquez Salazar. Methanol as a marine fuel report. Technical report, Methanol Institute, 2015. URL www.methanol.org.

[5] Carsten Baumgarten. Mixture Formation in IC Engines. pages 215–230, 2006.

[6] A. Bejger and J. Drzewieniecki. Analysis of tribological processes occuring in precision pairs based on example of fuel injection pumps of marine diesel engines. *Zeszyty Naukowe Akademii Morskiej w Szczecinie*, nr 41 (113(April), 2015. ISSN 1733-8670.

[7] Adnan Berber. The effect of Diesel-Methanol Blends with Volumetric Proportions on the Performance and Emissions of a Diesel Engine. *Mechanika*, 25(5):363–369, 2019. ISSN 20296983. doi: 10.5755/j01.mech.25.5.22954.

[8] R.B.; Bird, W.E.; Stewart, and E.N. Lightfoot. *Transport phenomena*. John Wiley & Sons, Inc., 2nd edition, 2002. ISBN 0471410772.

[9] Gary L. Borman and Kenneth W. Ragland. *Combustion Engineering*. McGraw-Hill, 1998. ISBN 0-07-006567-5.

[10] Murat Ciniviz, Hüseyin Köse, Eyüb Canli, and Özgür Solmaz. An experimental investigation on effects of methanol blended diesel fuels to engine performance and emissions of a diesel engine. *Scientific Research and Essays*, Vol. 6(15)(August 2015):3189–3199, 2011. doi: 10.5897/SRE11.230.

[11] J; Dierickx, L; Sileghem, and S; Verhelst. Efficiency and emissions of a high-speed marine diesel engine converted to dual-fuel operation with methanol. *CIMAC World Congress 2019*, 013, 2019.

[12] Yu Ding. *Characterising Combustion in Diesel Engines*. 2011. ISBN 9789065622891.

[13] G Doetjes. Het bepalen van een geschikte emulgator om F76 en methanol gemengd te houden. Technical report, Nederlandse Defensie Academie, Den Helder, 2020.

[14] F. dos Santos and L. le Moyne. Spray atomization models in engine applications, from correlations to direct numerical simulations. *Oil and Gas Science and Technology*, 66(5):801–822, 2011. ISSN 12944475. doi: 10.2516/ogst/2011116.

[15] Joanne Ellis and K Tanneberger. Study on the use of ethyl and methyl alcohol as alternative fuels in shipping. 46(0):8–31, 2015.

[16] Enerkem. W2C Rotterdam project welcomes Shell as partner, 2019.

[17] Yanfeng Gong, Shenghua Liu, and Yu Li. Investigation on methanol spray characteristics. *Energy and Fuels*, 21(5):2991–2997, 2007. ISSN 08870624. doi: 10.1021/ef0605089.

[18] L Grunnberg and Alfred Nissan. Mixture law for viscosity. *Nature Publishing Group*, (4175):799–800, 1949. doi: 10.1038/164799b0.

[19] Zhiqiang Guo, Tianrui Li, Jinlong Dong, Rongrong Chen, Peijun Xue, and Xuehong Wei. Combustion and emission characteristics of blends of diesel fuel and methanol-to-diesel. *Fuel*, 90 (3):1305–1308, 2011. ISSN 00162361. doi: 10.1016/j.fuel.2010.12.011. URL http://dx.doi.org/10.1016/j.fuel.2010.12.011.

[20] Shen Haosheng, Zhang Jundong, and Cao Hui. Visualization Simulation Research of fuel common rail system of marine intelligent diesel engine, 2014.

[21] Jorrit Harmsen, Nina Nesterova, Dick Abma, Praveen Balakrishnan, and Karin van Kranenburg. Green Maritime Methanol. Technical report, Green Maritime Methanol, 2019.

[22] John B Heywood. *Internal Combustion Engine Fundementals*, volume 21. 1988. ISBN 007028637X. doi: 10987654.

[23] Hiroyuki Hiroyasu. Development and use of a spray combustion modelling to predict diesel engine efficiency and pollutant emissions. *Bulletin of the JSME*, 26:569–575, 1983.

[24] Robert Holyst and Andrzej Poniewierski. *Thermodynamics for Chemists, Physicists and Engineers*. 1 edition, 2012. ISBN 978-94-007-2999-5. doi: 10.1007/978-94-007-2999-5.

[25] Z. H. Huang, H. B. Lu, D. M. Jiang, K. Zeng, B. Liu, J. Q. Zhang, and X. B. Wang. Engine performance and emissions of a compression ignition engine operating on the diesel-methanol blends. *Proceedings of the Institution of Mechanical Engineers, Part D: Journal of Automobile Engineering*, 218(4):435–447, 2004. ISSN 09544070. doi: 10.1243/095440704773599944.

[26] IMO. Methanol as marine fuel: Environmental benefits, technology readiness, and economic feasibility. *DNV GL Maritime Environmental*, 2:49, 2016. URL www.dnvgl.com.

[27] IMO, T. W. P. Smith, J. P. Jalkanen, B. A. Anderson, J. J. Corbett, J. Faber, S. Hanayama, E. O'Keeffe, S. Parker, L. Johansson, L. Aldous, C. Raucci, M. Traut, S. Ettinger, D. Nelissen, D. S. Lee, S. Ng, A. Agrawal, J. J. Winebrake, and A. Hoen, M. Third IMO Greenhouse Gas Study 2014. *International Maritime Organization (IMO)*, page 327, 2014. ISSN 0308-8839. doi: 10.1007/s10584-013-0912-3. URL http://www.imo.org/en/OurWork/Environment/PollutionPrevention/AirPollution/Documents/ThirdGreenhouseGasStudy/GHG3ExecutiveSummaryandReport.pdf.

[28] Methanol Institute. Safe handeling of methanol. 2013.

[29] Arkadiusz Jamrozik. The effect of the alcohol content in the fuel mixture on the performance and emissions of a direct injection diesel engine fueled with diesel-methanol and diesel-ethanol blends. *Energy Conversion and Management*, 148:461–476, 2017. ISSN 01968904. doi: 10.1016/j.enconman.2017.06.030. URL http://dx.doi.org/10.1016/j.enconman.2017.06.030.

[30] Kistler. Pressure sensor 7061B specifications sheet. Technical report, 2009.

[31] Kistler. Kistler charge amplifier specifications sheet. Technical report, 2015.

[32] Kistler. Kibox type 2893 specifications sheet. Technical report, 2017. URL https://www.kistler.com/?type=669{&}fid=71509{&}model=document.

[33] David R. Lancaster, Roger B. Krieger, and John H. Lienesch. Measurement and analysis of engine pressure data. *SAE Technical Papers*, 84:155–172, 1975. ISSN 26883627. doi: 10.4271/750026.

[34] Magín Lapuerta, Reyes García-Contreras, Javier Campos-Fernández, and M. Pilar Dorado. Stability, lubricity, viscosity, and cold-flow properties of alcohol-diesel blends. *Energy and Fuels*, 24 (8):4497–4502, 2010. ISSN 08870624. doi: 10.1021/ef100498u.

[35] Magín Lapuerta, Juan Pablo Hernández, and John R. Agudelo. An equation for the estimation of alcohol-air diffusion coefficients for modelling evaporation losses in fuel systems. *Applied Thermal Engineering*, 73(1):539–548, 2014. ISSN 13594311. doi: 10.1016/j.applthermaleng.2014.08.009. URL http://dx.doi.org/10.1016/j.applthermaleng.2014.08.009.

[36] Magín Lapuerta, José Rodríguez-Fernández, David Fernández-Rodríguez, and Rayda Patiño-Camino. Modeling viscosity of butanol and ethanol blends with diesel and biodiesel fuels. *Fuel*, 199:332–338, 2017. ISSN 00162361. doi: 10.1016/j.fuel.2017.02.101.

[37] Byungjoo Lee. The effects of methanol fuel on combustion in premixed dual fuel engine. 2016.

[38] Y Linden. NO-emission prediction in a Diesel Engine. (2826), 2017.

[39] Sebastián Galindo López. Three-Zone in-cylinder process model for DI diesel engines Sebastián Galindo López. 2014. doi: SDPO.14.010.m.

[40] MAN B&W. The Diesel Cycle Verified for Methanol Operation. 2014.

[41] MAN B&W. Using Methanol Fuel in the MAN B&W ME-LGI Series. page 16, 2014. URL https://www.mandieselturbo.com/docs/default-source/shopwaredocuments/using-methanol-fuel-in-the-man-b-w-me-lgi-series.pdf.

[42] Guenter Merker, Chirstian Schwarz, Gunnar Stiesch, and Frank Otto. *Simulating Combustion: Simulation of combustion and pollutant formation for engine-development*. Number 1. 2014. ISBN 9780874216561. doi: 10.1007/s13398-014-0173-7.2.

[43] Tony Miller, Tom Beer, Tim Grant, David Batten, David Lamb, and David Trimm. Methanol as an alternative transport fuel. *Proc. 14th International Union of Air Pollution Prevention and Environmental Protection Associations (IUAPPA) World Congress 2007, 18th Clean Air Society of Australia and New Zealand (CASANZ) Conf.*, (4000096701), 2007.

[44] A.F. Mills and C.F.M. Coimbra. *Basic Heat and Mass Transfer*. Temporal Publishing, LLC – San Diego, CA 92130, 2015. ISBN 9780996305303. doi: 10.1017/cbo9780511530142.005.

[45] Raul Payri, Jaime Gimeno, O. Venegas, and Alejandro H. Plazas-Torres. Experimental and computational study of the influence of partial needle lift on nozzle flowin diesel fuel injectors. *Atomization and Sprays*, 22(8):687–714, 2012. ISSN 10445110. doi: 10.1615/AtomizSpr.2012005810.

[46] Kun-peng Qi, Li-yan Feng, Xian-yini Leng, Jiang-ping Tian, and Wu-qiang Long. Simulation of quasi-dimensional model for diesel engine working process. *Central South University Press and Springer-Verlag Berlin Heidelberg 2010*, pages 444–449, 2009. ISSN 04381157. doi: 10.1007/s11771.

[47] C. D. Rakopoulos, K. A. Antonopoulos, D. C. Rakopoulos, and D. T. Hountalas. Multi-zone modeling of combustion and emissions formation in DI diesel engine operating on ethanol-diesel fuel blends. *Energy Conversion and Management*, 49(4):625–643, 2008. ISSN 01968904. doi: 10.1016/j.enconman.2007.07.035.

[48] Cenk Sayin. Engine performance and exhaust gas emissions of methanol and ethanol-diesel blends. *Fuel*, 89(11):3410–3415, 2010. ISSN 00162361. doi: 10.1016/j.fuel.2010.02.017. URL http://dx.doi.org/10.1016/j.fuel.2010.02.017.

[49] Cenk Sayin, Ahmet Necati Ozsezen, and Mustafa Canakci. The influence of operating parameters on the performance and emissions of a DI diesel engine using methanol-blended-diesel fuel. *Fuel*, 89(7):1407–1414, 2010. ISSN 00162361. doi: 10.1016/j.fuel.2009.10.035. URL http://dx.doi.org/10.1016/j.fuel.2009.10.035.

[50] Juhun Song, Kraipat Cheenkachorn, Jinguo Wang, Joseph Perez, André L. Boehman, Philip John Young, and Francis J. Waller. Effect of oxygenated fuel on combustion and emissions in a light-duty turbo diesel engine. *Energy and Fuels*, 16(2):294–301, 2002. ISSN 08870624. doi: 10.1021/ef010167t.

[51] D Stapersma. *Diesel Engines Volume 3, Combustion*, volume 3. 2003. ISBN 0693485000.

[52] D Stapersma. *Diesel Engines Volume 4 Emissions and Heat transfer*, volume 4. 2010. ISBN 0693485000.

[53] D Stapersma. Diesel Engines Volume 1 Performance Analysis. *Lecture notes WB4408A*, 1 (January), 2010.

[54] Douwe; Stapersma and Hans; Klein Woud. *Design of propulsion and electric power generation systems*. IMarEST, 2014. ISBN 1-902536-47-9.

[55] Gunnar Stiesch. *Modeling Engine Spray and Combustion Processes*. Springer-Verlag Berlin Heidelberg, New York, 1 edition, 2003. ISBN 9783642056291. doi: 10.1007/978-3-662-08790-9.

[56] Ivan Taritaš. *The development of a quasi-dimensional model for dual fuel combustion in engine cycle-simulation*. Doctoral thesis, University of Zagreb, 2018.

[57] Testo SE & Co. KGaA. Testo 350 Maritime V2 Flue Gas Analyzer Instruction Manual. *Testo Be Sure*, 2019. URL www.testo.com.

[58] Sebastian Verhelst, James WG Turner, Louis Sileghem, and Jeroen Vancoillie. Methanol as a fuel for internal combustion engines. *Progress in Energy and Combustion Science*, 70(January): 43–88, 2019. ISSN 03601285. doi: 10.1016/j.pecs.2018.10.001.

[59] Fang WANG, Jie YAO, Shaofeng YANG, Rui LIU, and Jie JIN. A new stationary droplet evaporation model and its validation. *Chinese Journal of Aeronautics*, 30(4):1407–1416, 2017. ISSN 10009361. doi: 10.1016/j.cja.2017.06.012. URL http://dx.doi.org/10.1016/j.cja.2017.06.012.

[60] J Warnatz, U Maas, and R.W. Dibble. *Combustion*. Springer-Verlag Berlin Heidelberg, 4th edition, 2006. ISBN 9783540259923.

[61] Lijiang Wei, Chunde Yao, Guopeng Han, and Wang Pan. Effects of methanol to diesel ratio and diesel injection timing on combustion, performance and emissions of a methanol port premixed diesel engine. *Energy*, 95(X):223–232, 2016. ISSN 03605442. doi: 10.1016/j.energy.2015.12.020. URL http://dx.doi.org/10.1016/j.energy.2015.12.020.

[62] G. Woschni. A Universally Applicable Equation for the Instantaneous Heat Transfer Coefficient in the Internal Combustion Engine. *Technical report: 670931*, 76:19, 1967.

[63] Jiyuan Zeng. Modelling and simulation of the Diesel Engine Injection Systems. *TU Delft Master Thesis*, 2019. ISSN 1098-6596. doi: 10.1017/CBO9781107415324.004.

[64] Xudong Zhen and Yang Wang. An overview of methanol as an internal combustion engine fuel. *Renewable and Sustainable Energy Reviews*, 52:477–493, 2015. ISSN 18790690. doi: 10.1016/j.rser.2015.07.083.

A

Pressure signals

A.1. Raw data

This section gives raw data per cylinder from pressure measurements for a single cycle for F76, M10 and M20. Cylinder one shows earlier ignition for methanol blends. Moreover, M20 causes cylinder two, three and four to ignite at divergent moments.

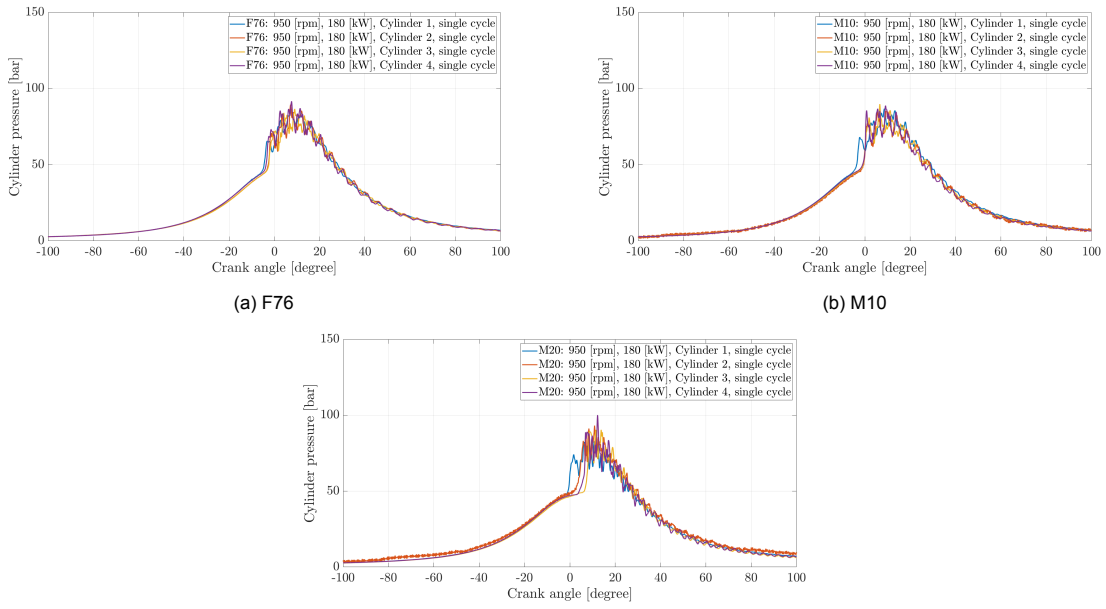

(a) F76

(b) M10

(c) M20

Figure A.1: Raw pressure data of a single cycle for each fuel type measured. Measurement point: 950 [rpm], 180 [kW]

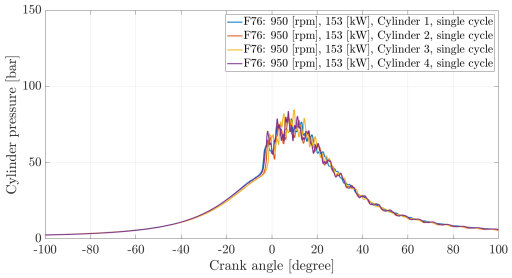

(a) F76

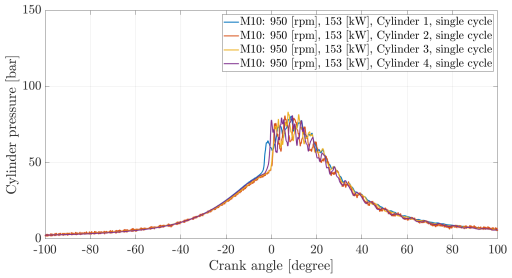

(b) M10

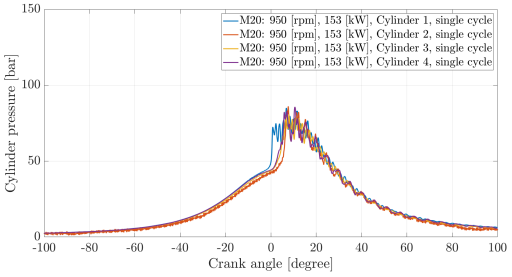

(c) M20

Figure A.2: Raw pressure data of a single cycle for each fuel type measured. Measurement point: 950 [rpm], 153 [kW]

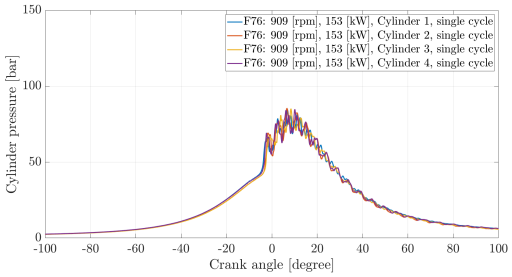

(a) F76

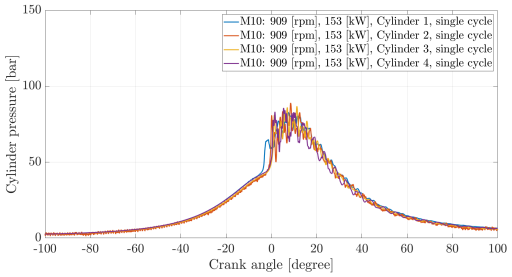

(b) M10

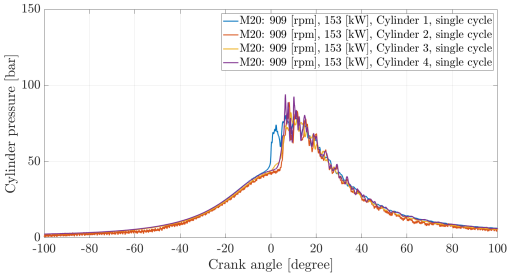

(c) M20

Figure A.3: Raw pressure data of a single cycle for each fuel type measured. Measurement point: 909 [rpm], 153 [kW]

A.1.1. Polytropic constant

The mechanical efficiency is considered to be the parameter to check whether the pressure signal is shifted correctly or not. Another way to look at the TDC-shift is the polytropic constant during the compression stroke.

Air is in principle the only gas that appears in the cylinder before injection during the compression stroke. Assumed for the first part of compression is that the air in the cylinder acts as an ideal gas. This implicates that the ideal gas law is valid. The in-cylinder gas temperatures must be low to behave like an ideal gas. For a polytropic process of a perfect gas, which has constant specific heat, the polytropic

constant must be between 1.3 and 1.4. However, due to heat transfer from and into the air in the cylinder as well as friction, the compression is not perfect or ideal. Therefore, the specific heats of the gas are varying at different temperatures. However, the first part of the compression takes place when the temperature and pressure are low. This justifies the assumption of an ideal gas for this phase. The polytropic constant can be determined by the logarithmic plot of the pV diagram of a pressure signal. The polytropic constant of the first phase is calculated based on theory described in Stapersma using eq. (3.32) [53].

$$\frac{p_2}{p_1} = \left(\frac{V_1}{V_2}\right)^n \tag{A.1}$$

where V_1 and p_1 are the volume and pressure at IC. V_2 and p_2 are the volume and pressure defined at IC+40 °CA. n is the polytropic constant. Figure A.4 shows the pV diagram of the engine running on F76 at 950 [rpm] at 180 [kW]. For this signal, after shifting the TDC, the polytropic constant is

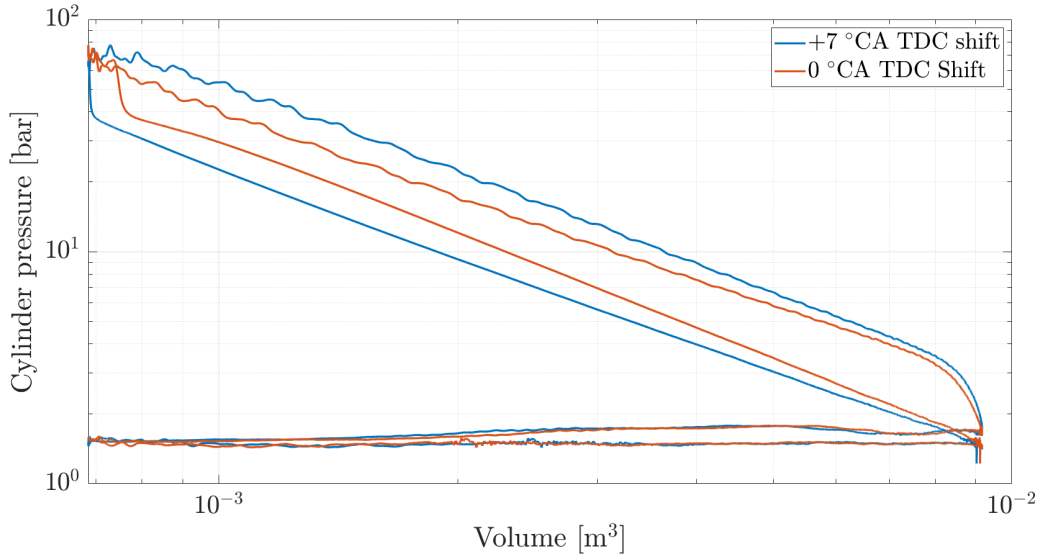

Figure A.4: Effect of TDC-shift to pressure signal: pV diagram of the engine running at 950 [rpm], 180 [kW].

around unity during the first 40°CA after IC. It is an indication that the polytropic process described by the polytropic constant does not represent a perfect or ideal gas. Besides that, the effect of residual gases in the cylinder also affects the polytropic process. Because the polytropic constant does not equal the theoretical value, the mechanical efficiency of the engine is taken as the main parameter to check if the pressure signal is well defined. Therefore, measurement data from Linden is used to check if the calculated engine mechanical efficiency is comparable [38].

B

Experiments

B.1. Experimental implementation

The experiments takes place at the Royal Netherlands Naval College over a for now unknown period. The fuel blends are direct injected to the cylinder. Below, the steps to complete a measurement are described.

1. Preheat engine
2. Check level daily supply tank
3. Open valves diesel supply to engine
4. Check for leakages
5. Start Engine (30 min)
6. Open valves methanol-diesel blend and close diesel supply valves
7. Run Engine (30 min)
8. Check cycle parameters in control room
9. Set engine torque and speed (stabilize 15 min)
10. Remote engine operation
11. Start measurement (41 cycles)
12. Check air consumption / fuel consumption / fuel leakage / Other parameters
13. Safe measurement data in control room
14. Repeat from point 9

Before starting the measurements, the engine runs on marine diesel oil for an hour to heat the system. After this, the blended fuel is injected, which also needs to stabilize for at least 15 minutes, because the marine diesel oil still in the fuel pipes also needs to burn first. Therefore, half an hour is planned to make sure the right mixture ratio is injected and measured.
The experiments contains the following targets:

- The measurements will follow a grid at 25, 50, 75 and perhaps 100% load following the propeller and generator curve burning pure marine diesel oil. These experiments are to benchmark the engine and get a clear reference point.
- Premixed methanol blends are measured at different ratios. Starting with 10%$_e$ and increasing until the engine starts to knock. These tests are also under increased load of 25, 50, 75 and if technically possible 100% following the propeller and generator curve.

During the measurements different parameters are measured to study the combustion parameters of the engine. The measured parameters are used in a simulation model to get an insight in the combustion properties inside the engine.

B.2. Parameters measured

The model needs input parameters and to get a clear understanding of the in-cylinder process, the following parameters are to get measured during the experiments.

1. Crank angle
2. In-cylinder pressure
3. Air and Fuel consumption
4. Engine Torque, Speed and Load
5. Blending ratios
6. Temperature at varying locations
7. Pressures at varying locations

Parameters such as valve and injection timings are known from the engines technical data. Crank angle and in-cylinder pressure are measured and correlated using a Kistler Kibox Type 2893. Engine torque and speed are set in the engine control room by a water brake and speed regulator.

C

Measurement equipment specifications

This chapter gives the specifications of the used measurement equipment.

C.1. Pressure sensor

The pressure sensor specifications are shown in table C.1

Table C.1: Kistler 7061B pressure sensor specifications [30]

Parameter	Unit	Value
Range	[bar]	0-250
Calibrated partial ranges	[bar]	0-50
	[bar]	0-5
Overload	[bar]	300
Sensitivity	[pCbar^{-1}]	≈ -80
Natural frequency	[kHz]	≈ 45
Linearity, all ranges	[% FSO]	≤±0.5
Acceleration sensitivity	[barg^{-1}]	<0.01
Operating temperature range	[°C]	-50-350
Sensitivity shift		
cooled 50 ±35 [°C]	[%]	≤±0.5
non-cooled 200 ±150 [°C]	[%]	≤±2
Load-change drift	[bars^{-1}]	≤±0.5
Thermo shock		
at 1500 [min^{-1}], 9 [bar] IMEP		
Δp	[bar]	≤±0.1
Δ IMEP	[%]	≤±0.5
Δ p_{max}	[%]	≤±0.5
Insulation resistance	[TΩ]	≥10
at 20 [°C]		
Tightening torque	[Nm]	25
Cooling water pressure	[bar]	≤6
Capacitance (incl. cable)	[pF]	11 (117)
Weight	[g]	27
Plug, ceramic insulator		10-32 UNF

C.2. Crank angle adapter

The crank angle is measured on the crank shaft of the engine by the crank angle adapter. Specifications are given in table C.2

Table C.2: Kistler crank angle adapter specifications [32]

Parameter	Unit	Value
Resolution of measurement data	[kHz]	312.5
	°CA	0.1
Speed range	[min^{-1}]	$\approx 0 - 15624$

C.3. Charge amplifier

The charge amplifier used is the Kistler type 5064C21. Specifications of this system are shown in table C.3. Because the engine has four cylinders, two of these amplifiers are used.

Table C.3: Kistler type 5064C21 charge amplifier specifications [31]

Parameter	Unit	Value
Number of channels	[-]	2
Measuring range	[pC]	±100 - ±100,000
Error (0-60 [° C])	[%]	<±0.5
typical (25 [° C])	[%]	±0.1
Measuring models	[-]	Short
	[-]	Long
	[-]	Drco*/Short
	[-]	Drco*/Long
Drift *Long*		
at 0-60 [° C]	[pCs^{-1}]	<±0.2
at 25 [° C]	[pCs^{-1}]	<±0.05
typical	[pCs^{-1}]	<±0.03
Reset-operate transition	[pC]	<±1.5
Time constant (*Long*)	[s]	>100,000
Drift compensation	[min^{-1}]	$\approx 100 - 20,000$
Output voltage	[V]	0-±10
Output current	[mA]	0-±2
Output impedance	[Ω]	10
Zero point error (Reset)	[mV]	<±5
Output noise (0,1 Hz - 1 MHz)	[mV_{pp}]	<8
typical	[mV_{pp}]	<4
Frequency range (20 [V_{pp}], -3 [dB])	[kHz]	$\approx 0 - > 200$
Group delay time	[□s]	<3
Low-pass filter (Butterworth, 2nd order, selectable, -3 [dB])	[kHz]	0.3 /1/3/5/10/ 30/50/100/off
Overload treshold	[V]	$\approx \pm 11$
Offset adjustable (gain 1.8)	[V]	-8.0±0.04
Common mode noise rejection (0-100 Hz)	[dB]	>70
Crosstalk attenuation Channel A, Channel B	[dB]	>60

C.4. Flow meter

Fuel flow measurements are executed with the Micro Motion ELITE CMF010M Coriolis Meter, 1/10 Inch (DN2), 316L Stainless Steel. Specifications of the equipment are shown in table C.4.

Table C.4: Specifications of the flow meter

Parameter	Accuracy
Mass flow accuracy (Liquid)	±0.10[%] of rate
Mass flow repeatability (Liquid)	±0.05[%] of rate
Volume flow accuracy (Liquid)	±0.10[%] of rate
Volume flow repeatability (Liquid)	±0.05[%] of rate
Mass flow accuracy (Gas)	±0.35[%] of rate
Mass flow repeatability (Gas)	±0.20[%] of rate
Density accuracy (Liquid)	±0.0005 g/cm3 (±0.5 kg/m3)
Density repeatability (Liquid)	±0.0002 g/cm3 (±0.2 kg/m3)
Temperature accuracy	±1 °C (±0.5[%] of reading)
Sensor maximum working pressure	1,812 psig (125 barg)

C.5. Testo 350 (Maritime) gas analyser

All emissions are measured using the Testo 350 Maritime gas analyser, except for the unburned hydrocarbons. These are measured with the Testo 350 gas analyser. Data is obtained from the specification sheets from Testo.com. Measurement tolerances for the Testo 350 Maritime are according to the Marpol, Annex VI [57].

Table C.5: Testo 350 gas analyser specifications

Parameter	Range	Unit	Tolerance
NO_x	0 to 3000	[ppmv]	±5 [%] (NO) ±5 [%] (NO_2)
SO_2	100 to 3000	[ppmv]	±5[%]
CO_2(IR)	0 to 40	[vol.%]	±0.5 [vol.%]
CO	0 to 3000	[ppmv]	±5 [%]
O_2	0 to 25	[vol%]	±0.2 [vol.%]
°C, flue gas	-40 to +1000	[°C]	±5 [°C]
C_xH_y	100 to 4000	[ppmv]	±400 [ppmv]

D

Measurement grid

A new 100% point of the engine is specified based on the energy and efficiency losses occuring while running on alcohol blends. From the nominal 100% point, the 75, 50, 25% MCR line is followed defined by IMO MARPOL. The new maximum load of the engine is based on the maximum mixing ratio according to previous research, which is based on 70% methanol on volume base done by the University of Gent by port injection. It is on beforehand not sure if this engine reaches this point.
The MCR line is calculated using a third power relation between engine power and speed, shown in eq. (D.1). Moreover, in this case the NO_x emission results can be calculated using the IMO standards.

$$N = (x \cdot P_{\mathrm{b}})^{(1/3)} \cdot N_{\mathrm{nominal}} \tag{D.1}$$

where N is the engine speed [rpm] based on the MCR-line varying from 0-100%. P_{b} is the nominal break engine power, x defines the point on the MCR-line (25-50-75-100%) and N_{nominal} is the nominal engine speed of 1000 [rpm].
The nominal engine power is 300 [kW] at 950 [rpm] running at F76 fuel. Normally, the nominal engine point was 340 [kW] at 1000 [rpm]. Technical issues with the engine and unexpected engine failures reduced the maximum engine load to 300 [kW]. Now, the new nominal point is calculated based on the new energy in a volume. For efficiency losses, a correction factor of 5% is used to be sure the new nominal point is reachable for each mixture ratio. Equation (D.2) gives the calculation of the new defined nominal power of the engine.

$$P_{\mathrm{b,100\%,new}} = \frac{0.7 \cdot LHV_{\mathrm{methanol}} + 0.3 \cdot LHV_{\mathrm{diesel}}}{LHV_{\mathrm{diesel}}} \cdot 340 \cdot 0.95 \tag{D.2}$$

The new maximum power defined for the engine during these experiments is 204 [kW] based on a nominal load of 340 [kW]. This point is corrected to 180 [kW] to be sure that the engine will reach this while running on methanol blends. The other engine loads are at 75, 50 and 25% of the nominal value of 204 [kW]. The torque is not equal for each power at different engine speeds. The torque per measurement point is calculated according eq. (D.3).

$$M_{\mathrm{b}} = \frac{P_{\mathrm{b}}}{2 \cdot \pi \cdot \left(\frac{N}{60}\right)} \tag{D.3}$$

where M_{b} is in [Nm]. This grid will be followed during the experiments, shown graphically in fig. 4.1. For each fuel blend, varying from 20 to 70% methanol by volume, the measurement grid is measured at least two times to avoid mistakes.

E

Dimensional analysis heating period

To describe the initial heating period of the droplet, the parameters involved in this process are selected. It is proven that the original model of Borman predicts a fast evaporation rate compared to experiments. Therefore, the results are tuned by using a self designed dimensionless number.
During evaporation, multiple parameters have an impact on the process. First of all, the initial heating period has a limited detailed description in an infinite conductivity model. Therefore, at least conductivity is of importance. Second, the length of the heating period takes a certain time before the linear evaporation progress starts. Comparison between the experiments and the model in 5.2 shows that the slope of the d^2-law is correct and the heating period is too short. Therefore, the time is included in the dimensional analysis. Furthermore, the heating period is related to the temperature of the droplet. The moment that the temperature of the droplet is constant, the d^2-law starts and is included in the analysis. Finally, droplet parameters decide whether the evaporation takes place. This is for the evaporation part mainly described by the diameter and density of the droplet. Parameters involved in the dimensional analysis are given in table E.1.

Table E.1: Parameters required for dimensionless analysis on initial heating period of a fuel droplet

Parameter	Description	Unit
t_h	Time of initial heating period	[s]
ρ_f	Droplet density	[kgm^{-3}]
d	Droplet diameter	[m]
k_f	Thermal conductivity	[Wm^{-1}K^{-1}]
T_d	Droplet temperature	[K]

In order to create a dimensionless number, the units of the parameters are evaluated in eq. (E.1)

$$ {t_\mathrm{h}}^{\alpha} \cdot {\rho_\mathrm{f}}^{\beta} \cdot d^{\delta} \cdot {k_\mathrm{f}}^{\gamma} \cdot {T_d}^{\kappa} \tag{E.1} $$

By solving the balances for each separate unit, the values of the unknown parameters in eq. (E.1) are calculated and shown in table E.2.

Table E.2: Parameter results of dimensionless analysis

Parameter	Value
α	3
β	-1
δ	-4
γ	1
κ	1

Table E.2 shows the unknown values shown in eq. (E.1), resulting in eq. (E.2).

$$t_{\mathrm{h}}{}^{3} \cdot \rho_{\mathrm{f}}{}^{-1} \cdot d^{-4} \cdot k_{\mathrm{f}}{}^{1} \cdot T_{d}{}^{1} \tag{E.2}$$

which is dimensionless. From this point, the time is described as a function of the diameter, density, thermal conductivity and temperature of the droplet. The heating period is therefore proportional to these parameters according to eq. (E.3).

$$t_{\mathrm{h}} \propto \left(\frac{\rho_{\mathrm{f}} \cdot d^{4}}{k_{\mathrm{f}} \cdot T_{d}}\right)^{\frac{1}{3}} \tag{E.3}$$

Implementing this dimensionless number to correct the infinite thermal conductivity in the droplet includes the effect of conductivity. Therefore, the heating period is extended and dependent of the droplet diameter.

F

Experimental setup and safety considerations

F.1. Fuel supply system

The experimental setup of the dual fuel engine is designed for this project. The general fuel system is schematically given in fig. F.1.

The fuel valves and three way connections are made of stainless steel suitable for both fuels chemical properties. Fuel pipes are made of chemical resistant materials, also suitable for oil and methanol.

Monitoring the fuel flow is executed by two manometers before and after the engine. Moreover, the F-76 and methanol tanks are filled with separate pumps. The fuel mix tank is equipped with a stirrer in order to blend the diesel and methanol. The flow meter is located before the fuel return pipe. Because the fuel pump is designed to keep the fuel system at a given static pressure, the pump supplies the fuel consumed by the engine. Therefore, the fuel consumption is measured before it enters the circular fuel loop. A disadvantage is that the residual fuel in the system stays in the fuel supply system until it is used by the engine. This could lead to slight differences in the fuel mixture in the fuel supply system.

F.2. Safety measures

Study to the properties of methanol has proven that personal protecting equipment is necessary when doing experiments with methanol. Table F.1 gives the toxic properties of methanol.

Table F.1: Toxic properties of methanol for human [28]

Flammable
Oral toxicity
Dermal toxicity
Inhalation toxicity
Specific organ toxicity by single exposure

Personal safety has high priority during the experiments. Therefore, multiple safety measures are taken in order to guarantee personal safety and decrease the risks on accidents. Table F.2 shows the measures taken for experiments containing methanol.

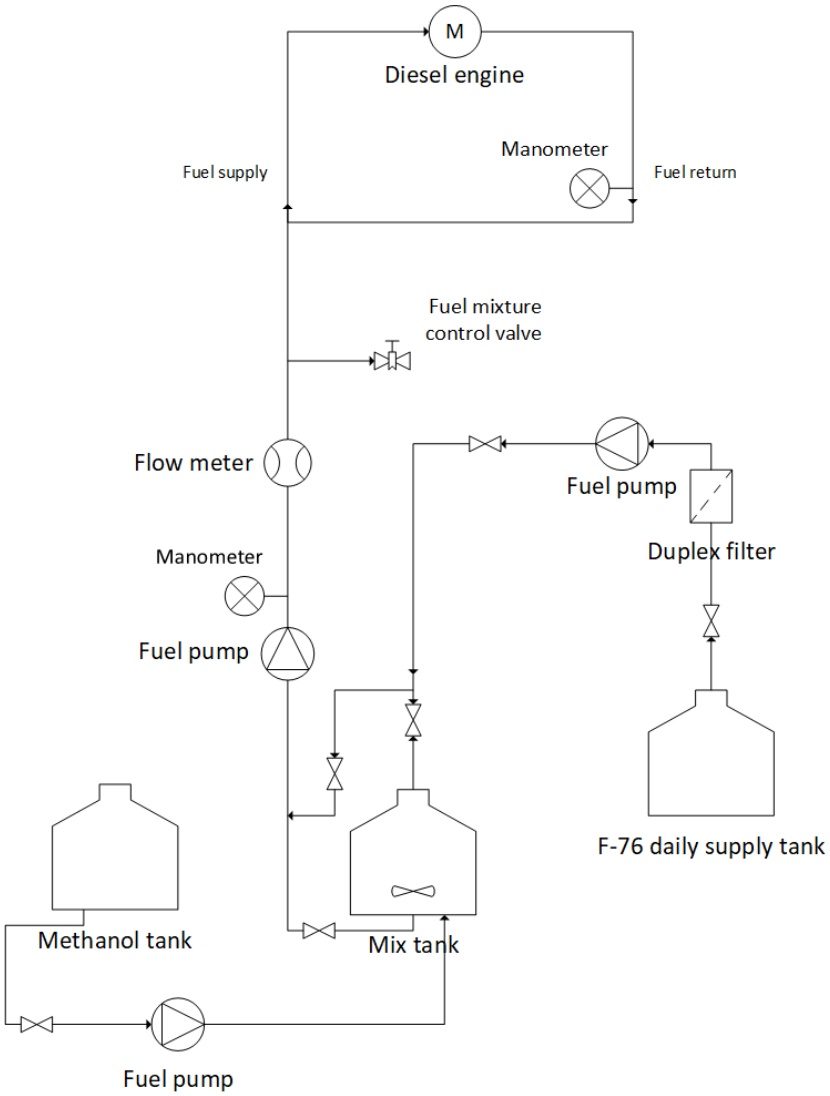

Figure F.1: General fuel supply system designed for dual fuel operation on the MAN 4L20/27 diesel engine

Table F.2: Safety measures according to toxicity of methanol

Equipment
Full face masks (AX filter)
Protective clothes (gloves, shoes and overall)
Thermal UV/IR^2 camera
Methanol detector (0-1000 ppm)

For specific technical data of the equipment and its safety requirements can be found in Safe Handling of Methanol of the Methanol Institute [28].

G

Sensitivity analysis

Since the pressure signal is shifted based on the engines performance, a sensitivity analysis of the in-cylinder model is performed. Effects on the heat release rate, temperature and the RCO by three different TDC-shifts are discussed.

G.1. Single zone model

The TDC shift affects the position of the pressure signal for a certain crank angle in time. As shown by figs. G.1a to G.1c, the position of the premixed combustion shifts with the crank angle position. Since the position of the crank angle determines the volume in the cylinder, the maximum heat release rate also increases with a larger TDC shift. The model is sensitive for the TDC shift, which has a impact on the model results. The shape of the heat release curve almost remains equal for each TDC shift. Except for the smallest shift shown, the heat release rate increases above zero before the fuel is injected. This is an inaccuracy by the model, which is possibly caused by the heat loss calculation and inaccuracy of evaporation heat calculation in the model. The location of the pressure signal affects the heat release period between SOI and SOC and shows nonphysical phenomena before injection starts. Unreal values are also seen in the RCO, which is -0.1 before the fuel is injected.

From this sensitivity analysis, it is clear that the position of the pressure signal has significant impact on the model results. Calibration of the Kibox could prevent that uncertainty of the pressure signal position occurs for this analysis.

G.1.1. Heat release rate

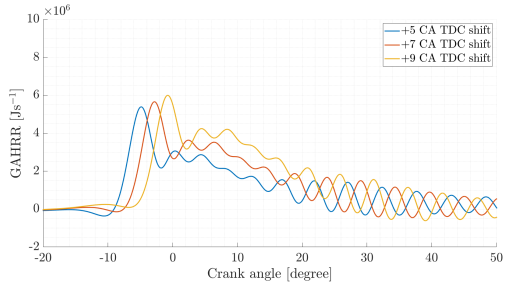

(a) F76

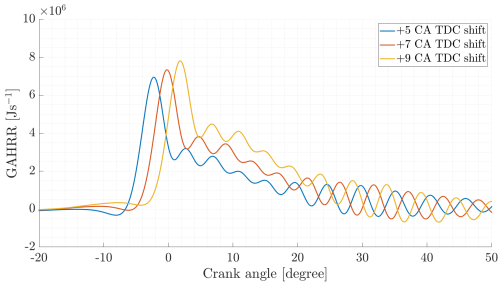

(b) M10

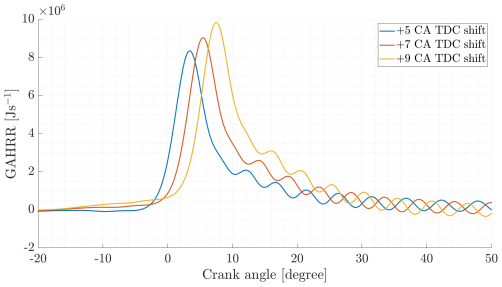

(c) M20

Figure G.1: Gross apparent heat release rate sensitivity analysis: effect of TDC-shift.

G.1.2. Temperature

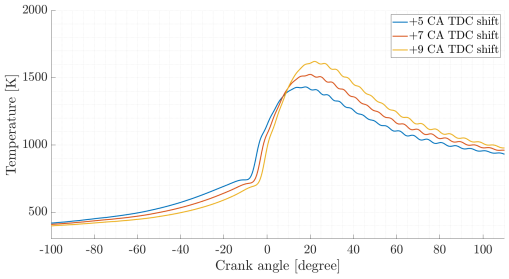

(a) F76

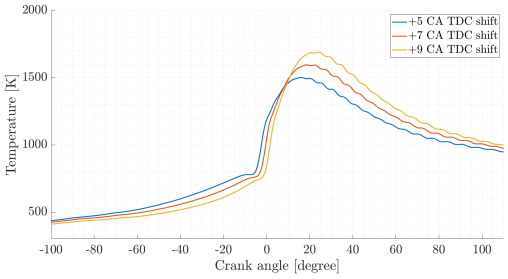

(b) M10

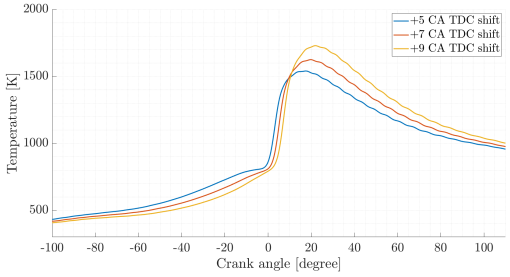

(c) M20

Figure G.2: Temperature sensitivity analysis: effect of TDC-shift.

G.1.3. RCO

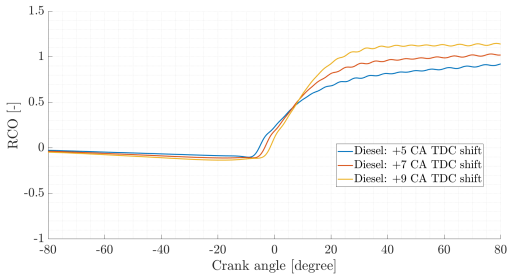

(a) F76

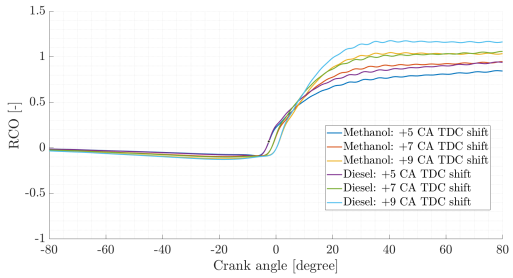

(b) M10

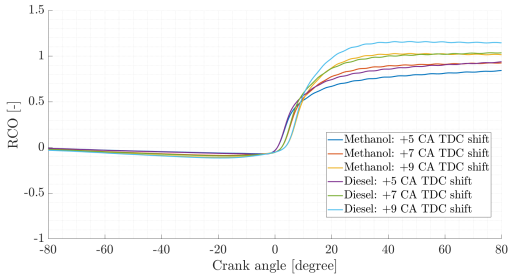

(c) M20

Figure G.3: Reaction coordinate sensitivity analysis: effect of TDC-shift

H

Cylinder comparison

Single zone model parameters per fuel are shown in this chapter. For each parameter from the single zone model, a comparison between the different fuels is given.

H.0.1. GAHRR

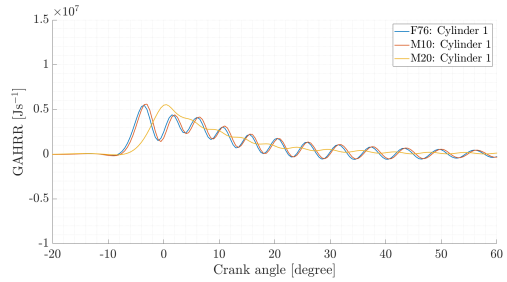

(a) Mean values of cylinder one

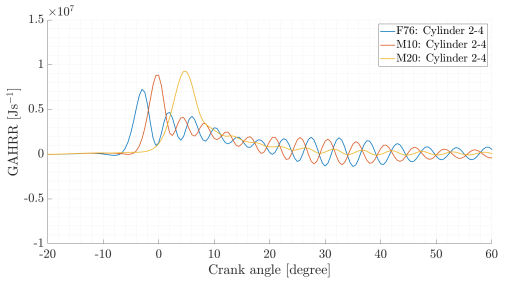

(b) Mean values of cylinder two, three and four

Figure H.1: GAHRR: Fuel comparison at constant engine speed and load of 909 [rpm] and 153 [kW] respectively. TDC-shift = 7°CA

H.0.2. Temperature

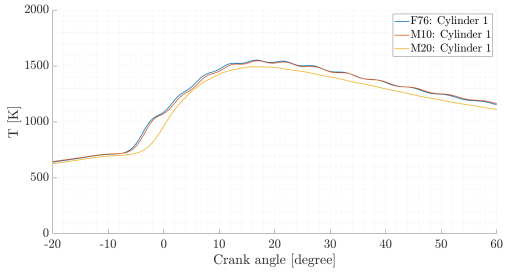

(a) Mean values of cylinder one

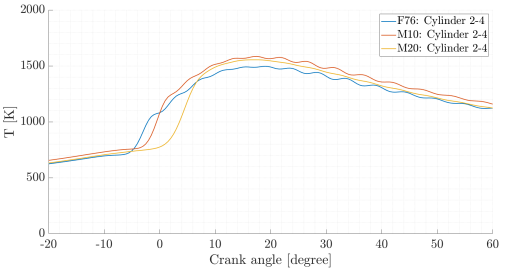

(b) Mean values of cylinder two, three and four

Figure H.2: Temperature: Fuel comparison at constant engine speed and load of 909 [rpm] and 153 [kW] respectively. TDC-shift = 7°CA

H.0.3. RCO

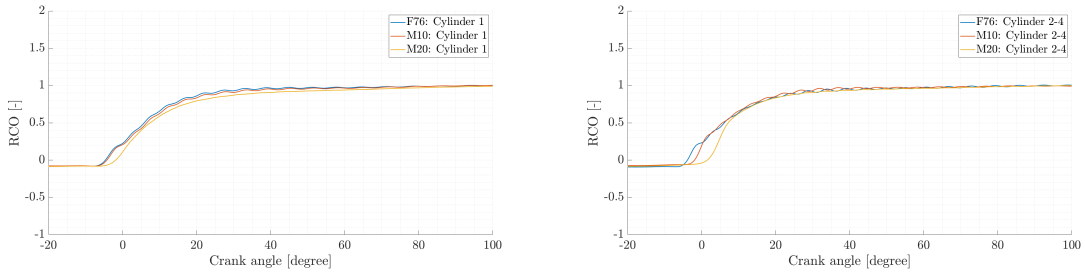

(a) Mean values of cylinder one

(b) Mean values of cylinder two, three and four

Figure H.3: RCO: Fuel comparison at constant engine speed and load of 909 [rpm] and 153 [kW] respectively. TDC-shift = 7°CA